（千葉大学審査学位論文）

Integration of Optical and Microwave Remote Sensing Data for the Estimation of CO_2 Sequestration by the Forests in Japan

January 2015

Chiba University
Graduate School of Science
Division of Geosystem and Biological Sciences
Department of Earth Sciences

Kotaro Iizuka

（千葉大学審査学位論文）

光学とマイクロ波リモートセンシングデータを用いた日本の森林による二酸化炭素固定量の算定

2015 年 1 月

千葉大学大学院理学研究科

地球生命圏科学専攻　地球科学コース

飯塚　浩太郎

Table of Contents

List of Figures

List of Tables

Abstract

This study aims on estimating the CO_2 sequestration by the forests in Japan using LANDSAT OLI and ALOS-PALSAR remote sensing data. The objective was obtained by integrating the optical data and the microwave data, where the former was used for developing a detailed land cover map and latter for estimating the stem volume information for the forests of Japan. Along with the CO_2 sequestration value for each forest types and for per tree age information from the forest inventory data, we have performed the estimation. It was found that total CO_2 sequestration based on tree age forest subclasses yields 85.0 $MtCO_2$ (coniferous), 4.76 $MtCO_2$ (evergreen broadleaf) and 21.61 $MtCO_2$ (deciduous broadleaf) summing up as total 111.27 $MtCO_2$. This methodology can thus help to investigate more in-depth the CO_2 sequestration values for trees of different ages and types, especially for the coniferous and also for deciduous or evergreen broadleaf forests, which are found over Japan. The result foresee that this would lead to even more realistic estimation of the CO_2 sequestration of the real environment. The detailed information about the spatial location and the status of the forest resources is more likely to provide the decision makers with a sound basis for more effective policies and actions aiming at the sustainable use and conservation of the environmental resources.

概要

本研究は、LANDSAT OLI と ALOS-PALSAR リモートセンシングデータを用いた日本の森林による二酸化炭素(CO_2)固定量の算定を目的とする。LANDSAT OLI を用いて詳細な土地被覆図を作成し ALOS PALSAR による林分材積量の推定を実施することで、日本の森林領域における樹種とその樹種別の成長期の情報を得ることが可能となる。これらの情報を統合し、かつ樹種毎とその林齢毎の CO_2 固定量の値を用いることにより、日本の森林におけるより詳細な CO_2 個定量の算定を実行することが可能となった。固定量の結果は、85.0 $MtCO_2$（針葉樹林）、4.76 $MtCO_2$（常緑広葉樹林）、21.61 $MtCO_2$（落葉広葉樹林）となり、総量は 111.27 $MtCO_2$ となった。本研究手法を用いることにより、それぞれの樹種毎と異なる林齢においての CO_2 固定量をより詳細に調査することが可能となった。我々はこの手法を用いることにより、実環境の CO_2 個定量をより現実的な数字の推定に繋がるであろうと考える。空間的位置と森林資源の状況についての詳細を把握することは、環境資源の持続可能な利用と保全を目的とした、より効果的な政策と行動のための意思決定としての判断材料になると考える。

1. Introduction

1.1. Research Background

Global Warming is considered as one of the most crucial environmental issues in the 21st century. Many research and conferences have been held to emphasize the importance of this issue and associated problems, and many nations are working together on policies if not for preventing the problem, but at least for mitigating its impacts (Hewitt & Jackson, 2003; Chiras, 2006). Japan, is one of the top nations which is involving in many activities related to this issue, and the Kyoto Protocol (adopted at the Kyoto Conference in 1997) has provided a new approach to finding solutions (UNFCC, 1998). Clean Development Mechanism (CDM), Emission Trading, Joint Implementation (JI) and Carbon Sink are the main Kyoto Mechanisms, and among them carbon sink is very important in the current research context, as 67 % of lands in Japan is covered by forests (MAFF, 2010a). Japan is considering the forests to be the top candidate for its CO_2 reduction process (METI, 2005). Many prefectures in Japan have done research about the forests carbon sequestration and have come up with policies for the implementation of reducing CO_2. However, some prefectures have not yet been involved in such processes that focus on CO_2 reduction through carbon sink although they have a great amount of forest cover (Sanga et al., 2012). Forests provides us with essential ecosystem services, such as regulating water flows, preventing landslides, providing pure oxygen from the photosynthetic activity, and much more it is known. One of the services that are often discussed is the role of forests in contribution to regulate the amount of greenhouse gas, in this case carbon dioxide (CO_2) in the atmosphere. As mentioned above Japan is the country where 67 % of land is covered by forests, and it is important to understand that forests store large amounts of carbon that would otherwise contribute to the one of the biggest environmental issue we are facing today: climate change.

Interests through the remote sensing society from applications to practical use of the various data sets to solve the challenging issues of the nature environment have been carried out, leaving many informative results that contributed to the understanding of our surrounding environment (Kato, 2004). The application of Synthetic Aperture Radar (SAR) is becoming one of the top interests among researchers to deal with issues that were facing difficulties when only optical data were opted. Developing algorithms for extracting information's from the Earth's surface (e.g. biophysical parameters) is especially one of them. Today in Japan, because of the changes in the demands of timber product and increasing imports from overseas for low cost productions, it made the forests in Japan widely to turn into an unmanaged green desert. As mentioned, the use of remote sensing data with GIS techniques has provided various benefits to the scientific society. Japanese government has recently begun to emphasize the use of GIS and remote sensing for developing information's to provide the status of our country, such as the land cover information (vegetation map) is one of them. However, still, the most important information of those forests are not known, which are to be the status of those resources, in terms of either the condition of the trees or the growing stages of those trees. By understanding the status of those resources through the remote sensing methods, the efficiency of managing those resources could turn out to become one step forward to actually maintain and manage it in a more strategic and operative way. It is thus time to reconsider the measure and the tools used for the making a step forward to achieve the goals.

1.2. Review of Previous Works

Traditional methods of estimating carbon/CO_2 through a site-based method (Tadaki & Hachiya, 1968; Bird, 2010) or using eddy covariance flux tower are sometimes expensive, time consuming and limits the coverage of the area. Even to expand the area or implementing continuous monitoring will be more costly and again time consuming. Remotely sensed satellite observations have provided the scientists with an alternative method of the way to

study the Earth's nature (atmosphere, vegetation, etc.). On the study of vegetation it has been demonstrated that the reflectance of the wavelength (red, green, infrared) radiation contains considerable information about plant biomass (Tucker, 1979), leading to the extraction of vegetation information and giving us the possibility of monitoring at lower costs and less time. Today, with further advancement of research, it is a common application not only even to produce maps to categorize the land cover type of the surface for allocating and managing the Earth's resources (Lo & Choi, 2004) but to analyze the changes and its impacts for future developments (Xiuwan, 2002). The remotely sensed method for evaluating the carbon/CO_2 sequestration have been implemented in various ways, and one is to use the land cover information to combine with the averaged carbon sequestration value of different land cover types to estimate regional sequestrations (Janssens et al., 2003). The strength of using land cover information based on remotely sensed images is to cover regional or even global scales of the area and also it can observe sites that are difficult to access when on the ground. Moreover it allows implementation of continuous monitoring of the area for analyzing the changes of the forest cover areas. However, it is important to determine not only the types of forests but also the differences of the tree age can result in a big difference in the estimation (Turner et al., 2004). The estimation implemented in Japan focuses mostly at identifying the forests to the natural and the planted forests. Hiroshima & Nakajima (2006) has focused on the potential carbon sinks in Japanese plantation forests during the first commitment period of the Kyoto Protocol. They have estimated that the private planted forests were expected to sequester 8.16-8.87 MtC/yr, depending on the different scenarios of the forest management based on silvicultural practices, employing subsidies and forest workers' wages as predictor variables. Sasaki & Kim (2009) has estimated potential sequestration of the forests in Japan and the eligible sequestration under the condition of the Marrakesh Accords. Using the land use model and carbon stock growth model, it has been estimated that the forests in Japan is likely to sequester 20.1 MtC/yr (planted forests: 15.3 MtC/yr, natural: 4.8 MtC/yr), and in the conditions

under the Marrakesh Accords, it is estimated at 10.2 MtC/yr (planted forests: 7.3 MtC/yr, natural: 2.9 MtC/yr). In very recent on 2014, National Institute for Environmental Studies (NIES) Center for Global Environmental Research (CGER) has output a result for the IPCC reports on the issue of forests carbon sink, estimating the CO_2 sequestrations from the forests of Japan. Using the forest registration data from each prefectural government, and differentiating the forests by each tree types, they have calculated the total CO_2 amount sequestered from the aboveground and from litter and soil. Their results showed an estimate of 77.67 $MtCO_2$ for the year 2012.

Few studies estimates the potential of the sequestration by the forests in Japan and not many considers to perform an analysis to look through in a local or regional scale focusing more on detailed forest types, which can be understood because the Kyoto Protocol consists at the national level so many studies estimates at that scale. However, in the case of estimations performed by those researches mentioned above are based on a modeling, or by site observation and statistics while the information of where and how much those resources exist is not considered, which is not good because it won't give a further information of then how to make decision for treating those resources. It must also take in consider that the forests are more diverse than just a natural or planted forests. Thus it must be analyzed more on a local or regional scale locating precise and detailed classes of the forests types or the tree types for a realistic estimation of the sequestration, because tree types and even tree ages makes differences in sequestration (Tadaki & Hachiya, 1968; MAFF, 2010b; Sanga et al., 2012). After locating the precise information of the forests, the true value of the forests capacity could be estimated. Once this information is obtained, it will become strong information which can be provided for important decision making on forest management and further for the carbon cycle contributing to the issues relating to global warming. To plan for future developments and taking decision for actions, the status and location of resource is a critical issue to effectively manage those resources over time.

1.3. Research Objective

The objective of this research is to re-assess the estimation of CO_2 sequestration by forest covers in Japan based on precise evaluation of forests extents and the use of remote sensing data. This will make it possible to quantitatively estimate their potential storage capacity, and therefore, maximize the usage of this environmental resource as a CO_2 sink. These findings will help Japan, or otherwise each Prefectural Governments devise better scenarios for mitigating the global warming issue.

1.4. Structure of the content

This thesis is structured by 6 chapters.

In the first chapter "**Introduction**" clarifies the research background and the issue of why this study was considered, along with the reviews of other researches relating to this issue.

The second chapter "**Synthetic Aperture Radar (SAR) for Forest Biophysical Parameter Modeling**" explains the current trends and issues of the usage of the SAR technology for the extraction of the forests characteristics and the challenge for doing such in the forests of Japan.

The third chapter "**Stem Volume Map Development using SAR**" takes its knowledge obtained from chapter 2 and applying the method for developing a stem volume map for the forests of Japan.

In chapter 4 "**Detailed Land Cover Mapping of Japan using LANDSAT OLI**", development of detailed land cover (forest cover) map was implemented to obtain the land information of our nation in order to use its output information of the forests in the final chapter of this work.

Chapter 5 "**Estimating CO_2 Sequestration from the Forests of Japan**" describes the compilation of the work obtained from the previous chapters and using its data to finally take an approach for the estimation of the CO_2 sequestration from the forests of Japan.

Last but not least, chapter 6 “**Concluding Remarks**” states the overall conclusion of this doctoral research work. Figure 1 shows the overall flowchart of the content.

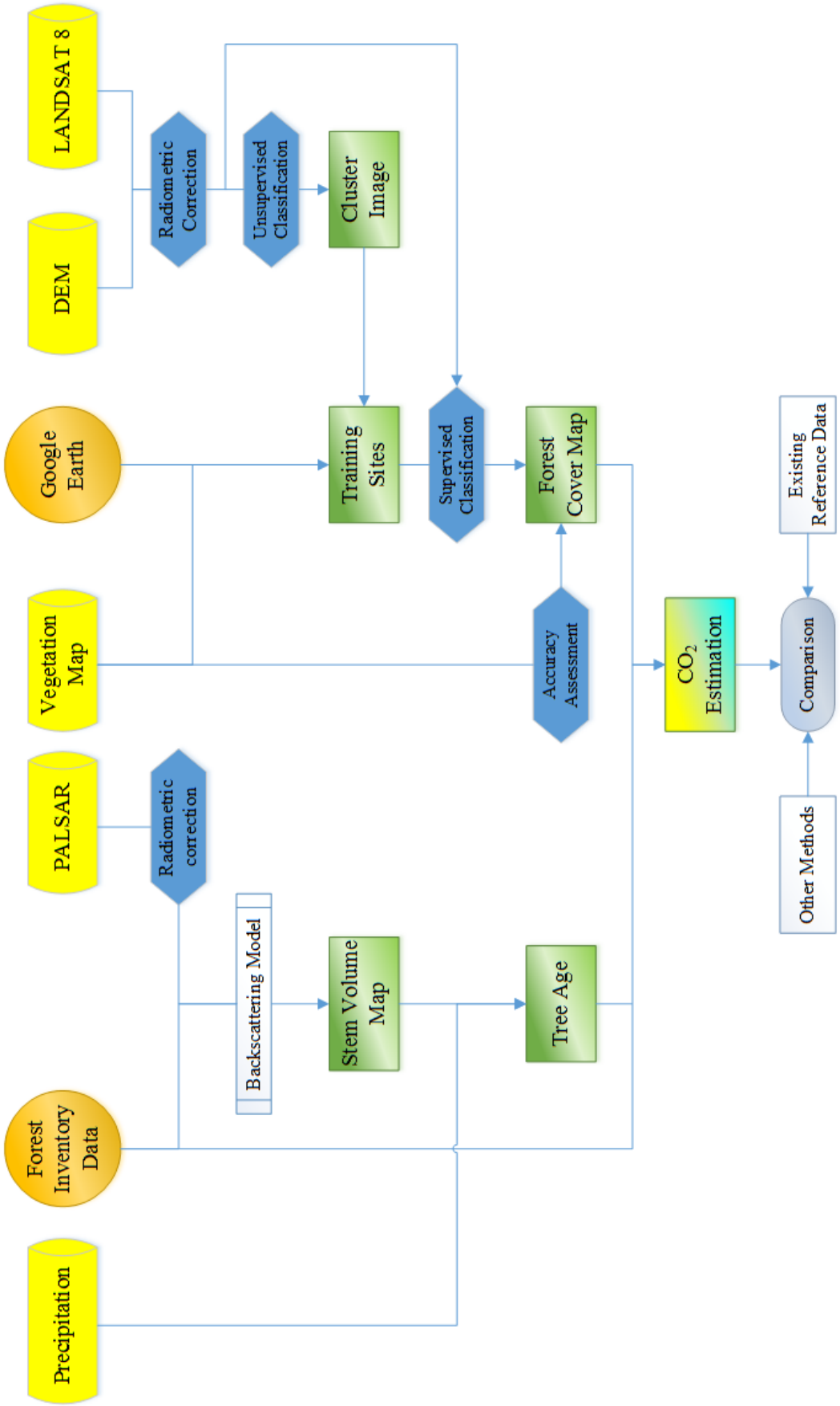

Figure 1. Overall flowchart of the methodology.

1.5. GIS Software

In this research, the Clark Labs IDRISI Selva GIS platform was used for all the analysis. Various modules mounted and the high compatibility to other file format is the advantage of this software which will support all the analysis.

2. Synthetic Aperture Radar (SAR) for Forest Biophysical Parameter Modeling

2.1. Introduction

Synthetic Aperture Radar (SAR) application in land remote sensing is becoming one of the top methods chosen among the researchers for solving issues that were facing difficulties when only optical data were selected. The field varies from land cover change, detection analysis, to disasters such as land degradation, earthquakes, and to the application in forest management. Developing algorithms for extracting information's from the Earth's surface (e.g. biophysical parameters) is especially of high interests because of the potential of the remote sensing technique where interpretation of areas which are remote and difficult to access, and furthermore becomes possible, for the use as performing continuous monitoring of the forests resources.

The use of SAR for a biomass/biophysical parameter application is likely to be processed with the relationship between the radar backscattering and the parameters of the forests. This works out because of the characteristics of the radar information; radar waves are longer than the optical waves. As a result, the scattering of the radar contributes from not only the surface of the top layer (e.g. canopy) but also from the medium of the objects (e.g. branches, stems) for the L-band radar (Castel et al., 2001; Dobson et al., 1992b; Fransson and Israelsson, 1999; Harrell et al., 1997; Hoekman and Quinones, 2000; Hyyppä et al., 2000; Saatchi and Moghaddam, 2000; Sandberg et al., 2011). Various studies have investigated the correlations between biomass/biophysical parameters with SAR backscattering information to understand the trend and reliability of the usage of SAR for the extraction of the forests information so that it could be further applied for the use in forest management (Fransson and Israelsson, 1999; Kuplich et al., 2000; Champion et al., 2008; Hamdan et al., 2011; Kobayashi et al., 2012a; Lucas et al., 2010; Luckman et al., 2011; Wijaya, 2009). However, most of the studies focus on forests that are located in regions that are on relatively flat areas, which is understandable due

to the difficulties of the SAR distortions caused by the hilly terrains (Richards, 2009; Small, 2011) making the interpretation of ground lying objects falling into an erroneous assumption. Some studies have shown the challenges in analyzing the trend at mountainous regions (Chen et al, 2009), but they still show the difficultness in applying studies on such areas. The majority of these studies concludes that their understanding of the relation to backscatter and forests biomass/biophysical parameter shows that the backscattering tends to increase with relating biomass and biophysical parameters such as stem volume or tree height and comparing with the co-polarized signal such as the HH polarization, the cross-polarized HV backscattering shows more sensitivity to the growing parameters (Balzter et al., 2002; Castel et al., 2001; Dobson et al., 1992b; Harrell et al., 1997; Hoekman and Quinones, 2000; Kellndorfer et al., 2003; Le Toan et al., 1992; Ranson and Sun, 1994, 2000; Suzuki et al., 2013). Although, not all of the studies shows clear increasing relationships of the parameters with the increasing backscattering, such as the works done by Kobayashi et al. (2012a) and Wijaya (2009) when studying the relation of the backscattering with the changes of the stand characteristics within the forests of Indonesia. They described that the backscattering increases with increasing biophysical parameter but it also starts to decreases at a certain point of the growing parameter. Clear description of this phenomenon isn't stated, however, Kobayashi et al. (2012a) states that the backscattering may be affected by the leaves of the tree due to its size and the moisture content.

Studies applied in the forests of Japan are rare, Motohka et al. (2011) investigated the relationship between the backscattering information of HH and HV polarized gamma nought values and biomass of Japanese natural forests for the retrieval of forests above ground biomass (AGB), showing a positive logarithmic relationship and showing also the usefulness with the performance of slope correction. However, not a significant relation can be seen through the study, which might be occurring that the forest inventory data in their study were used from different experimental sites with various forest types and species, which makes

difficult to determine the true backscattering relations, as Santoro et al. (2009) explains that accuracy of forest biometric parameter estimations are site dependent.

Leblon et al. (2002) describes that the influences to the backscattering at forested areas are affected by vegetation types, species and structures (Dobson et al., 1992a; 1992b; 1995; Leckie, 1990), vegetation biomass (Harrell et al., 1995; 1997; Kasischke et al., 1995; Pulliainen et al., 1996), topography and surface roughness (Shi et al., 1997) and canopy height (Dobson et al., 1992b; Harrell et al., 1997), flooding and the presence/absence of the standing water, and near surface moisture or fuel moisture (Abbott et al., 2007; French et al., 1996; Hess et al., 1990; Kasischke & Bourgeau-Chavez, 1997; Leblon et al., 2002; Lucas et al., 2012). If backscattering information changes from such various aspects, there needs to be a strong care when relationship analysis between the biomass/biophysical parameters is taken, because difference in region and environment would affect the changes in the response from the forests.

A number of studies have been implemented throughout various regions in the world, but not many studies have been applied at the forests of Japan for understanding the trends between the structure of the Japanese forests and SAR information. Even the work that has been implemented by Motohka et al. (2011) or Watanabe (2006) is limited to the natural forests, while it considers the AGB but not the actual biophysical parameters that influence to the resulting AGB. Most of the studies do not look through the characteristics of the backscattering with the relation on different tree types at different growing stages, and according to the former studies there might be some differences in the characteristics of the stands in the Japanese forests which could influence to the resulting backscatter, and those needs to be considered for when making relationship between the backscattering and the stand characteristics for a better understanding and development of accurate biomass/biophysical parameter extraction method.

Therefore, the objective in this chapter is to analyze the relationship between backscattering information with the biophysical parameters (diameter at breast height (DBH), tree height, stem volume) from different tree types (Sugi (Japanese cedar: *Cryptomeria japonica*) and

Hinoki (Japanese cypress: *Chamaecyparis obtusa*) at different polarizations in the forests of Japan.

2.2. Study Area

The study area is focused on the Prefectural owned forests of Chiba Prefecture, Japan. Chiba Prefecture is located on the east coast of Japan along the Pacific Ocean, just east of Tokyo metropolitan area where the peninsula sticks out, approximately between 139.75°E and 140.88°E, 34.89°N and 36.10°N, where a total land area of 5,156 km^2 (Figure 2). Official figure shows that 1,606 km^2 (about 1/3) of Chiba Prefectures lands are covered by forests. The terrain of Chiba is rather flat compared to the other places of Japan. The Boso hills, a chain of hills ranging from 200 m to 300 m in altitude, and the highest peak can be seen at Mt. Atago, which ranges up to only 408 m.

Climatic condition shows a warm oceanic climate, which is a condition that is high humidity, high precipitation on summer, and low humidity, low precipitation on the winter. However, compared to the southern and north eastern region of Chiba where the climate is warm throughout the year, the inland area shows more diversity such as a higher temperature drop in the winter. Annual precipitation shows highest at in the southern area with more than 2000 mm and next the northern area which is has about 1400 mm to 1600 mm. The difference in precipitation clearly shows the distribution of the forests being more dense at the south and sparse on the north.

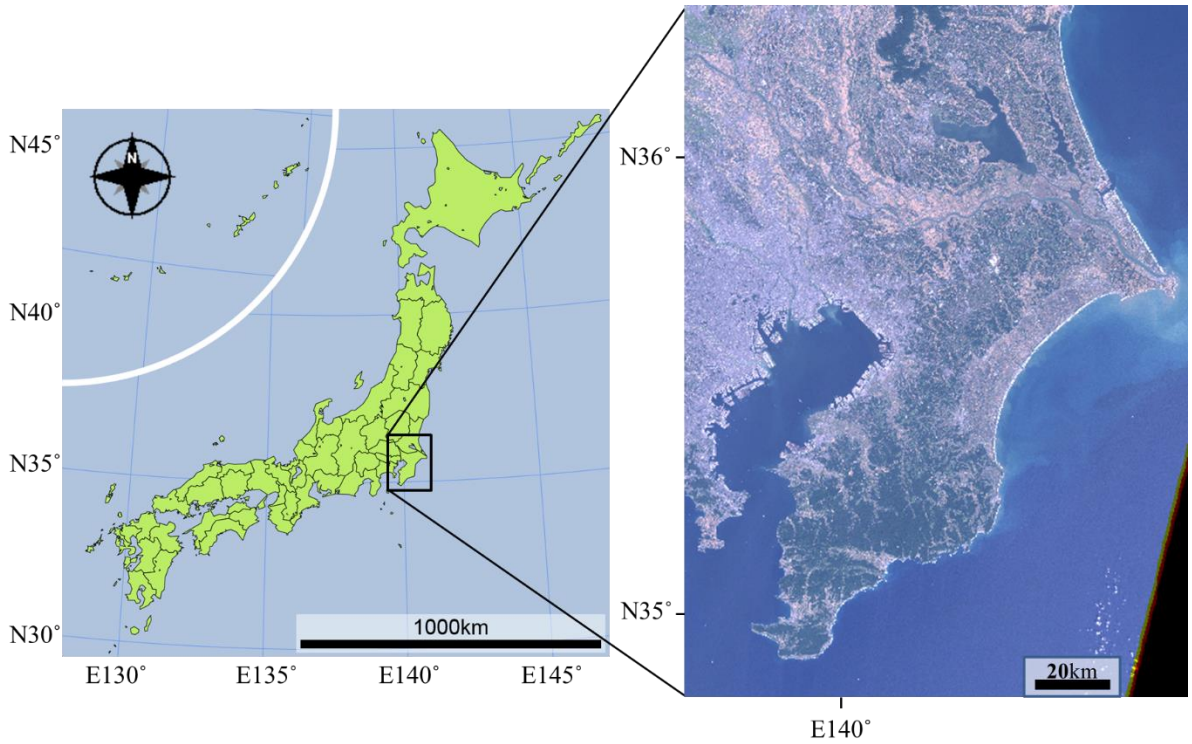

Figure 2. Study area, Chiba Prefecture, Japan.

2.3. Data Sets

2.3.1. Satellite Remote Sensing Imagery

For the analytical purpose, a microwave satellite data was considered in use. The Advanced Land Observing Satellite (ALOS) Phased Array L-band Synthetic Aperture Radar (PALSAR) provided by Japan Aerospace Exploration Agency (JAXA) was selected for the application. Remote Sensing Technology Center of Japan (RESTEC) has started to provide the PALSAR Global Mosaic (PGM) product which covers global range in the ground range pixel spacing of 10 m or 25 m, along with the process of ortho-rectification and slope correction (selective) from the beginning of 2013. Since the topographic effects that causes distortions to the observed SAR data is critical, both 10 and 25 m pixel spacing data of the study area for the comparison with the slope corrected option was selected. The observation date for the PALSAR image is July to September, 2009, where ranges in month occurs because the product is a mosaic image of the area with multiple scene tiles. The year 2009 data was used because both 10 m and 25 m data was available for that year for comparison. The PALSAR

specification of the study area is at ascending Fine Beam Dual (FBD) polarization, characterized by 34.3 degree of off nadir angle.

2.3.2. Field Observation Data

A forest inventory data provided by the Prefectural Government of Chiba were collected, which was obtained from the field observation implemented by the Chiba Prefectural Government, Agriculture, Forestry and Fisheries Department, Forest Division. Observations were made through 2011 and 2012 academic year at the prefectural owned forests located central to southern regions of the Prefecture (Figure 3). The data compiles with the information of tree type (Sugi or Hinoki), tree age, mean diameter at breast height (DBH), mean tree height, stem volume per unit area, stem density per unit area, mean basal area, and some other parameters which indicates the geological position of where the observations were made in terms of aspect and the position of whereabouts on the mountain (e.g. ridge). Information of the trees are collected within a plot area (0.01 ha) with the shape being similar to the satellite image pixel, which is normally square, and the coordinates of the plot is recorded only at the center of the plots. Total observation plot size results up to 1939 plots; 838 for year 2011 (Central: 588 Southern: 250) and 1101 for 2012 (Central: 672 Southern: 429). Central and southern plot data on 2011 and the plot data at the central of 2012 will be used for the statistical analysis between satellite data and the field observation data.

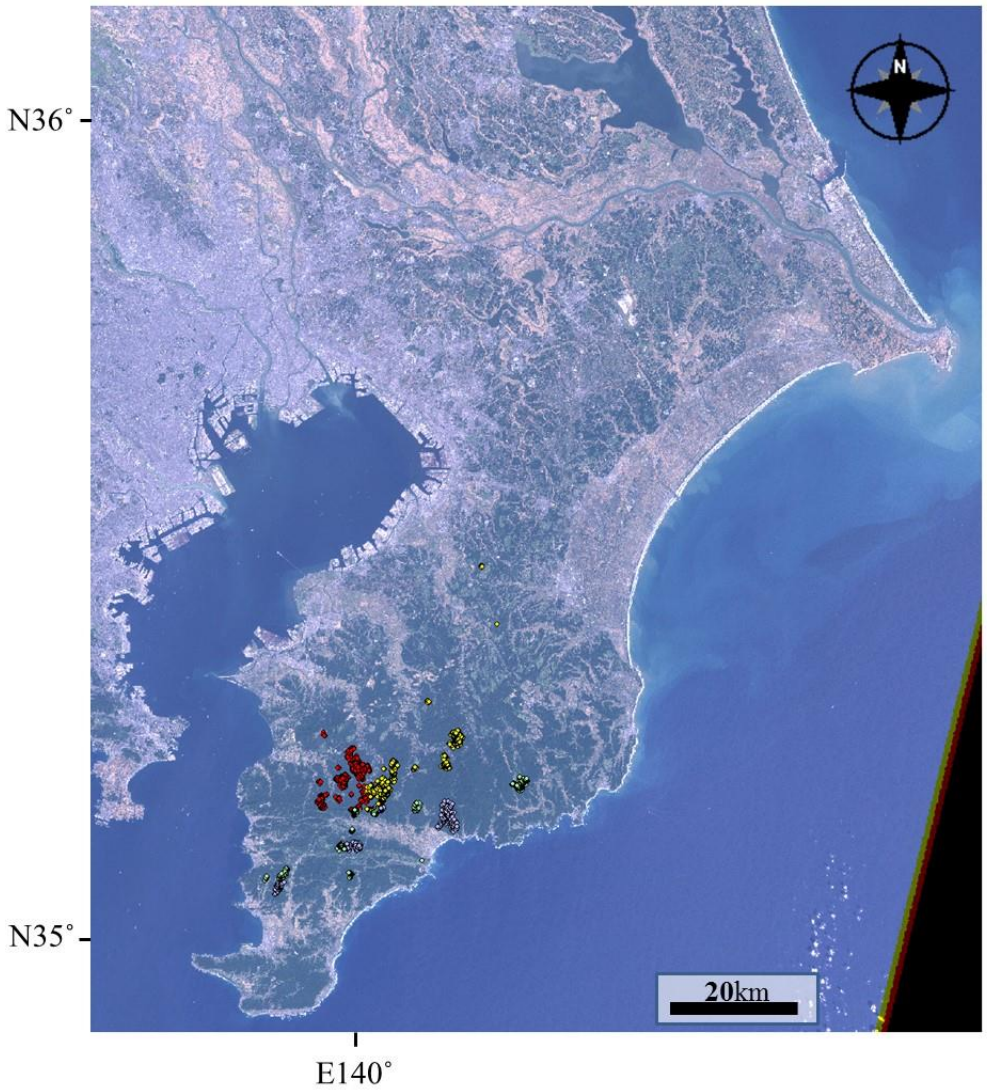

Figure 3. Location of the observation plots for 2011: Central (Red), Southern (Blue) and 2012: Central (Yellow), Southern (Green).

2.3.3. Vegetation Continuous Fields (VCF)

Vegetation Continuous Fields (VCF) data developed by the university of Maryland (DiMiceli et al., 2011) is utilized to quantitatively interpret the forest percent cover. By using this information better understanding of how the scattering behavior changes through the differences among the forested area differentiating it by each forest percentage cover could be known. The data is available online from the Global Land Cover Facility Website. The original resolution for the product is 250 m, while the data was resampled using bilinear method so it could match with the satellite image.

2.4. Analysis Methods

2.4.1. Image Preprocessing for PALSAR

The PALSAR image used in this study was converted from the provided format which is in the Digital Number (DN) values, to the backscattering intensity information also known as backscattering coefficients or the Normalized Radar Cross Section expressed using Equation (1):

$$\sigma^0 = 10 \times \log_{10}(\mathrm{DN}^2) + \mathrm{CF} \quad (1)$$

Where σ^0 is the backscattering intensity represented in decibel units (dB) and CF is the calibration factor for the data obtained, depending on the observation period and polarization (JAXA, 2010). The image is already in the process of ortho-rectification and slope correction, so further analysis is taken directly using this data without any additional correction. The difference of the obtained image of the area for non-slope corrected and slope corrected is shown on Figure 4 for the visual interpretation.

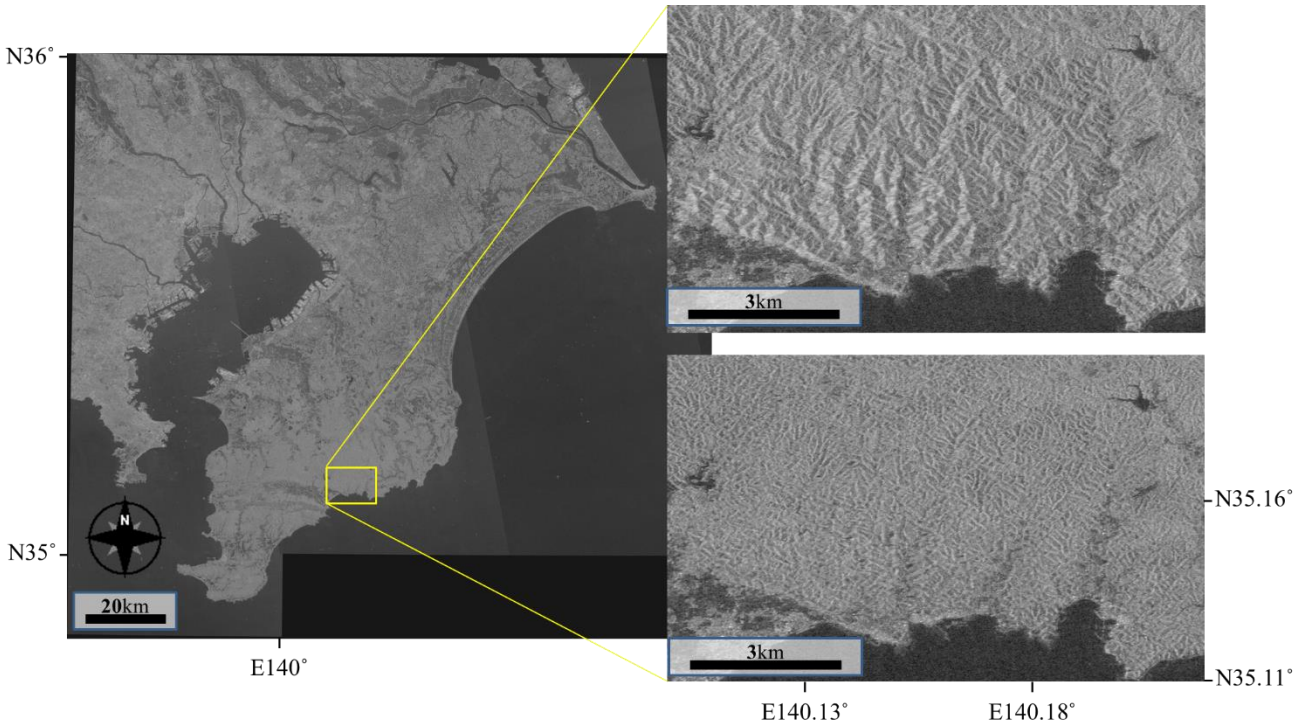

Figure 4. 25 m PALSAR Global Mosaic product (HV) of the study area, the left image shows the overall of the area and on the right shows the zoomed area with no slope correction (top) and slope corrected (bottom).

2.4.2. Statistical Analysis between Field Observation Data and Satellite Data

A statistical analysis for formulating relationships among the field observation data of the forest stand characteristics and the remotely sensed microwave satellite data was carried out. The process will be taken by analyzing the relationships between SAR backscattering intensity (σ^0) and the stand characteristics (DBH, tree height, and stem volume) for both 10 m and 25 m pixel spacing PALSAR image to compare the differences of the results from higher and lower pixel spacing. The procedure for the relationship analysis was taken through multiple approaches:

(A) Combine all the observation plots and make the analysis,

(B) Divide the plots into per forest percentage cover,

(C) Divide the plots to different stem volume range (lower range or higher range),

(D) Divide the plots into separate species (Sugi and Hinoki).

This method was attempted because the scattering mechanisms of the SAR backscatter in the vegetated areas are very complex; usually it is difficult to see any trends when relationships analysis are made with the stands in various range of the structure when combined (Brolly & Woodhouse, 2012). So the approach was to break down the whole to a smaller category to see how the backscattering will respond to those structures, The confidence of the image pixel was considered using the mask data attached together with the PGM product. Plots that do not match the needs were omitted from the analysis by using the mask data.

2.5. Results

2.5.1. Statistical Analysis of Backscattering vs. Forest Stand Biophysical Parameter (Methods A,B,C)

Statistical relationship between backscattering intensity (σ^0) and each forest stand characteristics (DBH, Tree height, Stem volume) is investigated by using least-square method on the basis of the field observation plot. For reference, a regression line is drawn using second order polynomial. First, all of the plot information was used for the relationship analysis (Figure 5).

(a)

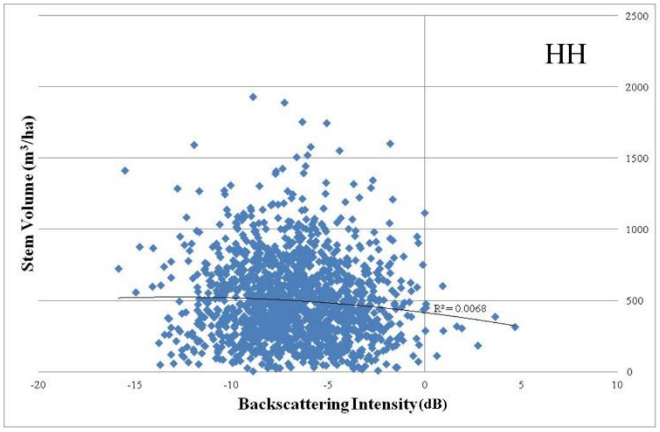

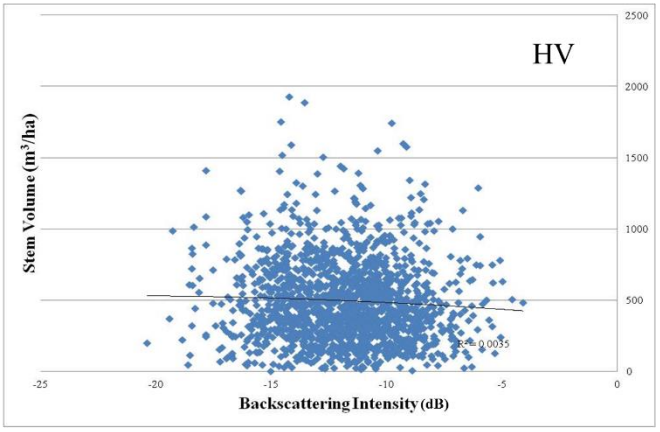

(b)

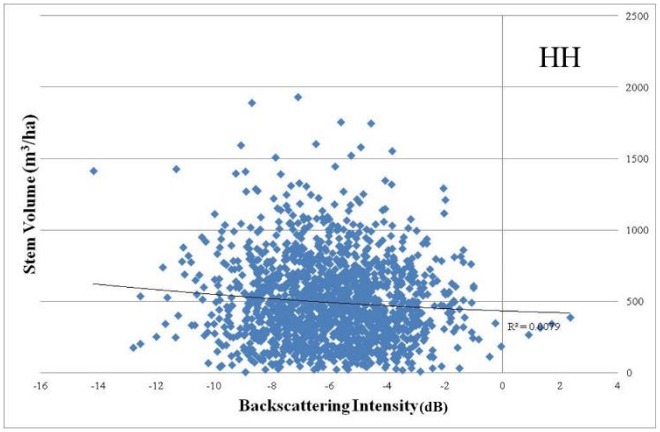

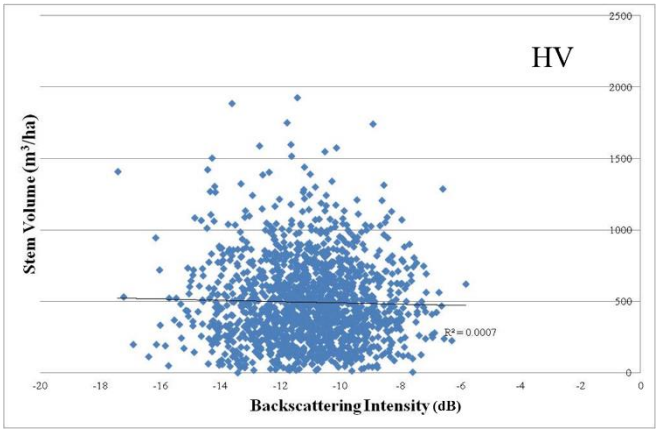

Figure 5. Relationship between backscattering and stem volume using all observation plots for the (a) 10 m and (b) 25 m pixel spacing data for both HH and HV polarizations.

It is obvious that no relationship can be seen between the two. Usually, when empirical approach is taken, it doesn't show much relation because of the complexity in the scattering at the forested areas (Brolly & Woodhouse, 2012). The trend shows the same for the other parameters also (DBH and tree height). Ulaby et al. (1990) identified the scattering components that comes from the tree canopy, and showed that 11 different kinds of scattering was occurring; Fernandez-Ordonez et al. (2009) shows 9 kinds of the scattering as a visual figure which consists of:

1: diffuse scattering from the ground (no vegetation),

2 and 3: direct scattering from various vegetation components,

4: double-bounce vegetation–ground interaction,

5: corner reflector between tree trunks and ground,

6: direct backscatter from the forest canopy,

7: volume scattering from within the forest canopy,

8: diffuse scattering from the ground (with vegetation)

9: shadowing by parts of the forest canopy of other parts of the canopy or the ground.

When relationship analysis is made with a forested area that is varied with different growth stages and at different density of the trees and different structure of the trees, it is very difficult to see a trend because of all of those different scatterings, which likely results as on Figure 5. Therefore the second and third approach was taken for the analysis, which is to make the relationship analysis using the plot data filtering it by the forest cover percentage using the VCF data and at different volume range.

Iizuka and Tateishi (2013) showed the relation between the mean backscattering intensity as a function of forest cover percentage at the forests of Chiba Prefecture using 50 m PALSAR mosaic product, and mentioned about the decrease in the backscattering after when the forest cover percentage exceeds over 80-85 % which might be occurring by the attenuation from the canopies. Similar method was performed to see the effect with this study and found that attenuation was occurring from the earliest, at 70 % forest cover percentage for the coniferous trees (Figure 6). So to avoid the uncertainties in the scattering, those areas were omitted that could lead in errors to obtain correct interpretation of the backscattering information which should then directly respond from the stand characteristics.

Figure 7a to Figure 7c shows the relationship between the backscattering and the stand characteristics for DBH, tree height and stem volume respectively for the 10 m and 25 m pixel spacing data on both HH and HV polarizations, on the area where the forest cover percentage is below 65 % coverage and at lower volume ranges (0-500 m^3/ha).

(a)

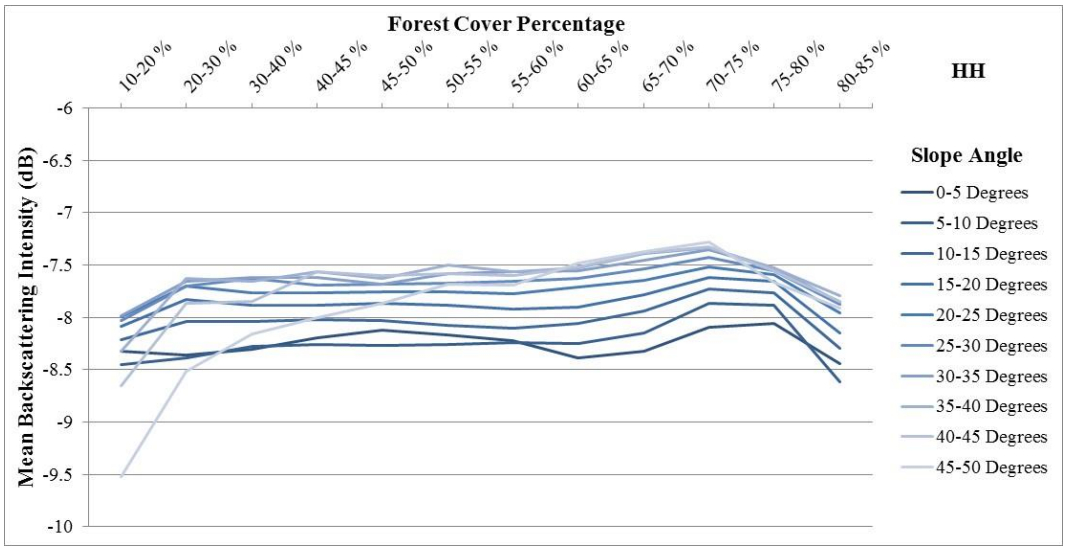

(b)

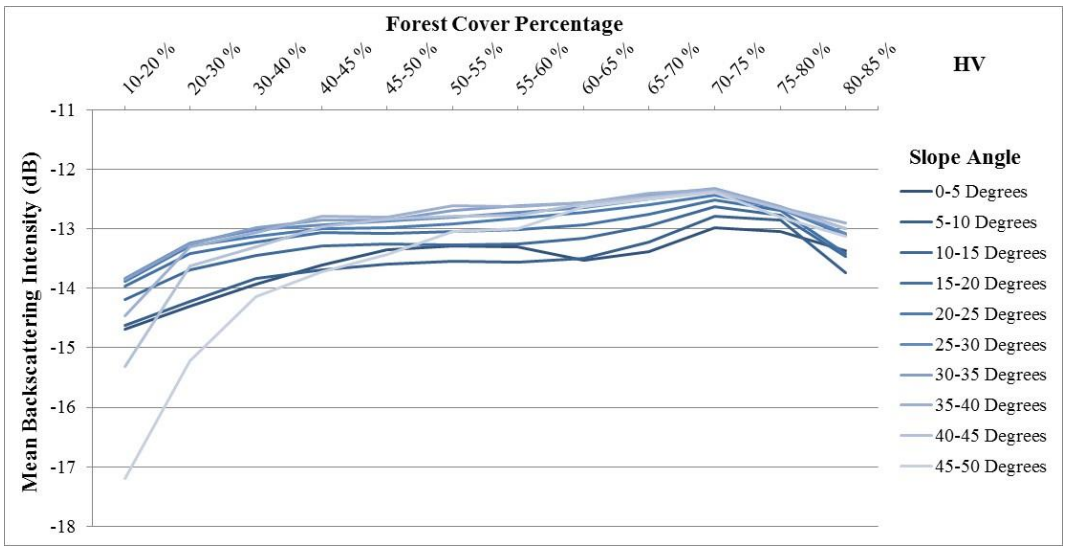

Figure 6. Mean backscattering response of 25 m PGM product from per slope angle as a function of forest cover percentage for (a) HH and (b) HV polarizations at foresloped areas (areas facing towards the sensor direction) from the forests of the study region.

(a)

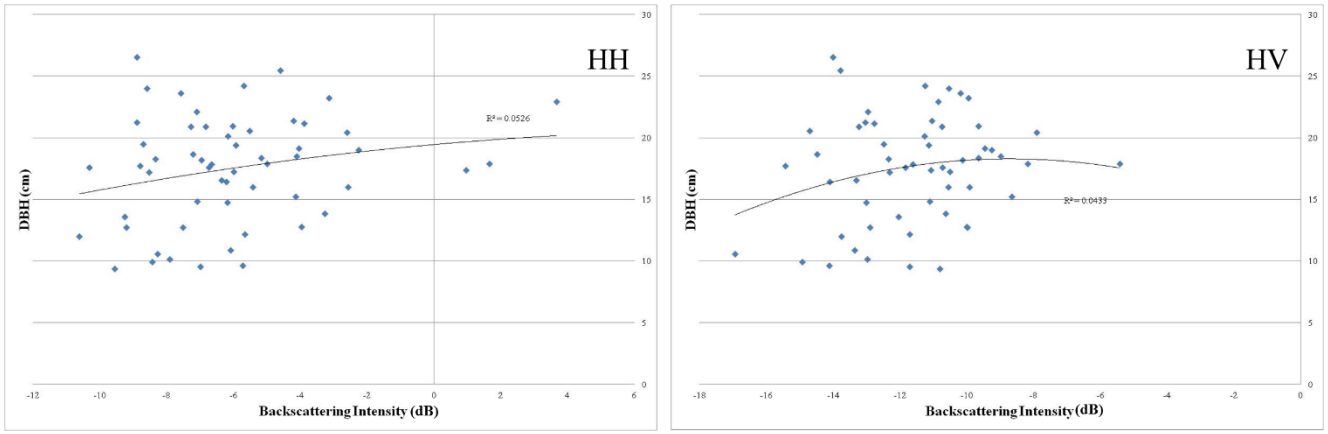

(b)

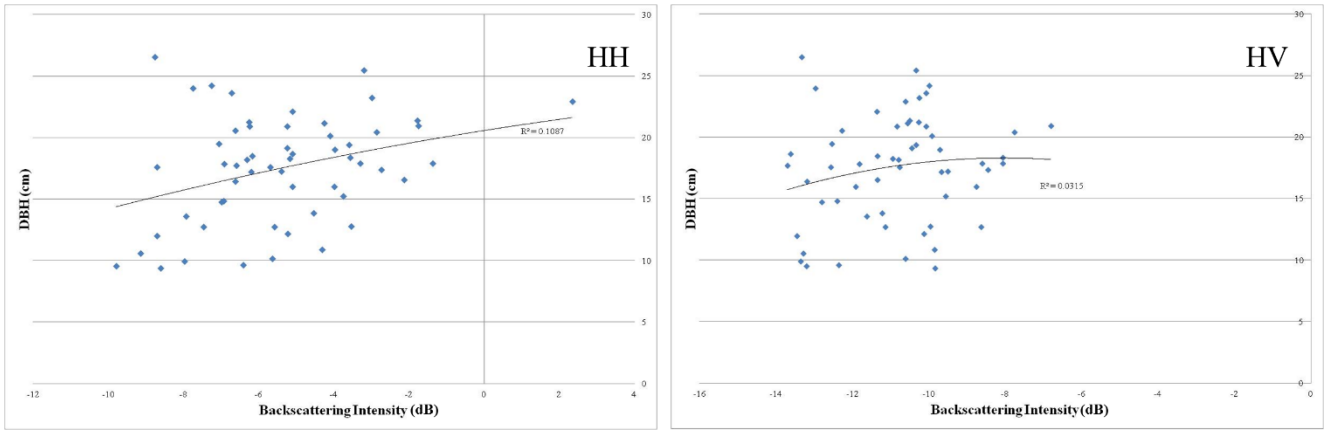

Figure 7a. Relationship between DBH (cm) and backscattering for (a) 10 m and (b) 25 m pixel spacing ((a) HH: R^2 = 0.053, HV: R^2 = 0.043; (b) HH: R^2 = 0.109, HV: R^2 = 0.032).

(a)

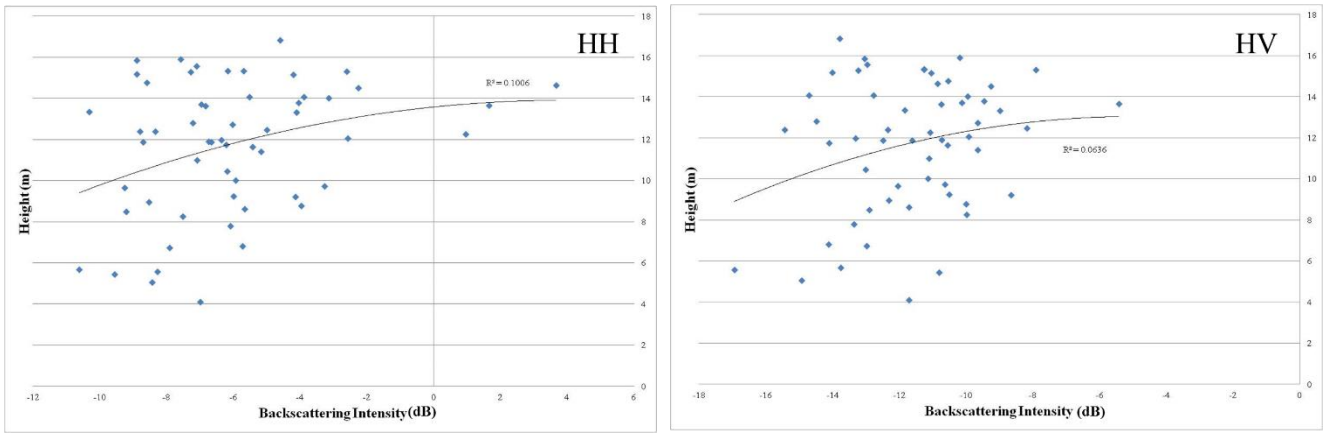

(b)

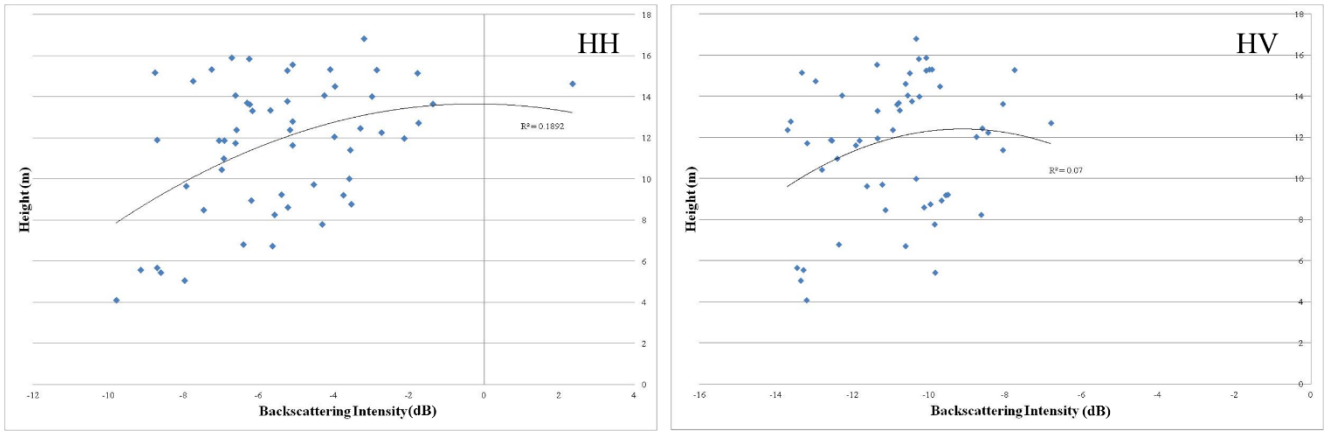

Figure 7b. Relationship between Tree height (m) and backscattering for (a) 10 m and (b) 25 m pixel spacing ((a) HH: R^2 = 0.101, HV: R^2 = 0.064; (b) HH: R^2 = 0.189, HV: R^2 = 0.07).

(a)

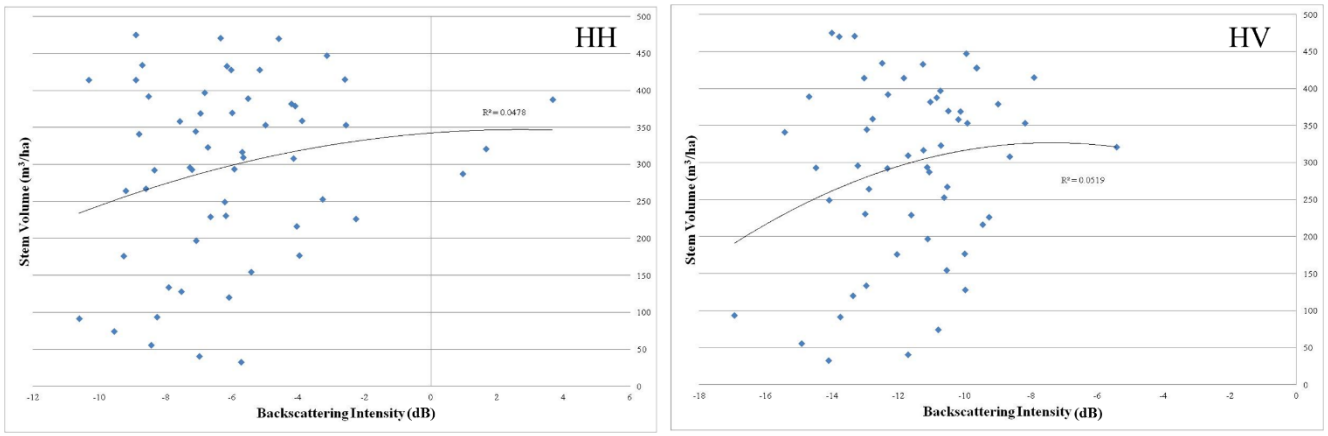

(b)

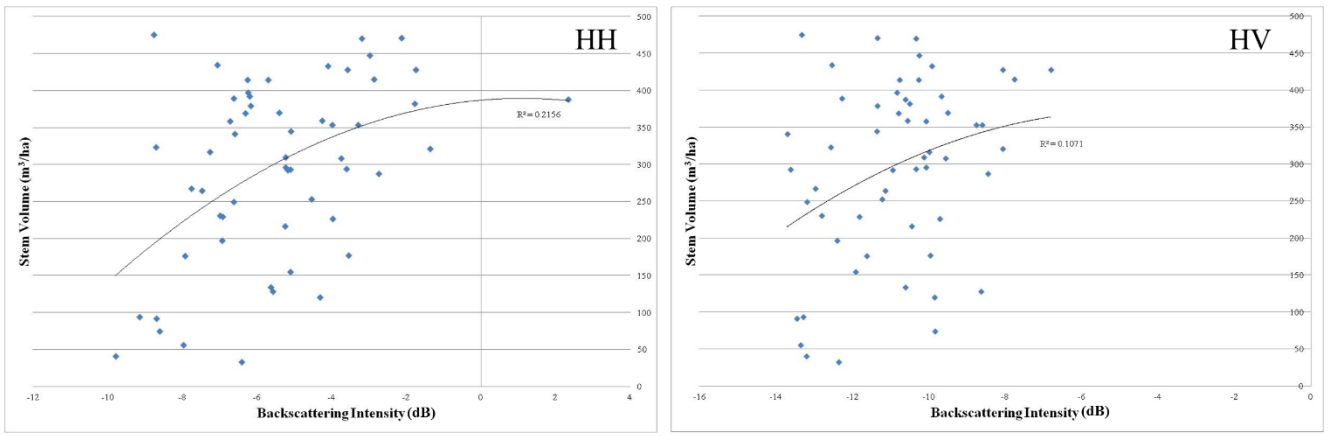

Figure 7c. Relationship between Stem volume (m^3/ha) and backscattering for (a) 10 m and (b) 25 m pixel spacing ((a) HH: R^2 = 0.048, HV: R^2 = 0.052; (b) HH: R^2 = 0.216, HV: R^2 = 0.107).

For DBH, 25 m pixel spacing HH polarization showed the highest correlation (R^2 = 0.109) among the others, which is similar for Tree height (HH: R^2 = 0.189), but for Tree height, also the 10 m pixel spacing data showed some correlation too (HH: R^2 = 0.1) although it is a very low trend. Of them all, stem volume shows the highest correlation with the backscattering, and in this case the HH polarization showed better correlation than the HV (HH: R^2 = 0.216, HV: R^2 = 0.107) at 25 m pixel spacing data. In the overall trend, it can be confirmed that comparing with the 10 m and 25 m pixel spacing data, the 25 m data shows higher correlation for all the biophysical parameters. This occurs from the smoothing of the local backscattering area generated at the low pixel spacing images. The differences to the local scattering would average out when the pixel spacing becomes lower; as a result, errors reduce and better correlations would be seen. Some studies also confirm the increase of the accuracy and higher correlation when the pixel spacing reduces (Santoro et al., 2011; Cartus et al., 2012).

2.5.2. Statistical Analysis of Backscattering vs. Forest Stand Biophysical Parameter (Method D)

Correlation between the backscatter and stand biophysical parameter showed better result in the 25 m pixel spacing PGM. So the third approach of the analysis will be based on the 25 m pixel spacing PGM (Figure 8a to Figure 8c). The figures show the relation between the backscatter for the same as figure 7a to figure 7c, but the plots were separated into differences of the species: Sugi (*Cryptomeria japonica*) and Hinoki (*Chamaecyparis obtusa*) trees. The relationship was analyzed for these species individually for each polarization.

(a)

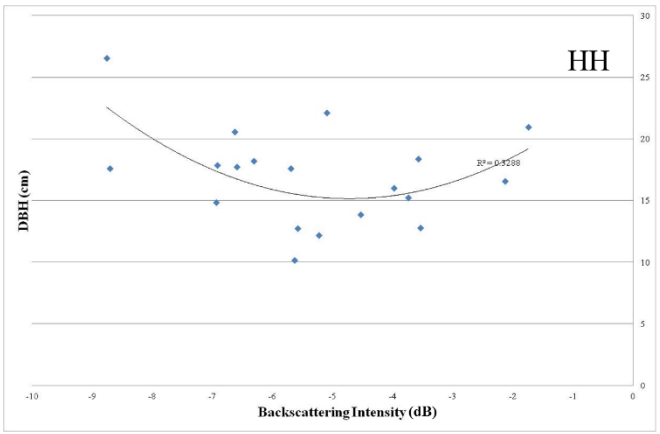

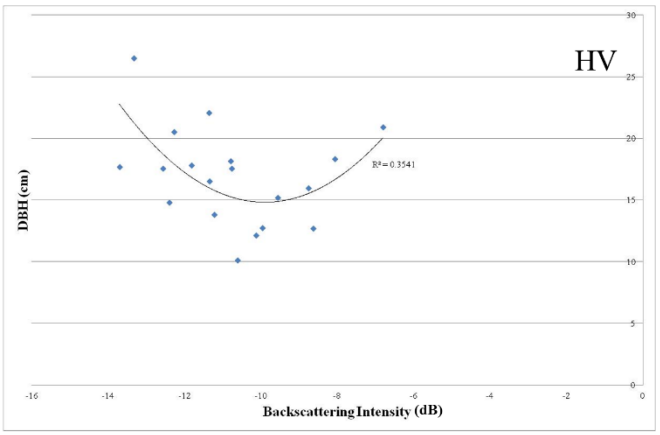

(b)

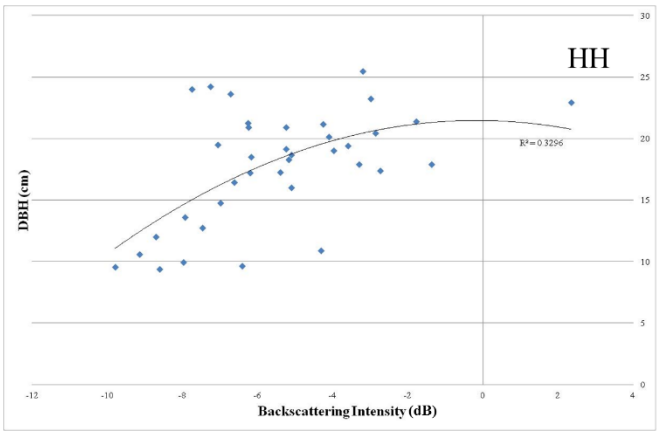

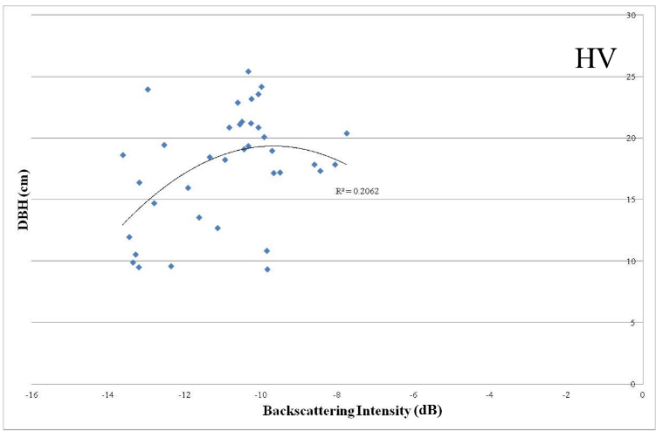

Figure 8a. Relationship between DBH (cm) and backscattering for (a) Sugi and (b) Hinoki tree at 25 m pixel spacing ((a) HH: R^2 = 0.329, HV: R^2 = 0.354; (b) HH: R^2 = 0.33, HV: R^2 = 0.206).

(a)

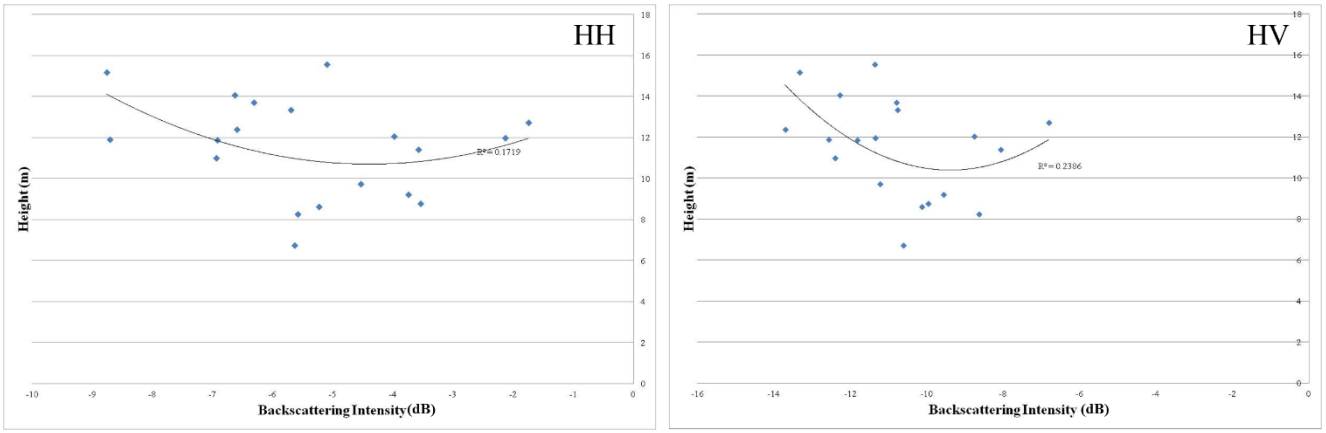

(b)

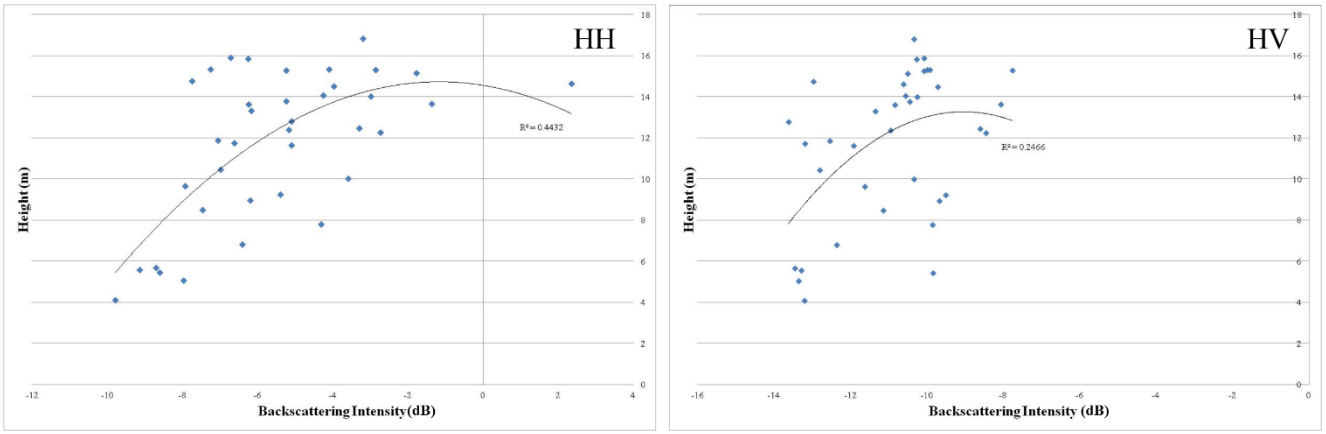

Figure 8b. Relationship between Tree height (m) and backscattering for (a) Sugi and (b) Hinoki tree at 25 m pixel spacing ((a) HH: R^2 = 0.172, HV: R^2 = 0.239; (b) HH: R^2 = 0.443, HV: R^2 = 0.247).

(a)

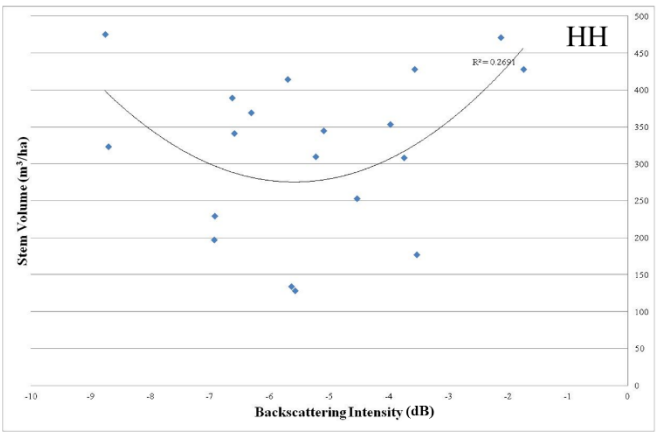

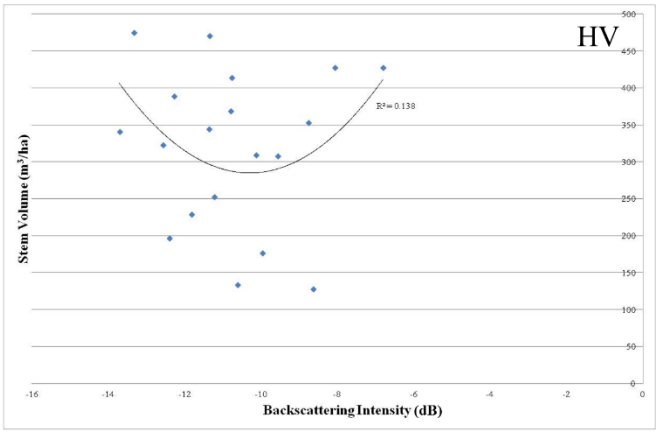

(b)

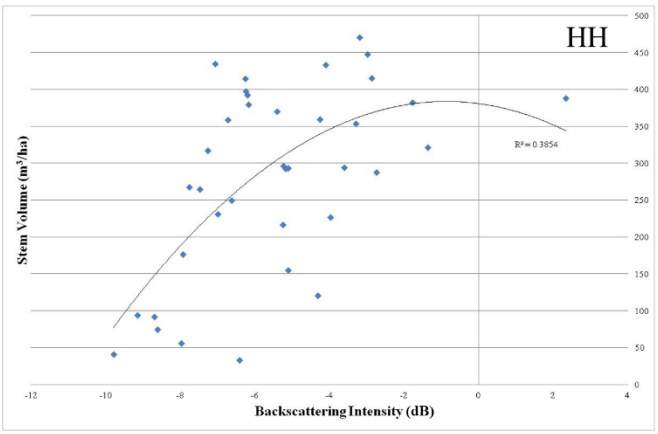

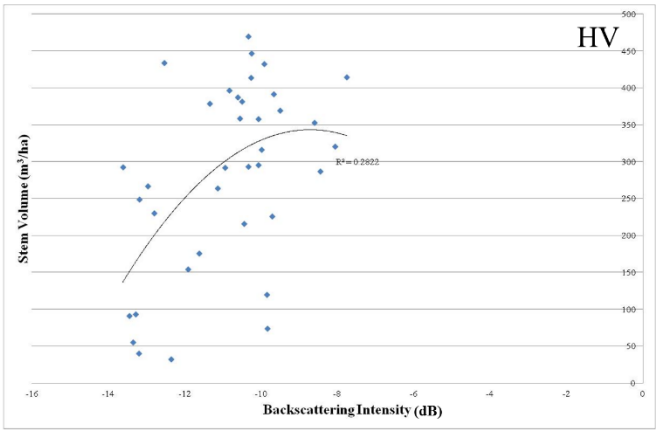

Figure 8c. Relationship between Stem volume (m^3/ha) and backscattering for (a) Sugi and (b) Hinoki tree at 25 m pixel spacing ((a) HH: R^2 = 0.269, HV: R^2 = 0.14; (b) HH: R^2 = 0.385, HV: R^2 = 0.282).

Compared to the analysis made using both species combined, better correlation can be seen for both species and the characteristics of those are conspicuous. For the Hinoki trees, increase in backscatter shows clearly with the increase in biophysical parameters, showing highest correlation for the tree height for HH (R^2 = 0.443) and stem volume for HV (R^2 = 0.282) however, for stem volume HH shows higher correlation (R^2 = 0.385) than the HV. While for the Sugi trees, stand biophysical parameter decreases with increasing backscatter but at the highest backscattering point, the parameters increase. This phenomenon for the Sugi trees shows only at the lower volume case, and at the higher stem volume range (over 550 m^3/ha), the relation of the biophysical parameter and the backscattering becomes obvious; backscattering decreases with increasing biophysical parameters (Figure 9). Unfortunately, the Hinoki trees mostly are in the range up to 500 m^3/ha and could not find relevant number of samples over 550 m^3/ha so the figure for the Hinoki trees to see the characteristics on that range is excluded. At the higher volume range, the tree height at HV polarization showed the highest correlation with the backscattering (R^2 = 0.214), and at this stage of the stands, HV polarization started to show better correlation than the HH, however for stem volume, still HH showed higher correlation. When looking at the other parameters, for the HH polarization it can still be seen that correlation shows the highest for the stem volume (R^2 = 0.113), and for the HV, tree height and DBH showed some correlation (DBH: R^2 = 0.177, Height: R^2 = 0.214) but the stem volume showed low correlation (R^2 = 0.095) compared to the other parameter and by HH polarization. Unless the site is covered with the early stage Sugi plantation, majority of the areas of the Sugi forests would have a chance to be in the higher volume range, so the actual trend between the parameter and backscatter might be seen as like on figure 9.

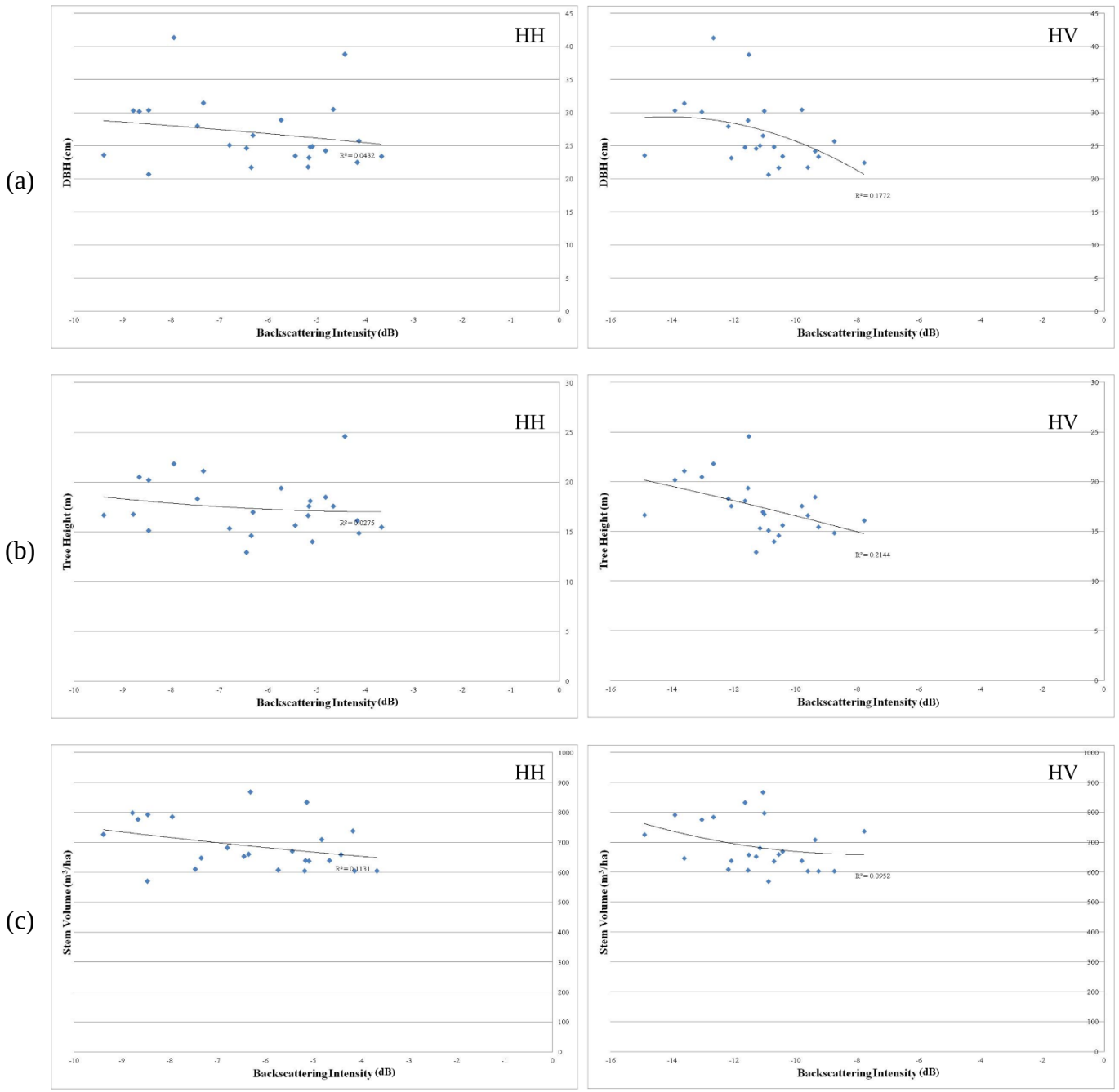

Figure 9. Relationship between (a) DBH (b) Tree height and (c) Stem volume against backscattering for both HH and HV polarization of Sugi tree at 25 m pixel spacing at higher volume range (over 550 m^3/ha). Coefficient of Determination are (a) HH: R^2 = 0.043, HV: R^2 = 0.177; (b) HH: R^2 = 0.028, HV: R^2 = 0.214; (c) HH: R^2 = 0.113, HV: R^2 = 0.095.

2.6. Discussion

2.6.1. Sugi Characteristics to Backscattering

Statistical relationship between the Sugi stand characteristics and the backscattering showed an astonishing result, showing that backscattering was decreasing with an increasing of the biophysical parameters. However, there were some questioning results for the Sugi trees at the lower volume range plots, where an increase in the parameter showed at the end of the increasing backscatter. To understand why this was happening closer analysis on those plots was carried out. From Figure 8 we have focused on the stem volume information and extracted 4 points from the figure to see what was causing the difference in the backscattering from those points (Figure 10). The points were chosen because of similar stem volume per unit area but with a totally opposite backscattering value. Table 1 shows the specifications of the Sugi tree characteristics at those plots, and from the table what can clearly be indicated is that the difference in the stem density (number of trees) of the plot area, where higher stem density has higher backscattering information.

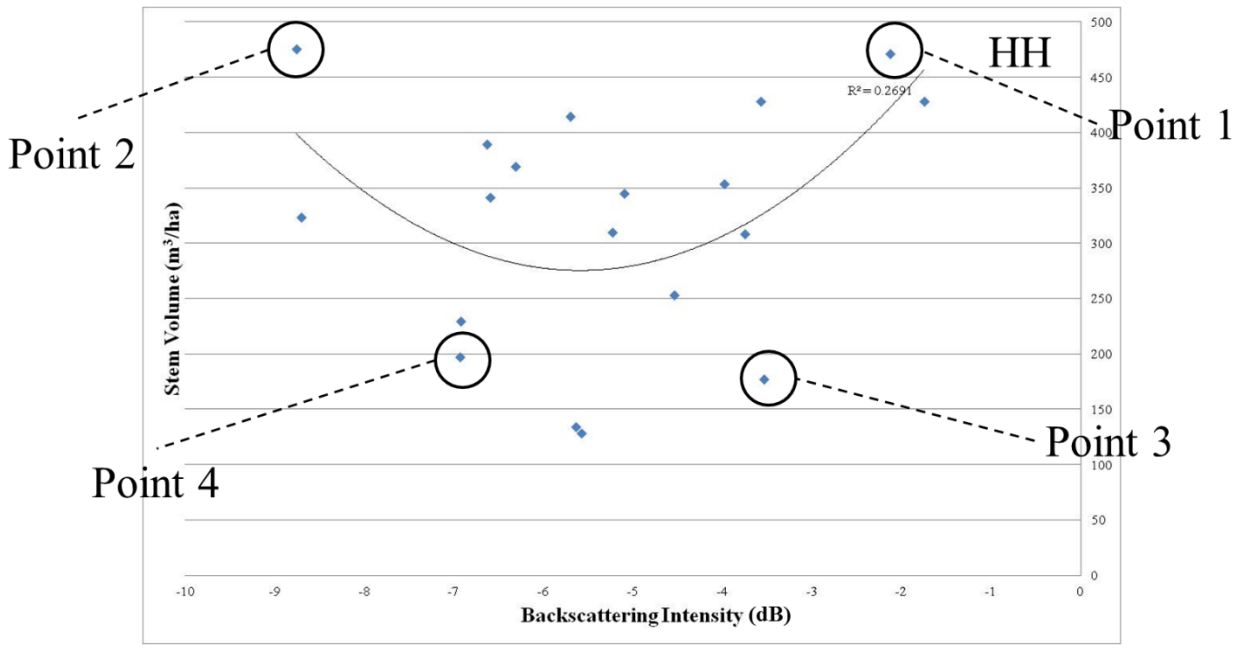

Figure 10. Extracted points where the stem volume per unit area lies on the similar value but with opposite backscattering value.

Table 1. Specification of the observation points extracted from Figure 9.

	dB	**Mean DBH** (cm)	**Mean Height** (m)	**Density** (*N*/ha)	**Volume** (m^3/ha)	**Age**
Point 1	-2.13	16.56	11.96	2,500	471	20
Point 2	-8.76	26.545	15.18	1,100	475	57
Point 3	-3.54	12.76	8.76	2,900	177	22
Point 4	-6.94	14.84	11	1,900	197	18

When the term stem volume per unit area is stated, we can describe this in various ways from the differences in the thinning process of the forests (Brolly & Woodhouse, 2012). For example, small sized stems with high numbers of stems could turn up to become large stem volume per unit area, while even the same volume per unit area could turn out to be from one large stem but with small number of stems. To be sure with this idea, a relationship between the stem density and the backscattering information was taken. As a result, Figure 11 shows that backscattering has positive correlation with the stem density for the Sugi trees, but for the Hinoki trees, no correlation could be seen for HV polarization but a decreasing stem density trend with increasing backscattering is shown in HH. From this result it may determine that there is something to the Sugi trees that can be different from the Hinoki trees, even they are in the same coniferous tree category.

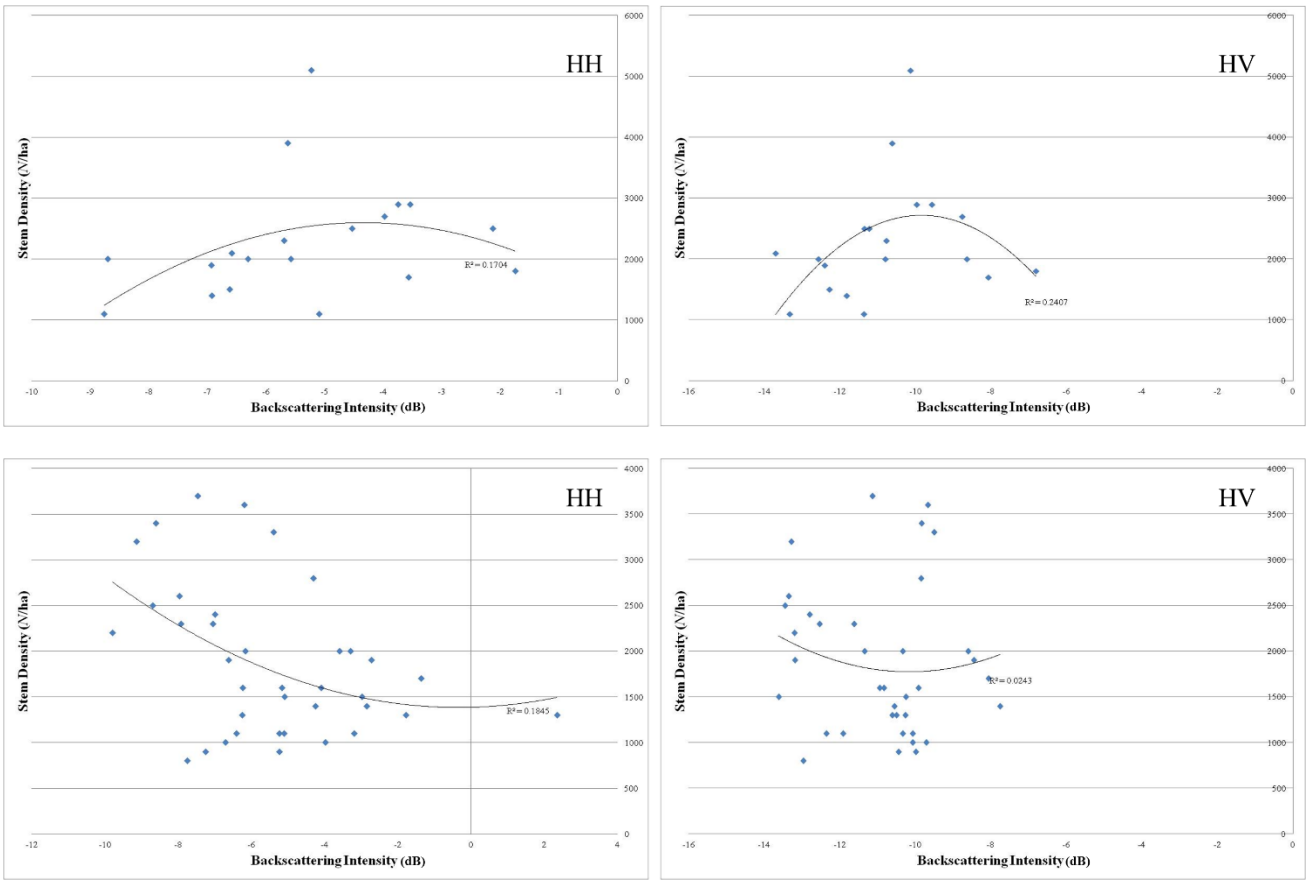

Figure 11. Relationship between Stem Density (*N*/ha) and backscattering for (a) Sugi and (b) Hinoki trees for both HH and HV polarization at 25 m pixel spacing ((a) HH: $R^2 = 0.17$, HV: $R^2 = 0.241$; (b) HH: $R^2 = 0.185$, HV: $R^2 = 0.024$).

One reason for this phenomenon could be considered from the differences in the moisture content in the stem of the Sugi and Hinoki trees. Minato et al. (1989) reports that in the 53 year age Sugi and Hinoki trees, the moisture content of those trees in the heartwood averages 132 % and 36 % respectively. Umebayashi et al. (2011) reports similar moisture content in the heartwood of Hinoki trees (28 %) at a younger aged trees (below 10 years), same by the work from Tsushima et al. (2006) showing again similar moisture content for the trees around the age of 20 to 32 of the Hinoki trees (31-39 %). Kawazumi et al. (1991) reports the similar high moisture content in the younger age of Sugi trees (20 years: 53-157 %). Uyemura (1960) studied the dielectric constant of different tree types as a function of moisture content in the stem, and showed the dielectric constant of about 4 to 5 for the Sugi and Hinoki tree when the moisture content is 25 %, while when the stem has contained saturated moisture content (180 %) the dielectric constant increased to 70. So maybe, here what can be said is that large number of stems with high dielectric constant is causing such increase in the backscattering even when the stem volume per unit area is showing similar value. But at the higher volume range (over 550 m^3/ha), the biophysical parameters were showing an decrease with increasing backscatter which is not like how we often understand as it is for the Hinoki tree case. This is not confirmed yet, however if the larger tree height and larger DBH trees contained with high moisture, affects the radar signal to attenuate, then it might be the reason here that backscattering was decreasing when the biophysical parameters increased, on the other hand trees with not enough size and volume for attenuation, leads to increasing radar signal scattering back to the sensor due to the large number of stems with high dielectric constant. This needs to be considered strongly in the future works for the validation.

2.6.2. Hinoki Characteristics to Backscattering

The Hinoki relationship with the backscattering is very similar to what is performed by other researchers with their relationships with the forests. Where, the backscattering increases with the increasing biophysical parameters. Compared to the Sugi trees, stem density was not much influencing the trend, and on HH polarization it can be seen that stem density was decreasing with increasing backscattering. When time passes and the trees grow, DBH and tree height increases and eventually the number of stems will reduce due to the thinning process. As an overall trend for both Sugi and Hinoki, this is likely to be the case. However, for the Sugi case backscattering decreased with decreasing stem density, but for the Hinoki trees, even when the number of stems reduced, the backscattering increased. For the Hinoki case, this trend could be answered that how it is described by Kobayashi et al. (2012b) that canopy scattering and double-bounce scattering increases with increasing tree height and DBH, resulting higher total backscattering. It can be assumed for the Hinoki trees that this mechanism implies even when the number of stems reduces.

2.6.3. Complexity of backscattering at forested areas

As mentioned in the former section, backscattering is occurring from various mechanisms within the forested area. For example Ulaby et al. (1990) Identified 11 different components that are affecting the total backscatter and this backscatter would differ due to the different environment in terms of species, structures, soil moisture and so forth. Moreover, it would also depend on the density of the forests, where there are attenuations, saturations, and maybe other more that is still unclear. In the case of this study in Chiba, Japan, most of the forested areas are generated over the hilly rugged terrains, even though various radiometric corrections are developed for the normalization (Ulander, 1996; Castel et al., 2001; Shimada et al. 2010; Small, 2011), there are still lot of issues we need to overcome, such as the radiometric accuracy of those correction methods.

In this study, the relationship between the biophysical parameters and backscattering was performed in very limited conditions, such as areas that are less than 65 % forest cover considering the attenuation from the dense forests. It is said that P-band SAR can sense more to the parameters than the L-band because it has longer wavelength. This is probably true if we look at the studies that use P-band radar for the relationship analysis, indicating higher saturation points than the L-band data (Le Toan et al., 1992; Imhoff, 1995; Sandberg et al., 2011). But for the case such as this study, it could be said that it can be applied at more dense forests to extract more precise information of the forests structure, and not only the saturation point for detecting higher AGBs. We need to note that backscattering does not measure direct AGB, but it gets affected to the structure of the forests relating to its growth that forms to the resulting AGB, so it is better to understand the scattering mechanism from the forest stand characteristics to make better prediction and extraction of the forest biophysical parameter or the AGB for the forests of each region in interest.

2.7. Summary

In this chapter, performance of a statistical analysis in relation of the backscattering intensity from the L-band PALSAR and the in-situ stand characteristics of Sugi (*Cryptomeria japonica*) and Hinoki (*Chamaecyparis obtusa*) trees was carried out. The relation showed acceptable result for the Hinoki trees, where backscatter increased with increasing biophysical parameters (DBH, tree height, stem volume). However, for the Sugi trees, the trend showed completely opposite where the backscattering decreased with increasing biophysical parameters. It was surprising that totally opposite trends showed for the same coniferous trees. This difference is assumed that it is coming from the characteristics of the Sugi tree, where it contains of high moisture content resulting with high dielectric constant to affect the backscattering with the increasing stem density, and attenuations caused from increasing DBH and tree height. However, there are still needs of validation for this hypothesis and it is necessary to verify on

more relationship analysis for different species other than the Sugi and Hinoki trees because it might have different trend in the scattering, this is considered to be one of the future works.

3. Stem Volume Map Development using SAR

3.1. Introduction

In the former chapter, analyzing the backscattering trend with the stand characteristics from the forests of Chiba Prefecture, Japan was performed. To carry on for the estimation of CO_2 sequestration, obtaining stem volume information for all the forested areas in Japan is necessary to collect the precise forests extent. The objective on this chapter is to develop a stem volume map from the forests of Japan considering the relationship analysis taken from the previous chapter.

3.2. Data Sets

3.2.1. PALSAR 50 m Ortho-Rectified Mosaic Product

The Advanced Land Observing Satellite (ALOS) Phased Array L-band Synthetic Aperture Radar (PALSAR) provided by Japan Aerospace Exploration Agency (JAXA) was downloaded from their webpage and used for the analytical objectives. The data is a product created from the ascending path for dry and wet seasons or summer and winter seasons globally, with a ground range pixel spacing resampled to 50 m resolution from the original. Specification of the PALSAR is in ascending Fine Beam Dual (FBD) polarization, OffNadirAngle of 34.3 degrees. Digital Number (DN) values of the data from 2007 and 2009 was averaged, and for the further analysis this data with the mean value was used for the procedure to avoid small changes of backscattering caused by local environmental factors on that particular observation time (e.g. precipitation). Just to note that for the stem volume map, the 50 m product is used, however for the development of the backscattering model, the 25 m PGM product was utilized.

3.2.2. Digital Elevation Model (DEM)

A digital model of terrains surface is obtained. 10 m resolution DEM published by the Geospatial Information Authority of Japan were downloaded from the web page and mosaicked to cover the study area. The DEM information was resampled to 50 m resolution

using bilinear method to match with the PALSAR product and was used to generate slope and aspect information and further for the topographic correction of the PALSAR imagery because the product is performed only with ortho-rectification however radiometric corrections for slopes were not applied.

3.3. Analysis Methods

3.3.1. Stem Volume – Backscattering Model

Backscattering vs. stem volume relationship was obtained using the methods described in chapter 2. 25 m PALSAR PGM product were utilized, however in this case we have averaged the value from the data of 2009 and 2010. We used the same filtering for the observed plots and made an analysis for the correlation of the model. Figure 12 shows the result of the relation for both HH and HV polarizations.

Figure 12. Relationship between Stem Volume (m^3/ha) and backscattering for HH (top) and HV (bottom) polarization at mean 25 m pixel spacing data from 2009 and 2010 (HH: $R^2 = 0.2123$, HV: $R^2 = 0.2198$).

Because that discriminating the differences of the Sugi and Hinoki trees individually on the categorical map is difficult, the relationship analysis was carried out using both two species together. According to this result, second polynomial function from the HV polarization was selected and applied since it had higher correlation compared to HH (HH: $R^2 = 0.146$, HV: $R^2 = 0.22$). The equation of the function is described as:

$$V = 1.4192\sigma_{HV}^{0^2} + 60.472\sigma_{HV}^{0} + 773.8 \quad (2)$$

Where V is the stem volume and σ^0_{HV} is the backscattering intensity from the HV polarization. The relationship analysis to achieve this model was done by using the field observation data provided by the Chiba Prefectural Government and the 25 m PGM product (mean data of 2009 and 2010). The model was then applied to the 50 m ortho-rectified PALSAR product so that it would cover the whole forest area of Japan. Central and southern plot data on 2011 and the central plot data of the year 2012 was used for the statistical analysis, while the southern plot data on 2012 was used for the validation of the model.

One another backscattering model was applied developed by Wijaya (2009). The model by the author is described as:

$$V = 256.85 - (65.458\sigma^0) - (6.8{\sigma^0}^2) \quad (3)$$

The former model developed in this study is used for the coniferous forested areas, while it is strongly dependent to those forests and we believe it is inappropriate to apply the model for the broadleaf forests because the architecture is different compared to the coniferous forests. So for the deciduous and evergreen broadleaf forested areas, the stem volume information obtained by the function of Wijaya (2009) is considered.

3.3.2. Radiometric Correction of PALSAR

Performing radiometric correction (slope correction) to the SAR imagery is important in terms of correcting the enhancements of the backscattering response affected by the inclination of the earth's surface. As Iizuka and Tateishi (2012) states, the mean backscattering difference from

each sloped areas would lead to high backscattering response at higher sloped areas compared to lower sloped areas at foreslopes (slopes facing the sensor direction) because of the difference in the local incidence angle making more radar signal to return back to the sensor (Richards, 2009).

So for this problem, a correction method stated by Zhou et al. (2011) was applied. The correction of the SAR imagery is done by applying the slope correction factor to the original SAR data. The equation of the correction follows:

$$\sigma_c^0 = SCF^q \times \sigma^0 \quad (4)$$

Where σ^0_c is the corrected sigma nought backscattering value, σ^0 is the original sigma nought backscattering data, q is the diffuse scattering which is polarization dependent and *SCF* is the slope correction factor for the correction of the topography expressed as:

$$SCF = \frac{\cos i}{\sqrt{1 + \left(\frac{\tan a \times \sin a \times \sin 2\beta}{2}\right)^2}} \quad (5)$$

Where cos *i* is the cosine of the incidence angle, *a* is the slope and *β* is the aspect. The HV polarization image of PALSAR was corrected using this method. The value for the diffuse scattering depends on the environment, and was unknown for this case due to the large area of the study region with different structure of the forests, so here it has been assumed q = 1.

3.4. Results

3.4.1. Evaluation of Radiometric Correction of PALSAR

Figure 13 shows the trend of the backscattering value as a function of the cosine of the incidence (cos *i*). As it shows, where higher local incidence angle gives lower backscattering value, while the backscattering becomes higher when the local incidence angle become lower. Quantitative evaluation of the performance of the correction is done by assessing the non-correlationship between cos *i* and the corrected data, shown on Figure 13. Compared to Figure

13 **(a)**, the trend of the backscatter becomes flat making less correlation between these two (Figure 13 **(b)**). Figure 14 shows the visual interpretation of the PALSAR 50 m product before (Figure 14 **(a)**) and after (Figure 14 **(b)**) the correction. From this result, it was presumed that the correction of the PALSAR was successfully performed.

(a)

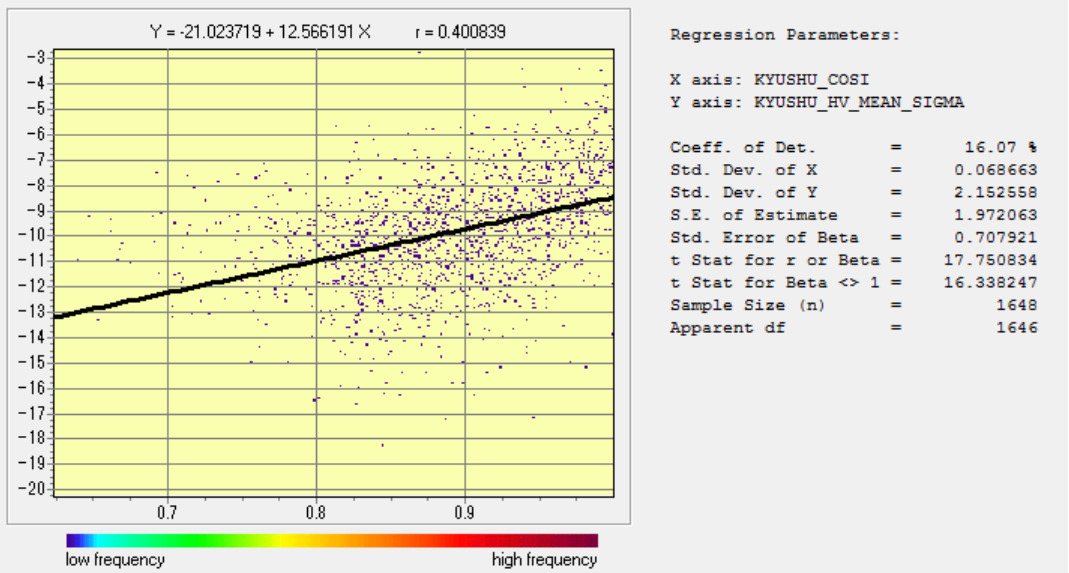

(b)

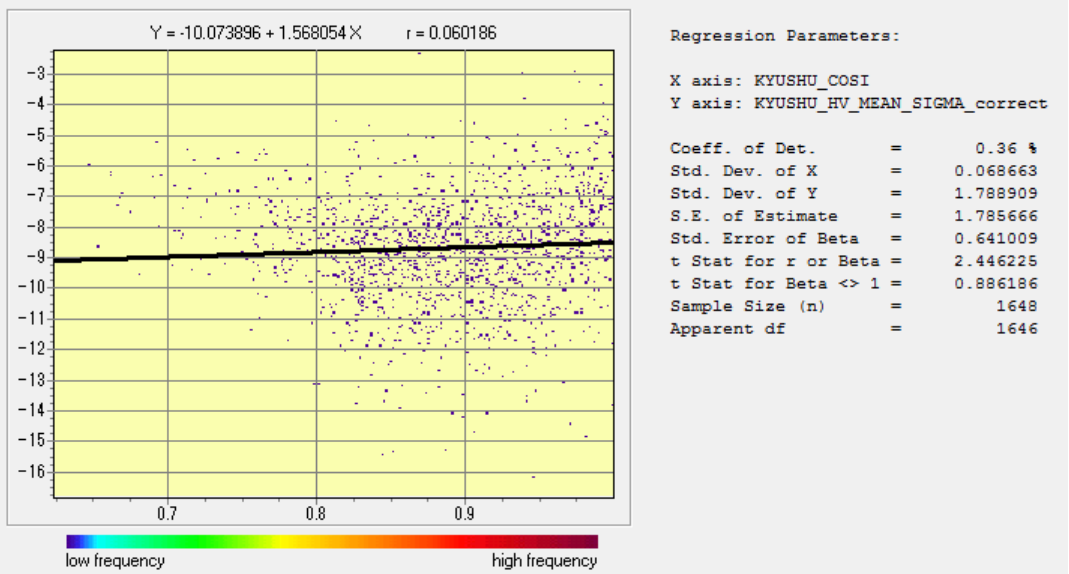

Figure 13. Regression analysis between cos *i* on x-axis, and the backscattering values (dB) on y-axis for the HV polarization: **(a)** non-corrected and **(b)** corrected data.

(a)

(b)

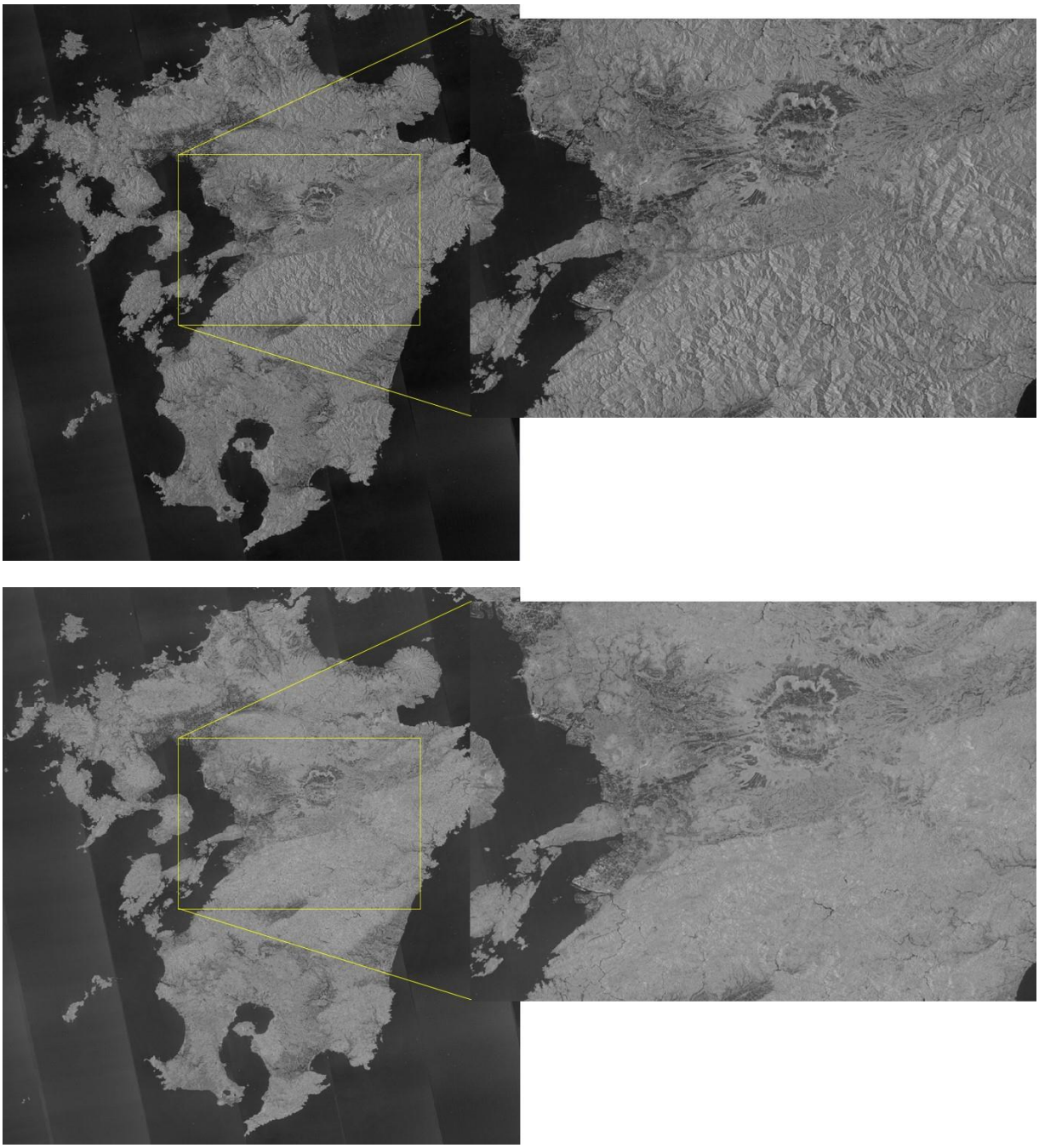

Figure 14. Visual interpretation of the PALSAR 50 m product at the Kyushu Island region, for the **(a)** original image and the **(b)** corrected image of the HV polarization.

3.4.2. Stem Volume Map and Validation

From the formula which was obtained in the above procedure, it was applied to the whole forest area of the study area (using the formula from the HV polarization result). By doing this, the spatial distribution of the estimated stand volume for the forests of Japan was obtained. However this model is specified to the coniferous stands and it should take into account that there are possibility of the backscattering characteristics to different forest types would give a different result due to the structure of the stand and leaf size. So for the broadleaf forests, instead a polynomial model developed by Wijaya (2009) from the evergreen trees of Indonesia was applied to fit the needs. Figure 15 shows the stem volume map of Japan for the coniferous forests (Figure 15 **(a)**) and for deciduous and evergreen broadleaf forests (Figure 15 **(b)**).

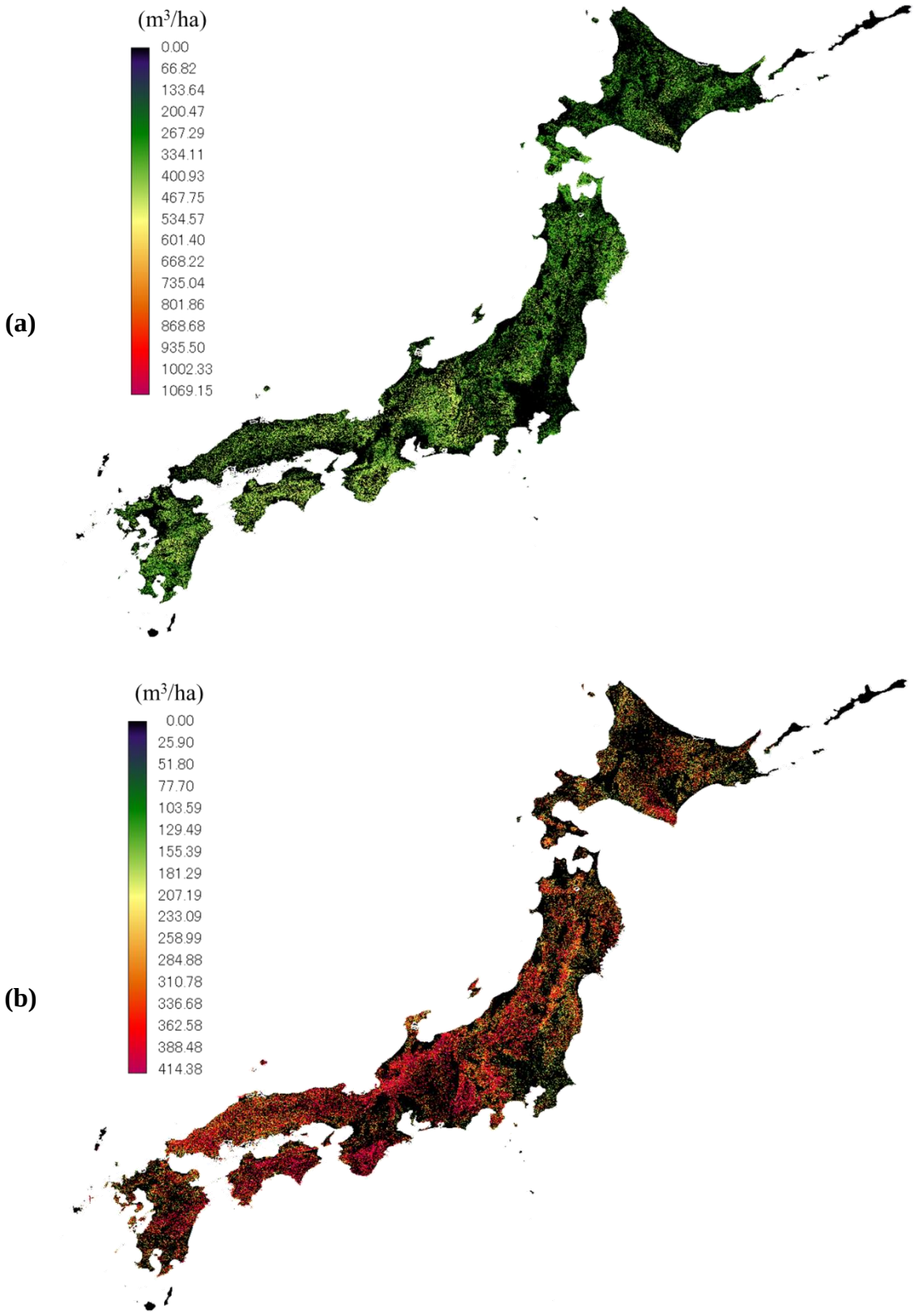

Figure 15. Stem volume map of Japan for the **(a)** coniferous forests and **(b)** deciduous and evergreen broadleaf forests. Forest cover data was overlayed with the stem volume map to extract the only forest types needed for each stem volume maps.

The maximum stand volume of the coniferous reaches up to 1000 m^3/ha using the model develop from the result of this study, and for the broadleaf forests, it reaches up to 414 m^3/ha. Although the coniferous stand volume gives a high maximum value, most of the distributed areas lies near 400-500 m^3/ha range, and it is rare to exceed over 700 m^3/ha. Using the detail forest cover map; which will be mentioned in the next chapter, the precise area of the coniferous and the broadleaf forests are extracted from the stem volume map which were made. As a result, now the data of the stem volume map for the different forest types for the whole Japan is so obtained. This information will be used in the final chapter of the work for estimating the CO_2 sequestration for the each forest types.

Validation of the backscattering model which was used for the coniferous forests was done by using the observation plot data from the southern 2012 explained on chapter 2. The plot data was used as ground truth information and the root mean square error (RMSE) between the estimated result and the reference data was calculated. The RMSE resulted 105.58 m^3/ha shown on figure 16.

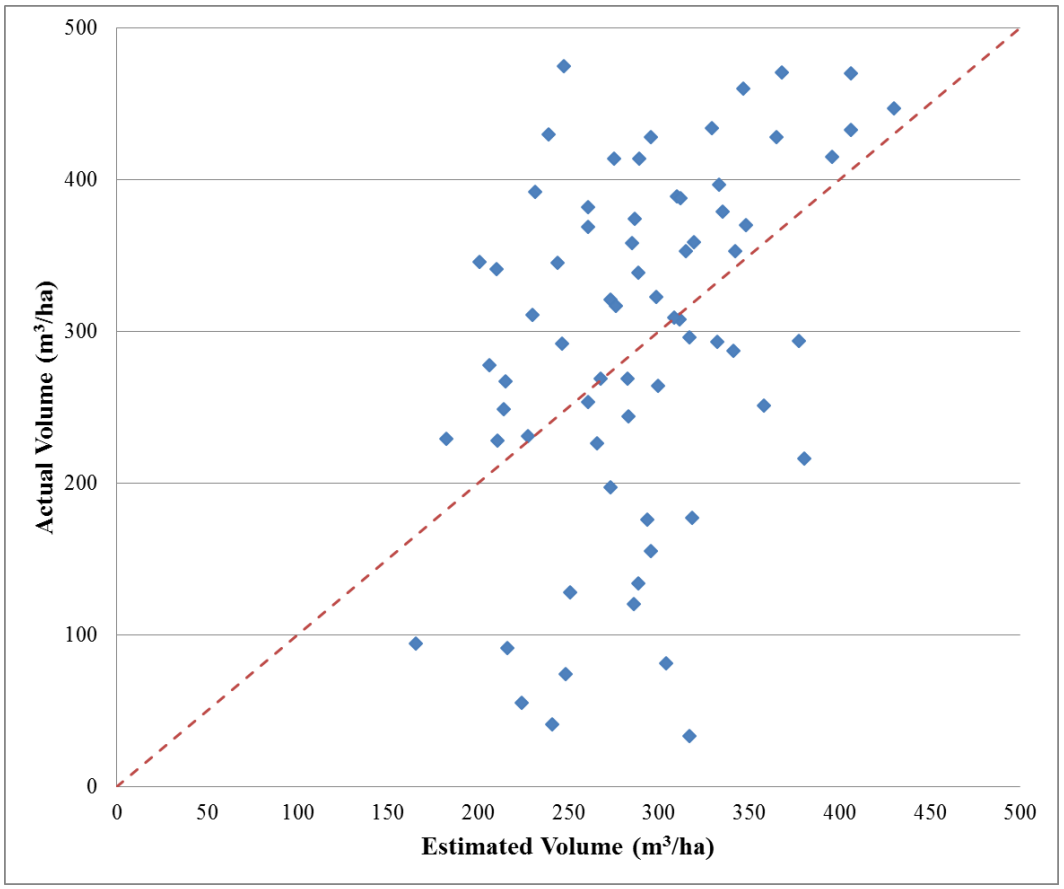

Figure 16. Validation of the backscattering model. X-axis is the estimated volume (m^3/ha) using the model, and Y-axis is the reference data from the observation plot. RMSE = 105.58 m^3/ha.

3.5. Summary

In this chapter mapping the estimated stem volume information spatially for the forests in whole Japan was performed. A backscattering model developed from the relationship analysis was used with the PALSAR 50 m ortho-rectified product, along with additional slope correction to obtain stem volume for the coniferous forests of Japan. On the other hand a polynomial model developed by Wijaya (2009) was used to extract the stem volume information precisely for the deciduous and evergreen broadleaf forests. Two different models were considered in use due to the difference in the backscattering trend which may differ from the stands architecture, so by using the more preferable model to the correct forest types should lead to better estimation of the stem volume of the forests in Japan. The validation of the backscattering model which was developed from this study resulted RMSE = 105.58 m^3/ha.

4. Detailed Land Cover Mapping of Japan using LANDSAT OLI

4.1. Introduction

Land Cover (LC)/Land Use (LU) information plays a major role in various scientific fields such as for to understand the processes and connections of the environment and the terrestrial systems, or for to consider the use of its information as a part of the decision making process for determining policy development for our living society, change detection, future prediction, and much more. This studies interests lay on regional scale analysis for to see more detail information of the land surface. Developing a detail land cover (forest cover) map of Japan is a critical process for identifying different forests types that lead to differences in the final estimation of CO_2 sequestration.

The objective in this chapter is to develop a detail land cover (forest cover) map of whole Japan. The method seeks its way through focusing on the spectral signature of the land cover types from the constructed training data and how to use those detail information to improve the land cover map.

4.2. Data Sets

4.2.1. LANDSAT 8 (OLI)

Optical Satellite data sets from the Land Remote Sensing Satellite (LANDSAT) Operational Land Imager (OLI) data published by the United States Geological Survey (USGS) were selected for the analytical objectives. 35 LANDSAT OLI scenes were used in total, captured within 2013 to 2014 to cover the whole study area of Japan. The date of the acquired scenes resulted 2 from March, 4 from April, 4 from May, 6 from June, 5 from August, 5 from September and 9 from October. Selections of the images were made by considering the general and most critical issues of the optical imageries: cloud-free. Not all scenes were complete cloud

free; however selections were made from the clearest images that could be found. Specifications of the chosen data are listed on Table 2.

Table 2. Specification of the LANDSAT Imagery used.

	LANDSAT OLI Data Sets				**LANDSAT OLI Data Sets**		
Region	PATH	ROW	DATE	Region	PATH	ROW	DATE
Kyushu Yamaguchi	112	36	2014-05-02	Tohoku	106	33	2014-05-08
	112	37	2013-04-13		107	31	2014-04-29
	112	38	2013-04-13		107	32	2013-10-19
	113	37	2014-04-23		107	33	2013-09-17
	113	38	2013-10-29		108	31	2014-04-20
Chugoku Shikoku Kinki	110	36	2014-03-17		108	32	2013-06-04
	110	37	2014-03-17		108	33	2013-06-04
	111	35	2013-05-24		108	34	2013-06-04
	111	36	2013-05-24	Hokkaido	105	30	2014-06-02
	111	37	2014-05-11		106	29	2014-06-25
	112	35	2013-08-19		106	30	2014-06-25
Chubu	108	35	2013-08-07		106	31	2013-10-28
	108	36	2013-08-07		107	29	2013-10-19
	109	35	2013-08-14		107	30	2013-10-19
	109	36	2013-08-14		108	28	2013-10-10
	109	37	2013-10-17		108	29	2013-10-10
	110	35	2013-05-17		108	30	2013-10-10
Kanto	107	34	2013-09-17				
	107	35	2013-09-17				
	107	36	2013-09-17				
	109	34	2013-08-14				

4.2.2. Ground Truth

In order to verify the contents of the pixel on the satellite images, it is necessary to obtain a reference data to compare what is there in reality. Here, two main sources were adopted to help determine the contents of the surface. One is the National Survey on the Natural Environment (6^{th} and 7^{th} surveys, performed from 1999 until the present), a vegetation map published by the Ministry of Environment of Japan which provides the status of lands, surface waters and coastal areas over the nation (MOE, 2013). It is used as a reference data for when constructing training sites for the classification process. Secondly, Google Earth was used also for as a reference but especially for when collecting ground truth information for the accuracy assessment of the outputted categorical map.

4.2.3. Digital Elevation Model (DEM)

As mentioned on section 3.2.2., again the same data is considered for the use. 10 m resolution DEM published by the Geospatial Information Authority of Japan were downloaded from the web page and mosaicked to cover the study area. The DEM information was resampled to 30 m resolution using bilinear method to match with the LANDSAT OLI and was used to generate slope and aspect information and further for the topographic correction of the LANDSAT imagery.

4.3. Analysis Methods

4.3.1. Radiometric Correction

Performing radiometric correction (atmospheric and topographic) to the remote sensing images is a crucial issue especially when dealing with such analysis that depends strongly on the information of the electromagnetic spectrum of the earth's objects. When the emitted or reflected electromagnetic energy is observed by a satellite sensor, the observed energy does not coincide with the energy emitted or reflected from the same object observed from a short distance. This is due to the solar azimuth and elevation, slope and aspects, atmospheric

conditions such as haze or aerosols, etc. which influence the observed energy. Therefore, in order to obtain the actual irradiance or reflectance, those radiometric distortions must be corrected. For the correction of the images, the Integrated Radiometric Correction (IRC) method developed by Kobayashi and Sanga-Ngoie (2008) was applied. This method is a comprehensive radiometric calibration method aimed at simultaneous correction of atmospheric, solar, and topographic effects inherent to remote sensing data, which makes it possible to retrieve the at-surface reflectance and radiance values as if the atmosphere were totally transparent and the underlying surface was absolutely flat (Kobayashi and Sanga-Ngoie, 2008). The correction method follows with the atmospheric correction using the Dark Object Subtraction method and for the topographic correction, the derivation of solar and land geometric parameters, calculation of topographic correction factor, and atmospheric transmittance functions follows, then after retrieving these parameters the IRC is performed to fully correct the remote sensing imagery. The images were converted from Digital Numbers (DNs) to radiance values before entering the process. Land geometric parameters can be derived from the DEM data. Using those parameters the cosine of the incidence angle (cos *i*) or the solar illumination and the h-factor which expresses the portion of the sky dome diffusing on to the tilted surface, can be given using equation (6) and (7):

$$\cos i = \cos\theta_z \cos e + \sin\theta_z \sin e \cos(\phi_e - \phi_s) \quad (6)$$

$$h = \frac{\pi - e}{\pi} = 1 - \frac{e}{\pi} \quad (7)$$

Where, θ_z is the solar zenith angle, e is the slope angle between the inclined surface and the horizontal plane, Φ_e and Φ_s represents the aspect angle of the inclined surface from the north and the solar azimuth angle from the north respectively. Topographic correction factor (A-factor) is then calculated with equation (8):

$$A = \frac{\cos\theta_z + Ch_0^{-1}}{\cos i + Ch_0^{-1}h} \quad (8)$$

Where, C is the parameter calculated as the quotient between the regressional intercept and slope of the expression between cos i and surface radiance as sensed by the satellite. h_0 is given by:

$$h_0 = \frac{\pi + 2\theta_z}{2\pi} \tag{9}$$

For the atmospheric transmittance functions, the Rayleigh scattering transmittance function (T_r) and water vapor transmittance function (T_w) was calculated. Expression (5) was used for the Rayleigh scattering transmittance ($T_{r\lambda}$) as a function of wavelength (λ), the ambient atmospheric pressure (P) and the sea level atmospheric pressure (P_0) in mbar.

$$T_{r\lambda} = \exp\left(-\frac{P}{P_0} \times M \times \frac{1}{115.6406\lambda^4 - 1.335\lambda^2}\right) \tag{10}$$

Where M is the relative air mass expressed as:

$$M = \frac{1}{\cos\theta_z + 0.15(93.885 - \theta_z)^{-1.253}} \tag{11}$$

For the atmospheric pressure (P) the parameter was not assumed $P \approx P_0$ as the author did since the elevation of the study area varies showing up to 3,776 m at the highest, so instead equation (12) was adapted to calculate the atmospheric pressure for each pixel locations.

$$P = P_0 \exp\left(-\frac{a_i}{a_0}\right) \tag{12}$$

Where, a_i is the altitude at a certain pixel and a_0 is the scale height. It has been assumed that the scale height to be 7,900 m so that the model could match with the standard pressure described as a function of altitude by Holton (1992).

The water vapor transmittance function is a function of water vapor absorption coefficients ($a_{w\lambda}$), relative air mass (M) and precipitable water vapor (W) measured in centimeters. Given as:

$$T_{w\lambda} = \exp\left[-\frac{0.2385\alpha_{w\lambda}WM}{(1+20.07\alpha_{w\lambda}WM)^{0.45}}\right] \quad (13)$$

For the precipitable water vapor, it was not possible to collect the spatial data of the certain area at the same period of time, so it has been determined here *W* to be a constant value.

With all the parameters calculated the expression for IRC yields finally:

$$L_g = (L_s^* - L_h)\frac{A}{0.5(1+T_r)T_rT_w^2} \quad (14)$$

Where, L_g is the corrected radiance from the surface, L_s^* is the at-satellite observed spectral radiance from a sloped terrain and L_h is the upwelling atmospheric spectral radiance. All the optical data from band 2 to 6 were corrected through this process.

4.3.2. Hybrid Classification

The Hybrid Classification method (Richards & Jia, 1999; Sanga-Ngoie & Kobayashi, 2003) is implemented for the classification process. This method uses both the unsupervised classification and supervised classification (Richards & Jia, 1999; Kato, 2004; Eastman, 2006), with the former classification first and on the base of the cluster image, which was produced by the unsupervised classification ISOCLUSTER module, the training site will be created and used in the supervised classification process. In the case of supervised classification, the software system delineates specific land cover types based on statistical characterization data drawn from known examples in the image (known as training sites). This "training sites" will be taken for each information classes (i.e. land cover types) and that information is then used to develop statistical characterization of reflectance/radiances for each information class as simple as the mean or the range of reflectance/radiances on each band, or as complex as detailed analyses of the mean, variances and covariances over all bands (Eastman, 2006). Data form the vegetation map published by the Ministry of Environment together with the Google Earth were used as ground truth references for land features identification. The strength of this method is

that the need of delineating unimodal spectral classes beforehand can be overcome based upon a representative subset of image data (Richards and Jia, 1999).

4.3.3. Maximum Likelihood

In the supervised classification, there are various methods for making decision about which pixel belongs to what classes. Parallelepiped, minimum distance to means, maximum likelihood, decision tree, linear discriminant analysis, etc. all of these methods differ only in the manner in which they develop and use statistical characterization of the training site data. In the analysis, the maximum likelihood method is used since this method estimates the posterior probability that a pixel belongs to each class, in other words, it gives the pixels to the most likely class based on the mean and variance/covariance data of the signatures from the training sites. This method is also the most widely used classifier in the classification of remotely sensed imagery.

The IDRISI Selva MAXLIKE (maximum likelihood) module and the LANDSAT OLI 5 bands (bands 2-6) along with Normalized Difference Vegetation Index (NDVI), Normalized Difference Water Index (NDWI) (Li et al., 2013) and Green Red Vegetation Index (GRVI) (Motohka et al. 2010) were used in order to perform the supervised classification. This yielded an original classified image with 20 to 30 categories in total depending on the scene tiles (regions). These were reclassed later on to give the final product: a classified image with 4 LC/LU categories, designed with a special attention to the forests types found over the analysis area.

The calculations of *NDVI*, *NDWI* and *GRVI* can be performed using the equations (15)-(17) respectively:

$$NDVI = \frac{\mathrm{IR} - \mathrm{R}}{\mathrm{IR} + \mathrm{R}} \tag{15}$$

$$NDWI = \frac{\mathrm{G} - \mathrm{SWIR}}{\mathrm{G} + \mathrm{SWIR}} \tag{16}$$

$$GRVI = \frac{\mathrm{G} - \mathrm{R}}{\mathrm{G} + \mathrm{R}} \quad (17)$$

Where IR, R, G and SWIR represents the infrared, red, Green and short wave infrared band of the satellite imagery respectively. *NDVI* is strongly correlated to vegetation, which can be used as information for discriminating vegetation and non-vegetative areas, and the *NDWI* can enhance open water features while efficiently suppressing and even removing built-up features as well as vegetation and soil features. *GRVI* is similar to *NDVI* however it is sensitive to the phenology change of the forests giving an advantage as a phonological indicator for the difference in the forest types (e.g. deciduous trees).

4.3.4. Accuracy Assessment

After the process of classification for producing land cover maps, accuracy assessment is an obligating process for evaluating the accuracy or the reliability of the map produced (Congalton and Green, 2009). Using Google Earth, points of the land surface were collected for the use as ground truth information. The collected points were then merged together with the vegetation map from the Ministry of Environment to extract the exact matches of the land category for avoiding errors: Miss-location of the points due to errors in the map projection and miss-interpretation of the classes. Final number of points yields 3,550 points, however the number of points were normalized for each class to 1,000 points to make the calculation and interpretation easier in the accuracy assessment. Figure 17 shows the location of the points taken within Japan.

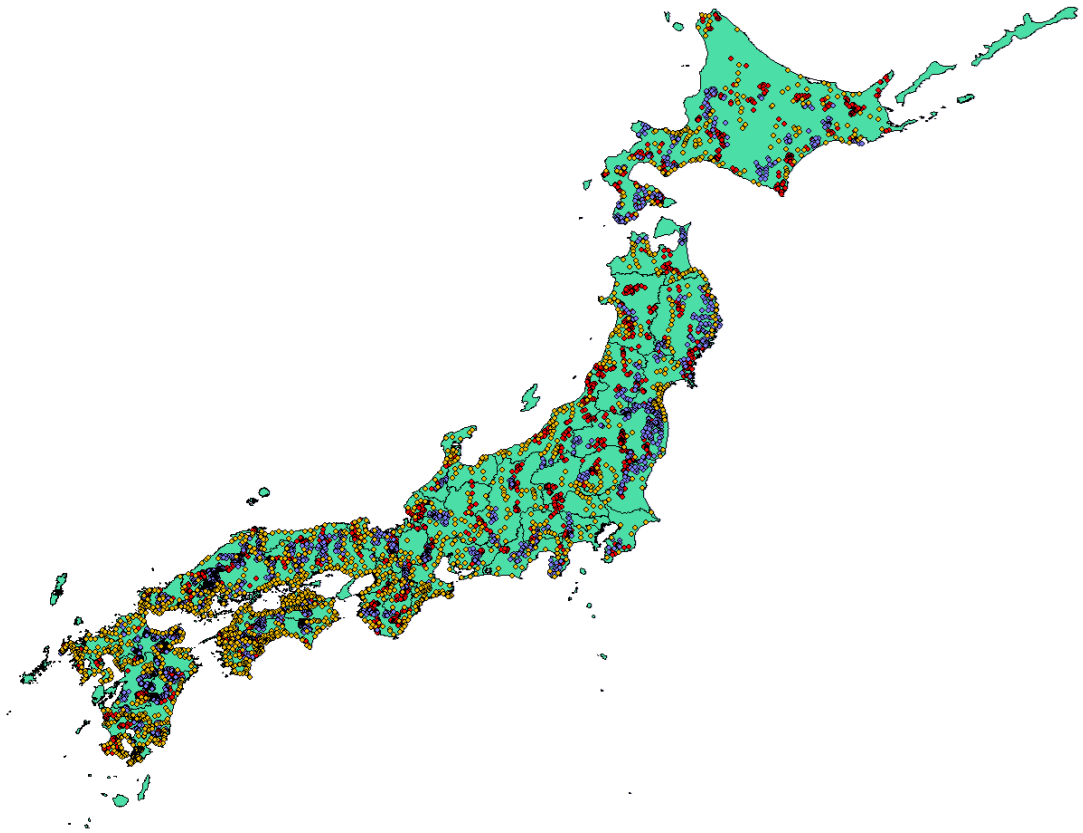

Figure 17. Distribution of the ground truth points taken through using Google Earth.

4.4. Results

4.4.1. Evaluation of Radiometric Correction

Quantitative evaluation of the performance of the correction is done by assessing the non-correlationship between the solar illumination (cos *i*) and the corrected data. In Figure 18, it shows the regression analysis between the solar illumination and non-corrected data on the left, which can be seen with a high correlation, with higher radiance for higher cos *i* value because of topographic effects. However, in the same Figure 18 on the right, the correlation between those two can be seen with lower or mostly non correlation which is the data after the correction. Figure 19 shows the example of the difference of images before the correction and after shown as a true color composite (RGB = band 432). The zoomed area is a mountainous location with forests, surrounded by water bodies and urban areas and it can be seen that the radiance values are corrected in those forests areas where shadows are generated. Compared to the uncorrected image, the dark areas are more enhanced clearly.

(1) **(2)**

(a)

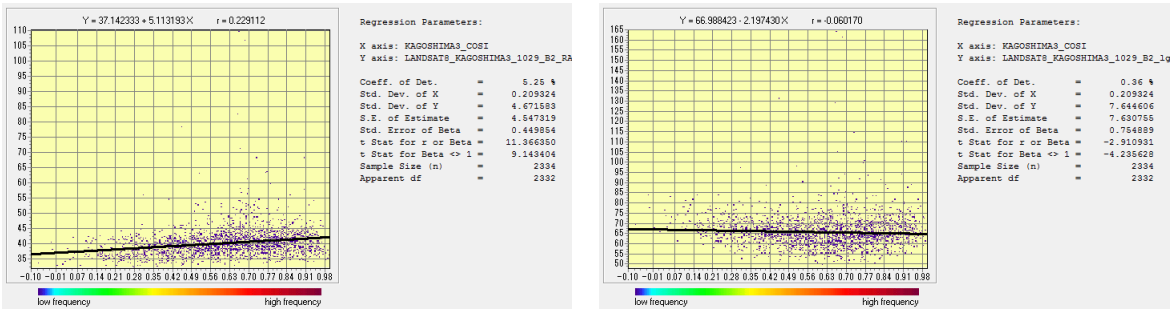

(b)

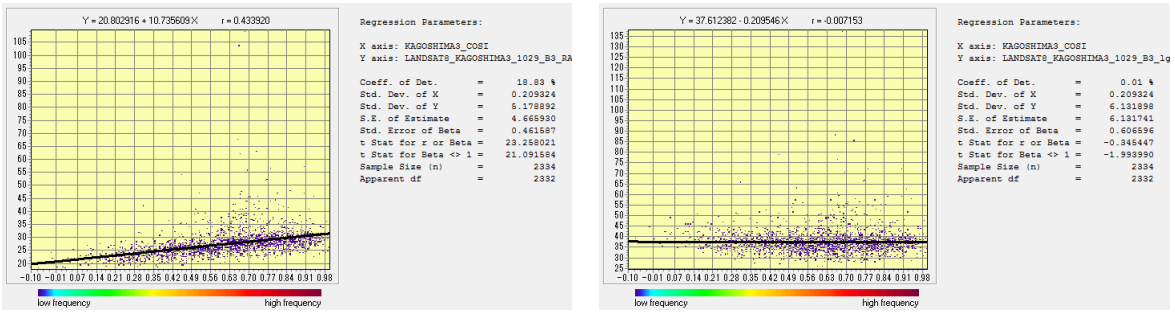

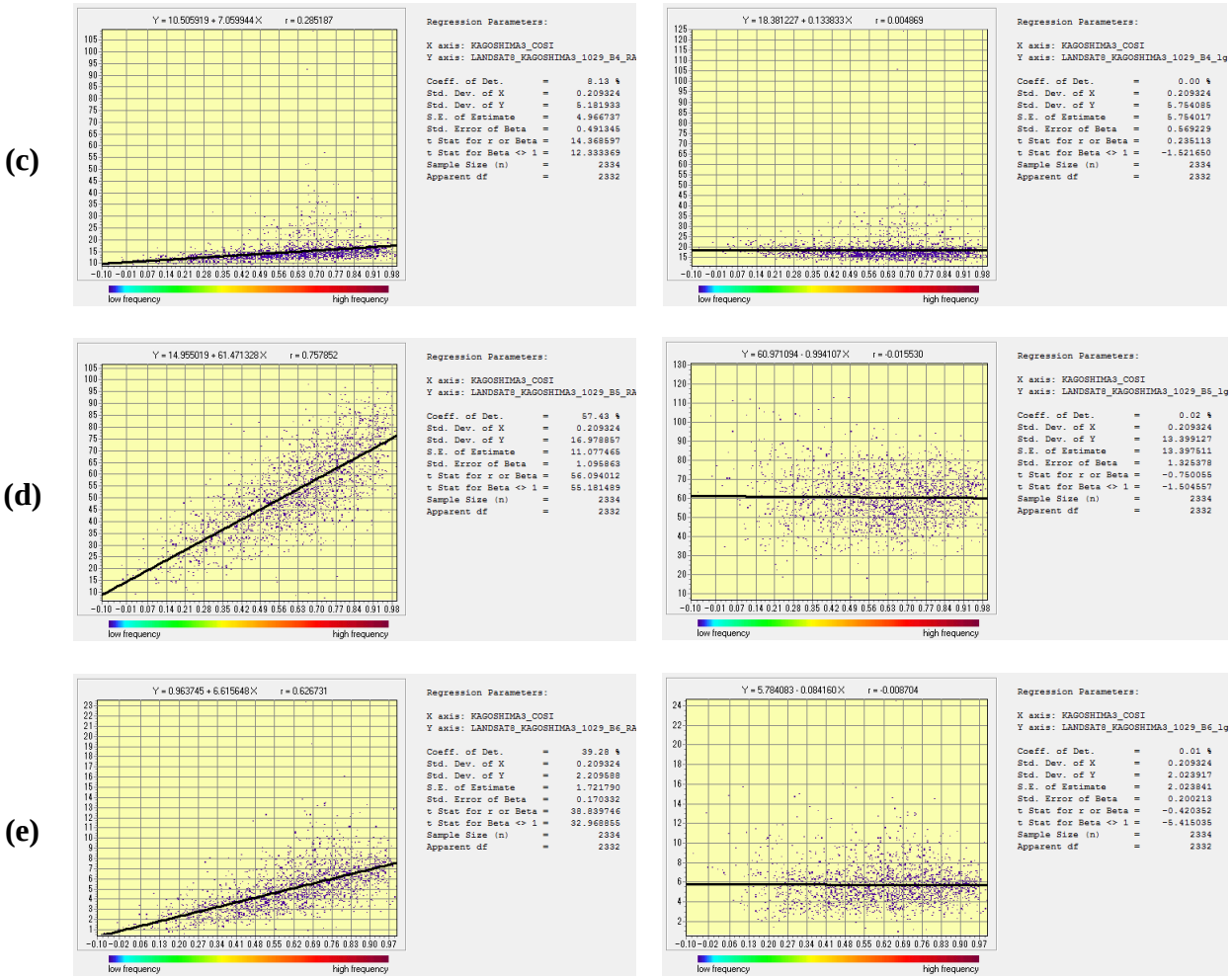

Figure 18. Regression analysis between cos *i* on x-axis, and radiance values on y-axis, for **(a)** band 2 **(b)** band 3 **(c)** band 4 **(d)** band 5 and **(e)** band 6, for the **(1)** non-corrected and **(2)** the corrected radiance data, respectively.

Figure 19. True color composite of the LANDSAT OLI image for the comparison before the radiometric correction (top) and after (bottom) for visual interpretation (RGB = band 432).

4.4.2. Detail Land Cover (Forest Cover) Mapping

4.4.2.1. Spectral Signatures of Land Cover Types

The spectral signature of the land cover classes extracted from the constructed training sites were analyzed and determined for the use in the latter supervised classification process. In the supervised classification process, consideration was made to take three different schemes to compare how different the results appear.

1. Using all training classes for the classification
2. Merging similar spectral classes then perform the classification
3. Merging all subclasses into one general class then perform the classification

To take the second approach of the classification, a mean radiance value of each training classes were extracted using the corrected LANDSAT imagery (Figure 20).

(a)

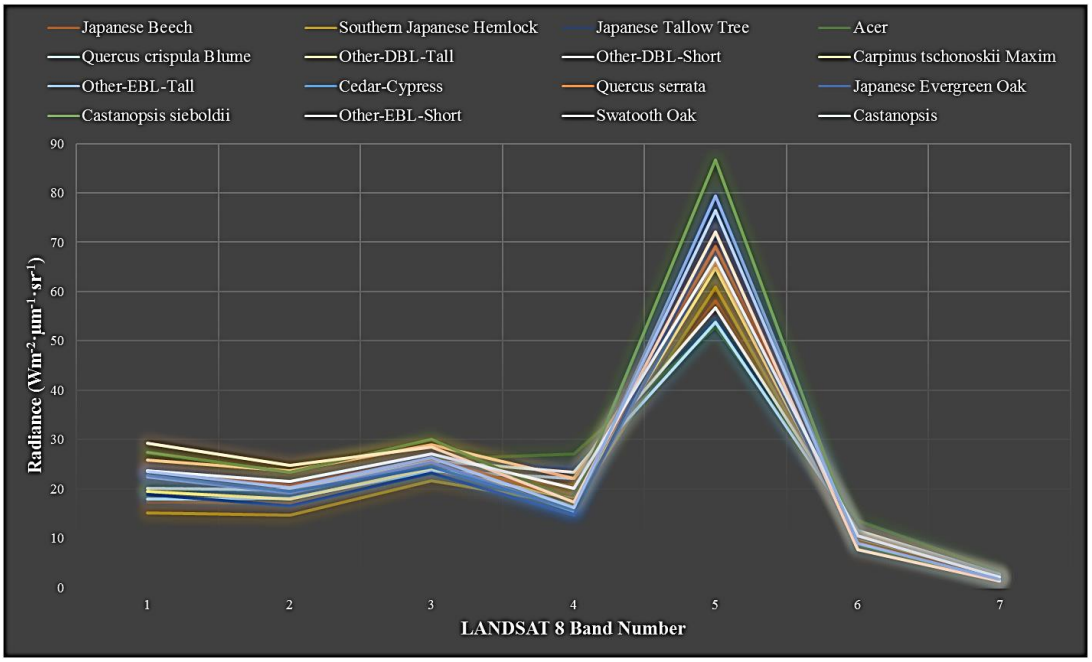

(b)

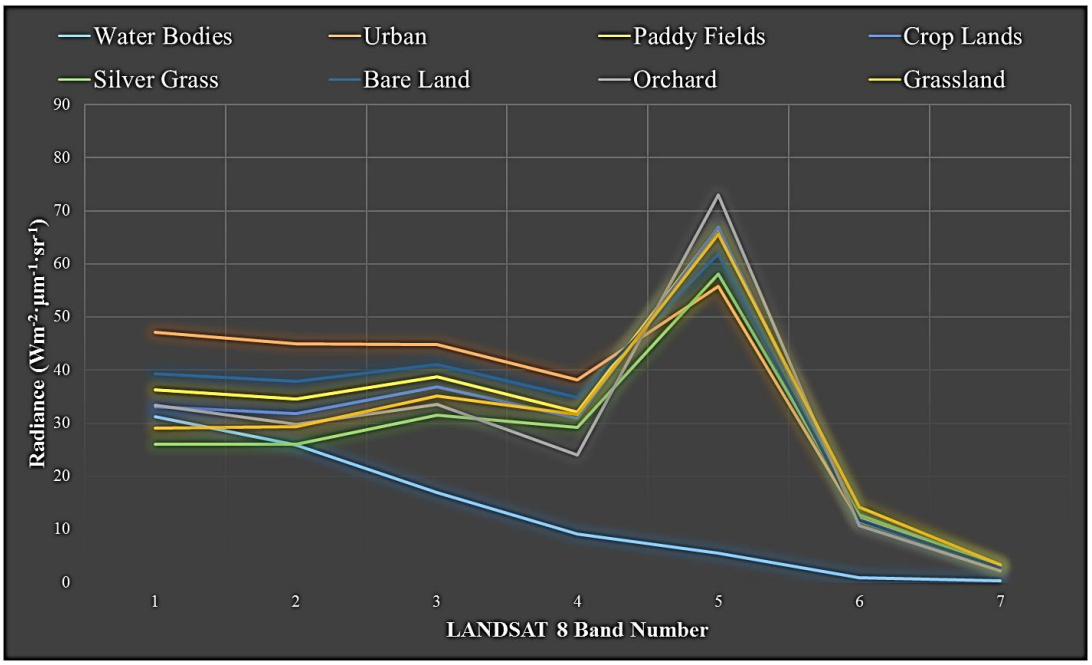

Figure 20. Spectral signatures of each land cover classes. Mean radiance value is extracted for each bands from LANDSAT OLI using the constructed training data. **(a)** is classes of forests and **(b)** is other than the forest classes.

According to this information, selection of which class to be merged were determined. We can see that some of the classes have different mean radiance values even within the similar forest types, showing around 30 $Wm^{-2} \cdot \mu m^{-1} \cdot sr^{-1}$ difference between the lowest and the highest value (band 5). However the trend of those among the bands is very similar while totally different signature can be seen in some other classes such as the water bodies or urban classes. It is noted here that for the comparison of the approaching method for supervised classification, the Kyushu Island area was chosen as the test site. Depending on the result which is obtained, the most preferable method will be further processed to develop a categorical map of whole Japan.

4.4.2.2. Maximum Likelihood

MAXLIKE module uses the spectral signature of the classes with the images to be fused, and the pixels will be classed to the most likely classes they would belong according to the algorithm. The pre-final product of the land cover map of Japan is shown in Figure 21 which is the reclassified map from the original number of classes to 12 classes. The category of original classes and the reclassed 12 classes are shown on Table 3 with which class was merged to what class (example from the Kyushu region). The difference of the accuracy of the map made by different approaches described in above section is also outputted, shown on Table 4.

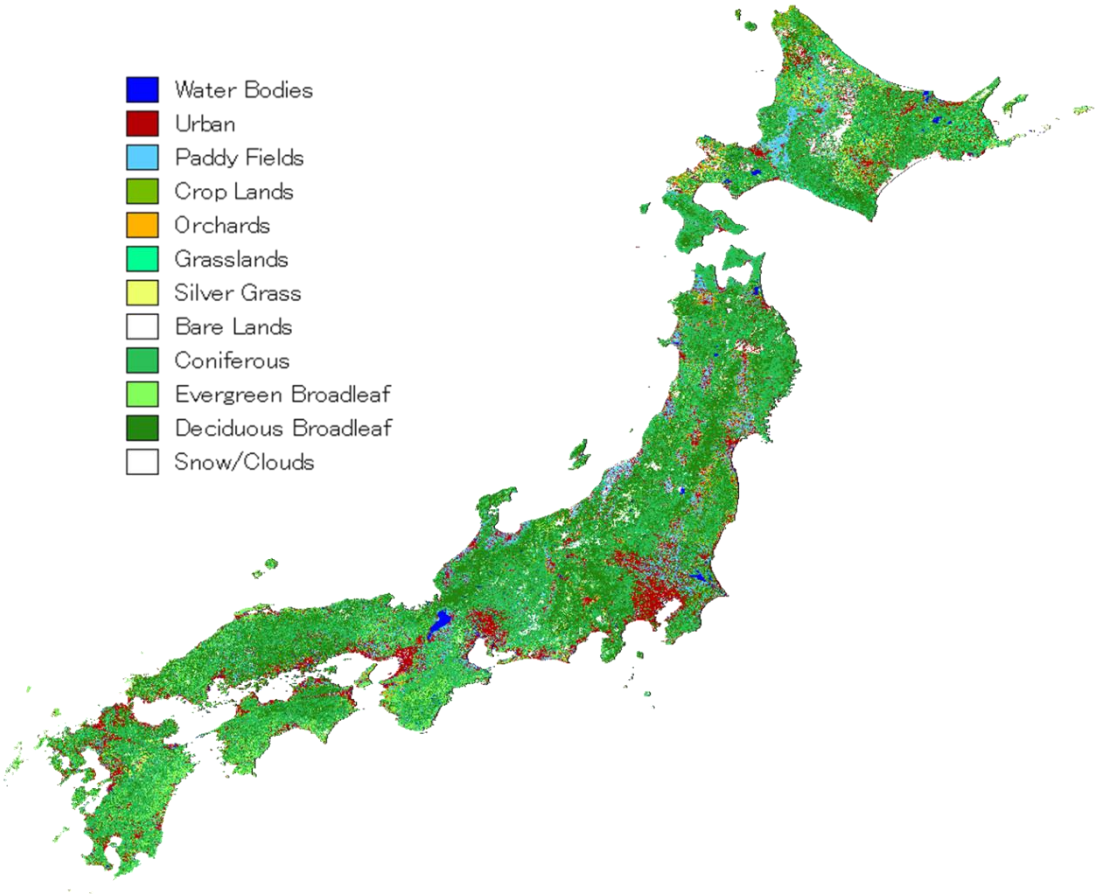

Figure 21. Land Cover map of Japan developed using 35 LANDSAT OLI scenes yielding 12 classes in total.

Table 3. Land cover classes for example from the Kyushu area: (a) original outputs (b) reclassified outputs.

Num	Cover Type (a)
1	Water Bodies
2	Urban
3	Paddy Fields
4	Crop Lands
5	Orchard
6	Grasslands
7	Silver Grass
8	Bare Lands
9	Japanese Hemlock (Conifer)
10	Cedar-Cypress (Conifer)
11	Evergreen Oak (EBL)
12	Castanopsis sieboldii (EBL)
13	Castanopsis (EBL)
14	Other-EBL-Tall (EBL)
15	Other-EBL-Short (EBL)
16	Acer (DBL)
17	Quercus crispula Blume (DBL)
18	Carpinus tschonoskii Maxim (DBL)
19	Quercus serrate (DBL)
20	Japanese Beech (DBL)
21	Japanese Tallow Tree (DBL)
22	Sawtooth Oak (DBL)
23	Other-DBL-Tall (DBL)
24	Other-DBL-Short (DBL)

Num	Cover Type (b)
1	Water Bodies
2	Urban
3	Paddy Fields
4	Crop Lands
5	Orchard
6	Grasslands
7	Silver Grass
8	Bare Lands
9	Coniferous
10	Evergreen-BL
11	Deciduous-BL
12	Snow/Clouds

Table 4. Accuracy of the classes for when different approaches were taken for the classification. Assessment was taken at the Kyushu area for the case.

Methods	**Coniferous**	**Evergreen Broadleaf**	**Deciduous Broadleaf**	**Others**	**Overall**
All Training Data	78.7 %	64.3 %	86.7 %	81.7 %	81.3 %
Merged Training Data	88.0 %	78.6 %	85.8 %	87.2 %	87.0 %
General Training Data	92.9 %	28.6 %	53.1 %	97.1 %	85.6 %

Overall accuracy of the classified map shows highest of 87 % when the approach was taken merging the similar spectral signature classes, second was using general training data resulting 85.6 %, and the last was when all detailed training data were used showing 81.3 %. Each class accuracy represents the producer's accuracy. Also an assessment was made comparing the difference of the accuracy when non-radiometric corrected imageries were used. The result showed 5-7 % increase when the corrected imagery was used. If we only take attention to the overall accuracy, it will seem that using merged training data gives the best result, however it needs to be focused more onto each class information and see what is really happening. This will be mentioned in the discussion section.

4.4.3. Accuracy Assessment

The ground truth points obtained from Google Earth together with the vegetation map was used with the land cover map to perform the accuracy assessment by outputting the error matrix (Table 5). Because the purpose of the use of land cover information is limited to the forests areas, we have reclassed the 12 class category to general 3 class forest category plus 1 (other than forests), resulting 4 classes in total for the accuracy assessment.

Table 5. Modified Error Matrix showing the reference data (ground truth) versus the image classification. Overall accuracy shows approximate 74 % and Kappa Index of Agreement (KIA) as 0.65.

KIA = 0.65		Reference					
		Coniferous	Evergreen Broadleaf	Deciduous Broadleaf	Others	Total	ErrorC
Classified	Coniferous	**852**	253	149	24	1278	0.3334
	Evergreen Broadleaf	41	**533**	113	30	717	0.2566
	Deciduous Broadleaf	59	200	**680**	54	993	0.3152
	Others	48	14	58	**892**	1012	0.1186
	Total	1000	1000	1000	1000	4000	
	ErrorO	0.1480	0.4670	0.3200	0.1080		0.2607

Here, the reference data (ground truth) is presented in the column and the classified category is in the row. Major diagonal of the error matrix represents agreement between the reference data and the classified map, and is represented by a single cell in the matrix for each map class. It is computed with the user's accuracy (Error of Commission) for the row total and the producer's accuracy (Error of Omission) for the column total. The overall accuracy is considered with sum of the points which has the exact match between the reference data and the classified data (major diagonal in bold) divided by the total number of points (in this case it shows as overall error). The overall accuracy of the land cover (forest cover) map resulted at 73.93 % which was produced with the method of when all detail training classes were used, and the overall Kappa Index of Agreement (KIA) resulted 0.65. KIA is a statistical measure adapted for accuracy assessment in the remote sensing fields by Congalton and Mead (1983), values range from 0 to 1 saying if it is 0, the total agreement of the categorical map is occurring from chance, while 1 means a perfect true agreement. In the case of this study KIA = 0.65, which could be said that the produced map is 65 % better agreement than just by chance.

4.5. Discussion

Producing a land cover map was made not only defining the areas as simple forests and non-forested area, but more in details (i.e. subclasses) such as for forests; coniferous, deciduous or even more classes, so that the information could be used and applied in various ways. Sanga-Ngoie (2003) has stressed on the need to produce a detailed digital land cover (or DVM) map, especially for the vegetation categories, in order to allow for more precise estimations of CO_2 sequestration values. Various combinations and data were examined to see which makes the best result for a high accurate land cover map. In the case of this study, only single scene data sets were used for developing a land cover map for each area. Sanga et al. (2012) states the usefulness of applying temporal data sets for improving the land cover accuracy due to the clear difference of the radiance values which changes during the different seasons of the year. In the case of forest classes, similar spectral signature would be seen through the season after blooming finishes, but clear difference can be seen and able to distinguish the difference of the forest types such as trees where the leaf fall in the winter seasons. It could not be managed to apply such method because of less frequency of cloud free product captured which made us difficult to find a set of scenes with two different seasons. Operation of LANDSAT 8 is still in its second year, the database of scenes are still less compared to LANDSAT 5 or 7, so such method would either be possible in a limited region or when time passes and number of data becomes available.

Rather instead, the method which was stated on above section was applied. Making a difference in the usage of the constructed training sites and then classify. As shown on Table 4, the best result of the classification was when the training classes were merged with similar spectral classes. Of course this term “best” would mean in the overall accuracy, however when each classes are taken into focus, there are differences among them. For example, overall accuracy of using general class training data is higher than using all detailed training class, but if we look at the evergreen and deciduous broadleaf class, using all detailed training data

improves the class accuracy by 36 % and 33 % for evergreen and deciduous broadleaf forests respectively. On the other hand the coniferous class drops by 14 %. In this case the merged training data has shown high accuracy among all the classes along with the overall accuracy. Compared to using all the training data, coniferous improves by 9 %, evergreen broadleaf improves by 14 %, other class improves 5 %, and only the deciduous broadleaf decreases but only 1 % and it is still near the highest accuracy for that class.

It is presumed that this difference in the result has occurred because when constructing more detailed and precise land cover classes would lead to making more chances of unclear pixels to turn into the more likely class that which it is supposed to belong to. However not all classes shows the increase in the accuracy and if one class improves either one or both other classes declines. Figure 22 shows the two band scatterplot (scattergram) of the LANDSAT OLI and the signature class which is overlayed on the scattergram giving the analyst a sense of how well the classes are distinguishing between the cover types in the two bands that are plotted. In this case X axis is band 4 and Y axis is band 5. Figure 22 **(a)** shows the scattergram of the two bands, along with each land cover classes when general classes are used, **(b)** shows when similar class is merged and **(c)** shows when all detail classes are used.

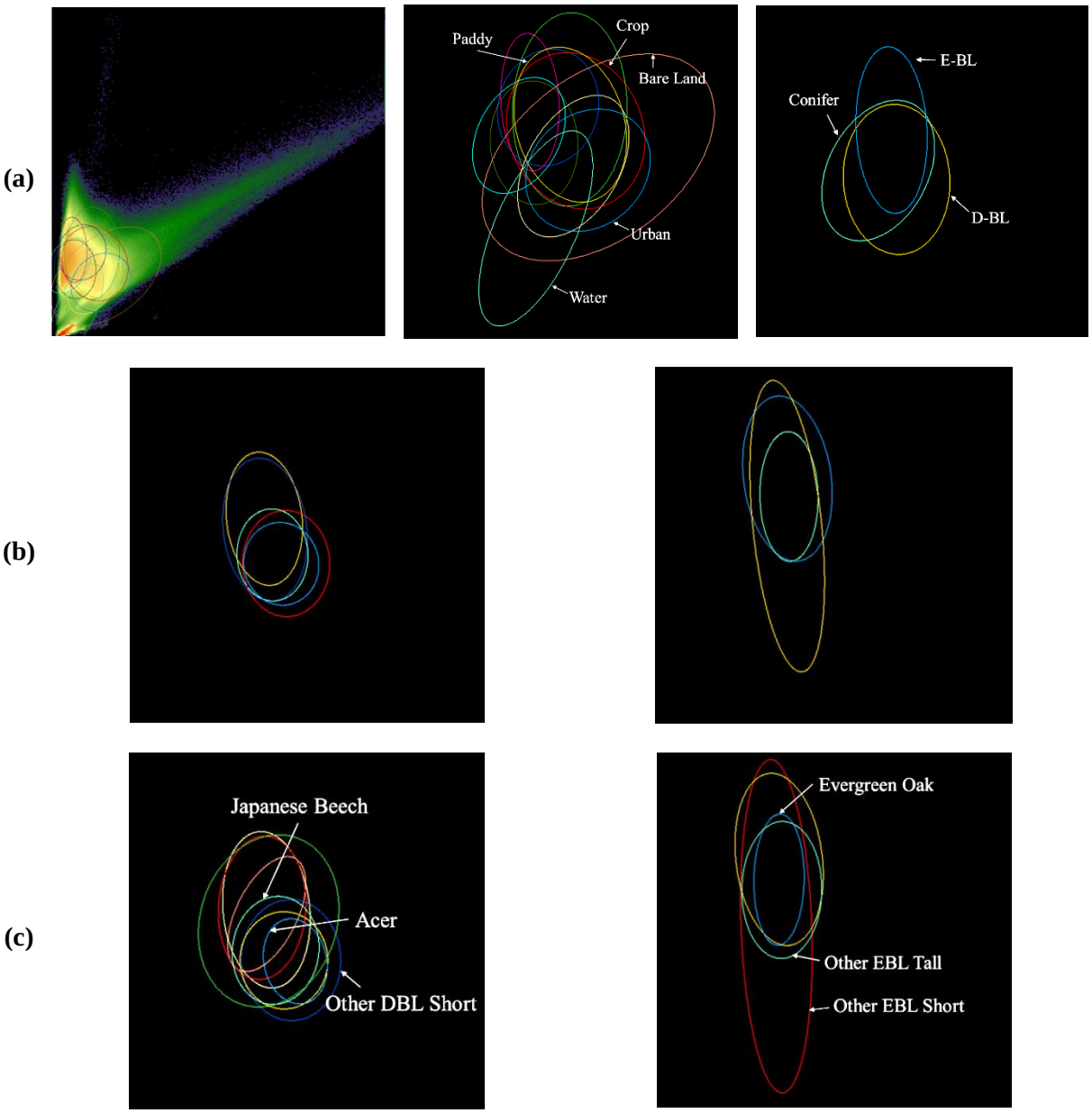

Figure 22. Two band scatterplot of LANDSAT OLI band 4 (x-axis) and band 5 (y-axis) and the interpretation of the each class category in distribution for (a) when using general classes, (b) merging similar spectral classes and (c) all detailed classes are used.

Figure 22 **(a)** on the left shows the overall of how the scattergram shows with all general class which can be seen in the right side in the same row. Figure 22 **(b)** to **(c)** shows the class distribution for when similar spectral classes are merged and all detail training classes are used respectively for deciduous broadleaf classes on the left and evergreen broadleaf forest on the right. It is clear that, when all classes are merged together into one general class, the two standard deviations from the mean (center) becomes more larger hence resulting more chances

of one signature class to overlap with another class. Now the problem is that these pixels that belong to the range which is overlapping with each other would have a possibility of getting misclassified to one or another class. However comparing with Figure 22 **(b)** or Figure 22 **(c)**, if more detail training classes are constructed within the same category class, each pixel where it was overlapping might fall into more likely classes which they are supposed to be. This is the case that describes why the improvements of the each land cover classes were seen when using such method. Just to note that some signatures overlap because of the inadequate nature of the definition of land cover classes. It can also indicate mistakes in the definition of the training sites. At last, it likely to occur because certain objects truly share common reflectance patterns in some bands (Eastman, 2006). Constructing precise training data for various land cover types in detail is useful for classifying the pixels to the correct classes, but too many of them might cause more probability in misclassifying those classes also. So this is a try and error for each region and environment to obtain the best result for its area. In the case of this study, all training data was applied in the further procedure, because we wanted to keep the precise radiance information for each class to develop better categorical maps. The result in Kyushu was easier to show due to high diversity of species and size of area to actually show the difference, however on some regions, such number of class cannot be constructed, so all training classes' information was kept for the classification.

4.6. Summary

In this chapter, a development of detail land cover (forest cover) map of Japan, using LANDSAT OLI was proceeded. The mapping scheme was considered by different ways of the usage of the training sites, either applying all detail classes, merging similar spectral classes or merging all classes into one general class. Final output of the categorical map of Japan resulted overall accuracy of 73.93 % (coniferous: 85.2 %; evergreen broadleaf: 53.3 %; deciduous broadleaf: 68 % others: 89.2 %). It was confirmed here also that by applying the radiometric

correction, the accuracy improves by 5-7 % compared to when the imagery is not corrected. This chapter made it possible to extract precise information of the forest cover distributed along the nation of Japan, and gave us convincing results in order to step forward to the final chapter of estimating the CO_2 sequestration by the forests of Japan.

5. Estimating CO_2 Sequestration from the Forests of Japan

5.1. Introduction

In this chapter, it is progressed to seek the way through to estimate the CO_2 sequestration from the forests in Japan, by using the two main information which was obtained in the early chapters: Detail forest cover map and stem volume map. By doing so, it becomes possible to estimate the potential amount of CO_2 sequestered by the forests of Japan, considering difference sequestration rate depending on the growing stages of the forests and its types. The result should lead to better understandings of the CO_2 trend and thus become one useful source of information for further uses in the carbon cycle, policy making or other various fields for the contribution.

5.2. Data Sets

5.2.1. Detail Forest Cover Map

One of the main sources for procedure is using the detail forest cover map developed in chapter 4. Different forest types has its unique value in the amount of sequestration and by understanding the distribution of its forest type, more precise estimation of the result could be obtained. The forest cover map is developed by using 35 LANDSAT OLI images from the year 2013 to 2014.

5.2.2. Stem Volume Map

Another main source for the procedure is to use the stem volume map of the forested areas developed in chapter 3. Even within each forest types, the growing stages of the forests leads to the difference in the amount of sequestration they can capture annually. By considering this information, even further detailed estimation of the sequestration becomes possible. The stem volume map is developed by using the model developed by us and together with the model

developed by Wijaya (2009), using PALSAR 50 m ortho-rectified mosaic product for to cover whole Japan.

5.2.3. Forest Inventory Data

Additional data which is used for the analysis is the forest inventory data provided by two Prefectural governments. One is the stem volume – age relationship data provided by the Oita Prefectural Government. The data shows the growing trend of each tree types depending on the regions within Oita. The data is used as a representative to output the tree age information transformed from the stem volume map information. Second is the CO_2 sequestration table published by the Tochigi Prefectural Government. The data consists of the amount of CO_2 sequestered by each tree types per tree age from different regions within Tochigi Prefecture. This information is used as a representative for the final output in the estimation of the CO_2 sequestration from each forests types at per tree ages of Japan.

5.2.4. Precipitation Data

Annual precipitation data published by the Ministry of Land, Infrastructure, Transport and Tourism (MLIT) of Japan is utilized for the use for the analysis of the site productivity for considering the different growth rates of the forests. This data is used together with the Oita data to consider the transformation of stem volumes to ages depending on its regional growth dependency.

5.3. Analysis Methods

5.3.1. Stem Volume – Age Conversion

The stem volume values for various tree ages as provided by the Oita Prefectural Government are shown in the graphs in Figure 23. Then, the so-obtained stem volume map (Figure 15) is reclassified into range of ages, by considering the different growth rates among the various regions of the study area.

(a)

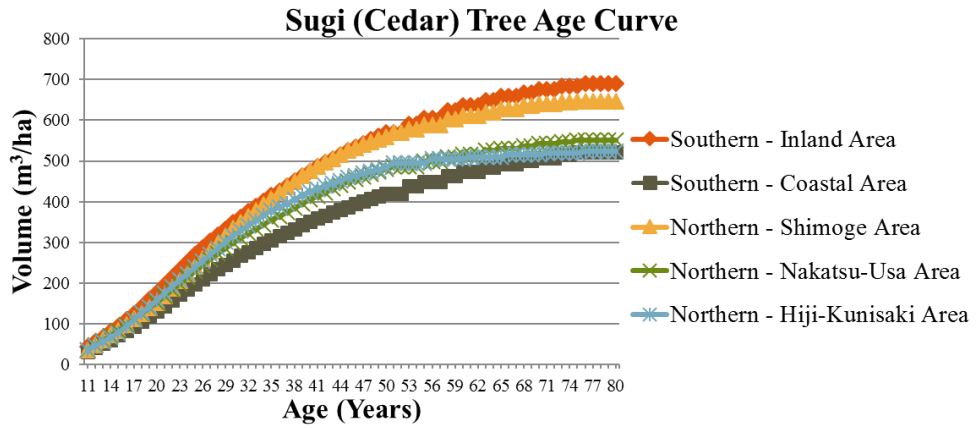

(b)

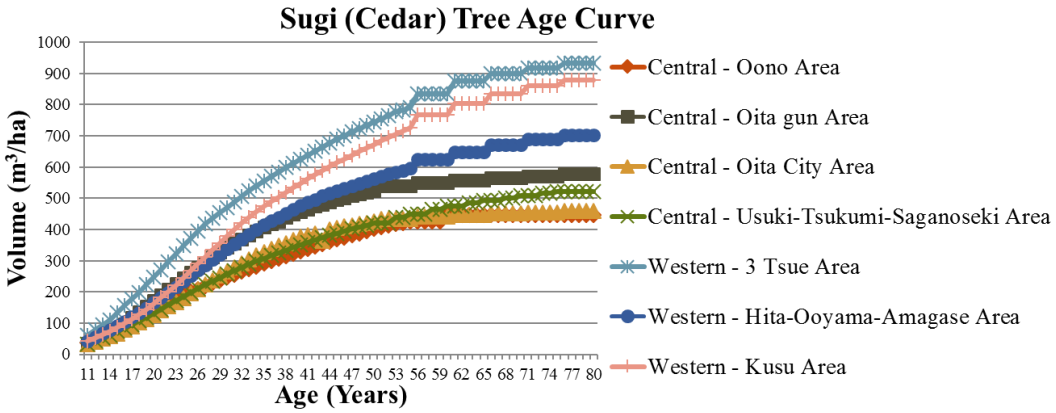

(c)

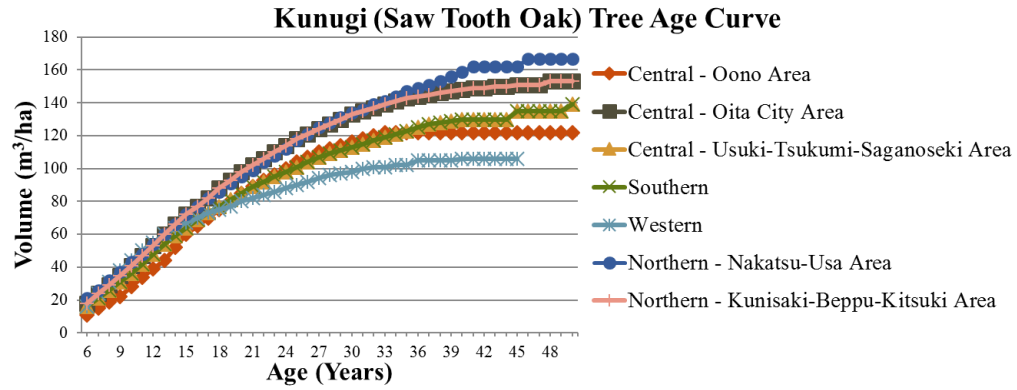

Figure 23. Stem Volume as a function of tree ages for **(a), (b)** the Sugi (cedar) and **(c)** the Kunugi (saw tooth oak), in Oita Prefecture. The difference of stem volume growth among the different regions in Oita is remarkable.

As seen in Figure 23, the growth rates of the tree differ for each region, and the dependency of the growth is characterized by various factors of the environment (Perry et al., 2008). Because it was necessary to apply the tree age conversion considering its growth rate for whole Japan, a relationship analysis was made using the precipitation data of the region together with the total volume growth made between the two periods of time. Precipitation data was used assuming that it to be one of the limiting factors for the growth of the forests. The result of the analysis shows on Figure 24 **(a)** and **(b)** for the Sugi (cedar) and Kunugi (sawtooth oak) tree respectively.

(a)

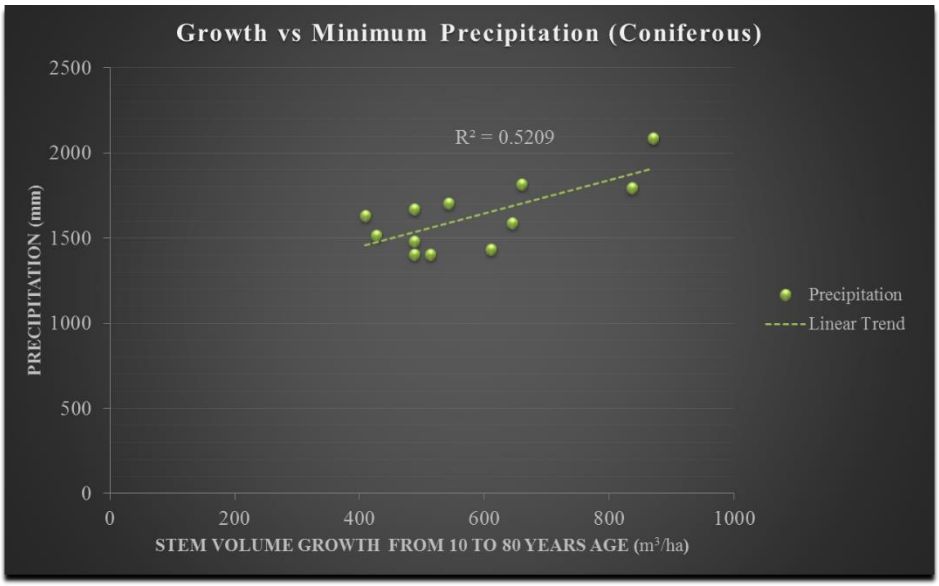

(b)

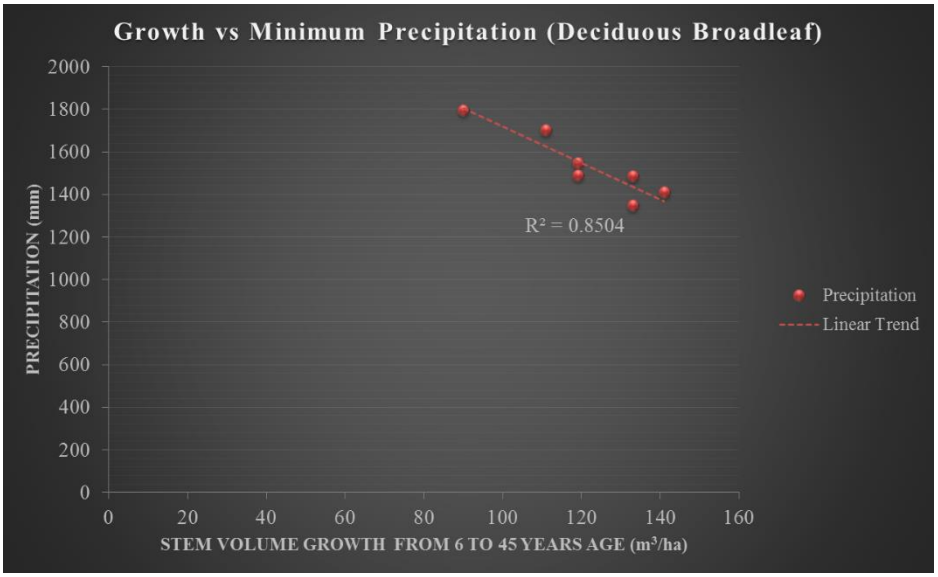

Figure 24. Relationship analysis between precipitation and tree growth for **(a)** Sugi (cedar) trees and **(b)** sawtooth oak trees.

The results show clear trend of the relationship between the precipitation and the tree growth. For the Sugi trees (coniferous) increasing precipitation results larger growth of the trees, on the other hand for the sawtooth oak (deciduous broadleaf) the trend shows an opposite where tree growth increases with decreasing precipitation. Using this information, a threshold of the precipitation value was set and classified the area of region to lay on which growth curve they would most likely fit. The Sugi data is used as a representative of the coniferous forests and sawtooth oak data is used as a representative for the deciduous broadleaf forests. Unfortunately a data for the evergreen broadleaf forests were lacking, so the growth rate is considered only for the first two classes. The distribution of the precipitation class and the threshold is seen on Figure 25.

(a)

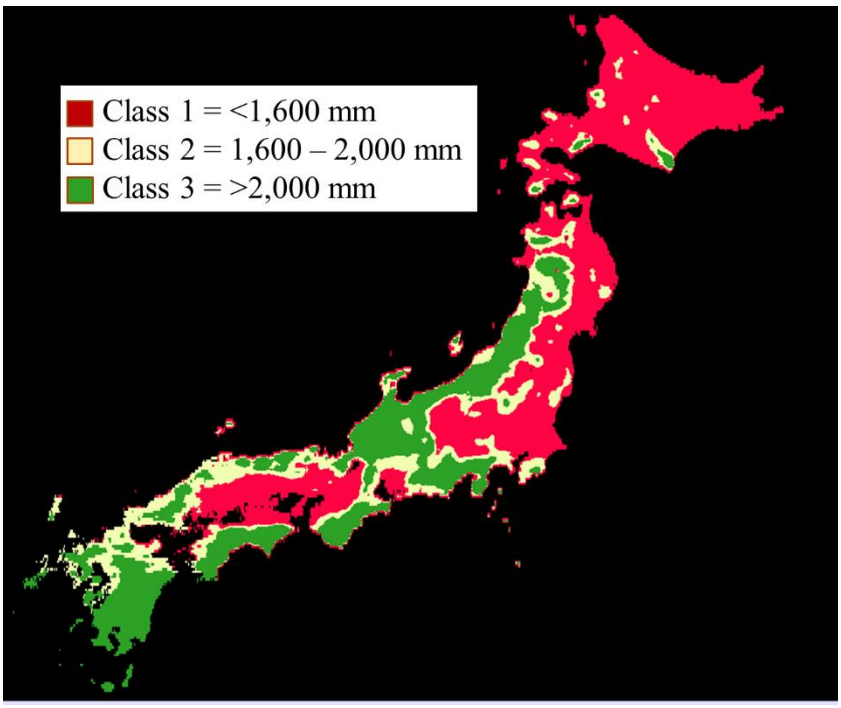

(b)

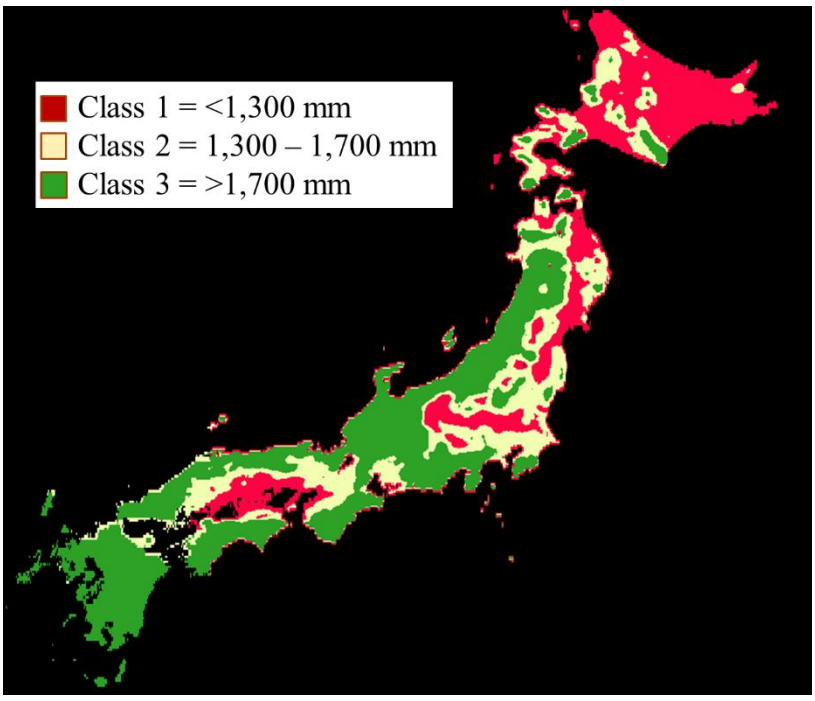

Figure 25. Precipitation data classified using the threshold values for the consideration of the growth rate of the forests for **(a)** coniferous and **(b)** deciduous broadleaf forests.

If the coniferous category falls into such classes seen on Figure 25 **(a)**, depending on the class number, the growth rate will be considered and tree age conversion will be process according to the reference data from the Oita prefectural Government. Same along with the deciduous broadleaf forests. Just to note, for the coniferous forests, class 1 will be areas with low growth rate, class 2 is moderate and class 3 is high growth rate. For deciduous broadleaf, class 1 are with high growth rate, class 2 moderate and class 3 is the low growth rate areas. This is done because age information is truly important to the estimation of sequestration. Even the same stem volume per unit area may differ its tree age due to the growth rate of the trees, and the difference of tree age leads to differences in the amount of CO_2 that the tree captures (Sanga et al., 2012).

5.3.2. CO_2 Sequestration estimation

Information from the Tochigi Prefectural Government was modified to calculate the sequestration value for each forests types at per tree ages. Estimation of total CO_2 sequestrations are obtained by multiplying the observational CO_2 sequestration rates by the total area of each forest type and tree age.

5.4. Results

5.4.1. Tree Age Map

Stem volume map information was transformed into the tree age map considering the growing rates of the forests on each regions of Japan, using the precipitation data for the coniferous and deciduous broadleaf forests. Figure 26 shows the graph of the distribution of tree age overlayed with the forest cover data to extract the exact forest types. Now, for the coniferous and deciduous broadleaf forests, it is examined to consider the growth rates for the age conversion, however the evergreen broadleaf was not and it has been converted directly from the stem volume map using the stem volume – age relationship information investigated by Sasaki et al. (1989).

(a)

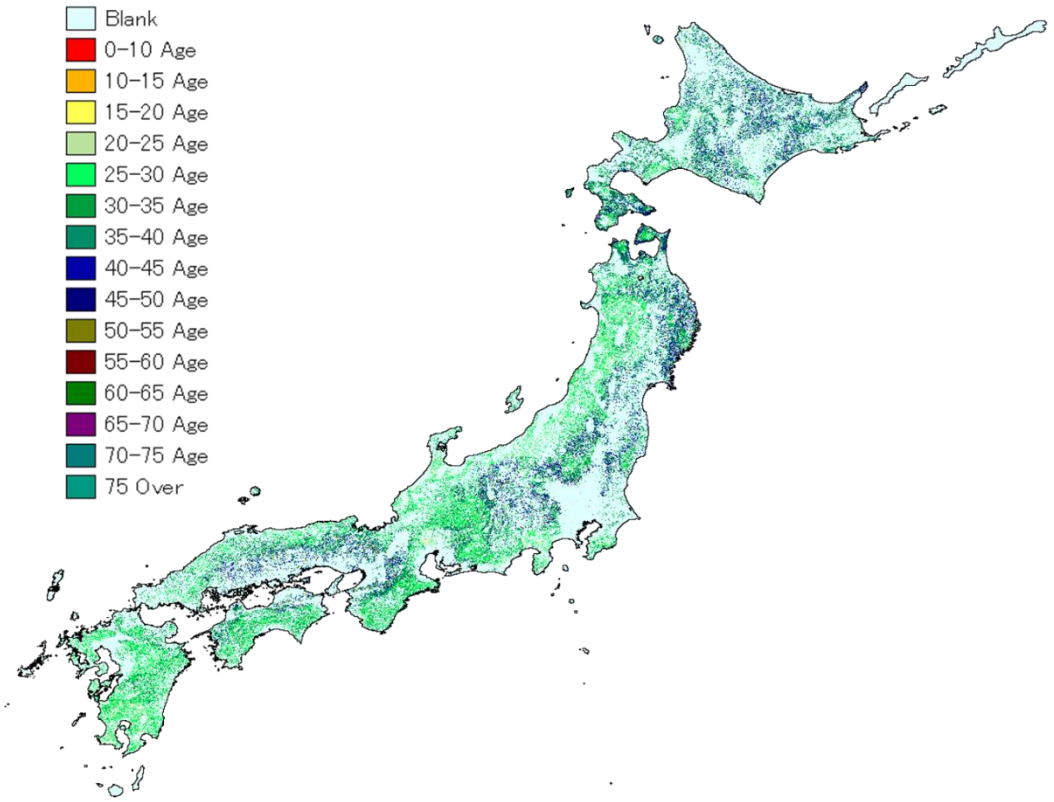
Blank
0–10 Age
10–15 Age
15–20 Age
20–25 Age
25–30 Age
30–35 Age
35–40 Age
40–45 Age
45–50 Age
50–55 Age
55–60 Age
60–65 Age
65–70 Age
70–75 Age
75 Over

(b)

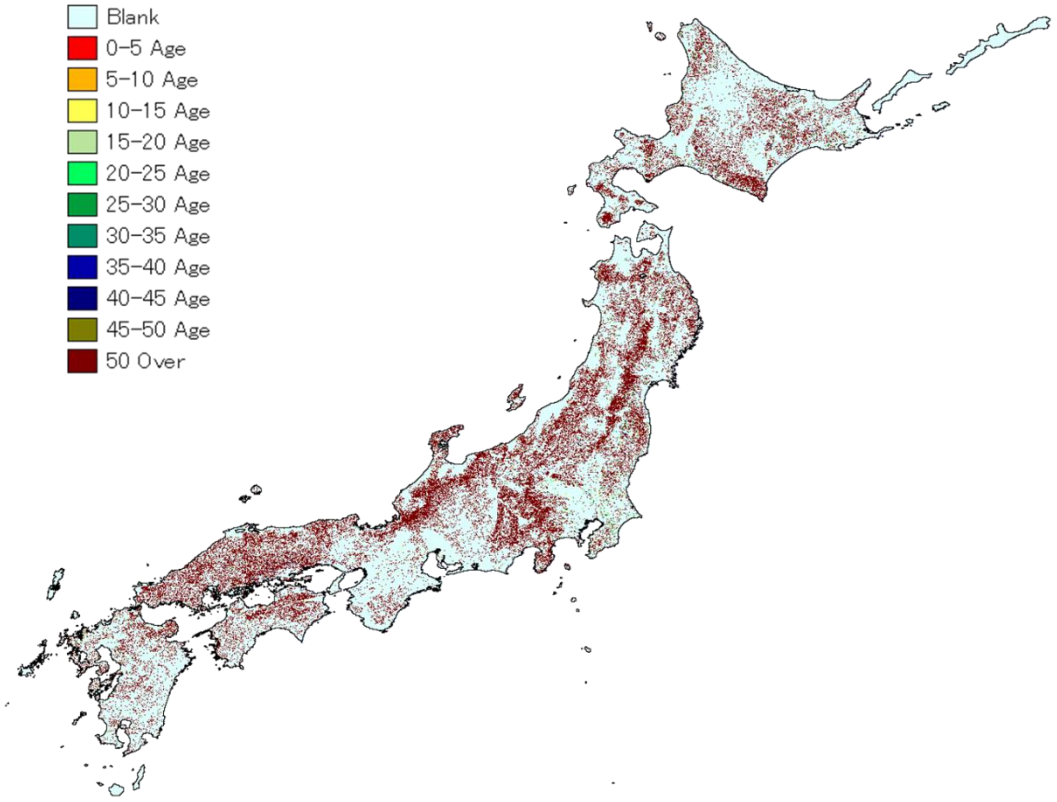
Blank
0–5 Age
5–10 Age
10–15 Age
15–20 Age
20–25 Age
25–30 Age
30–35 Age
35–40 Age
40–45 Age
45–50 Age
50 Over

(c)

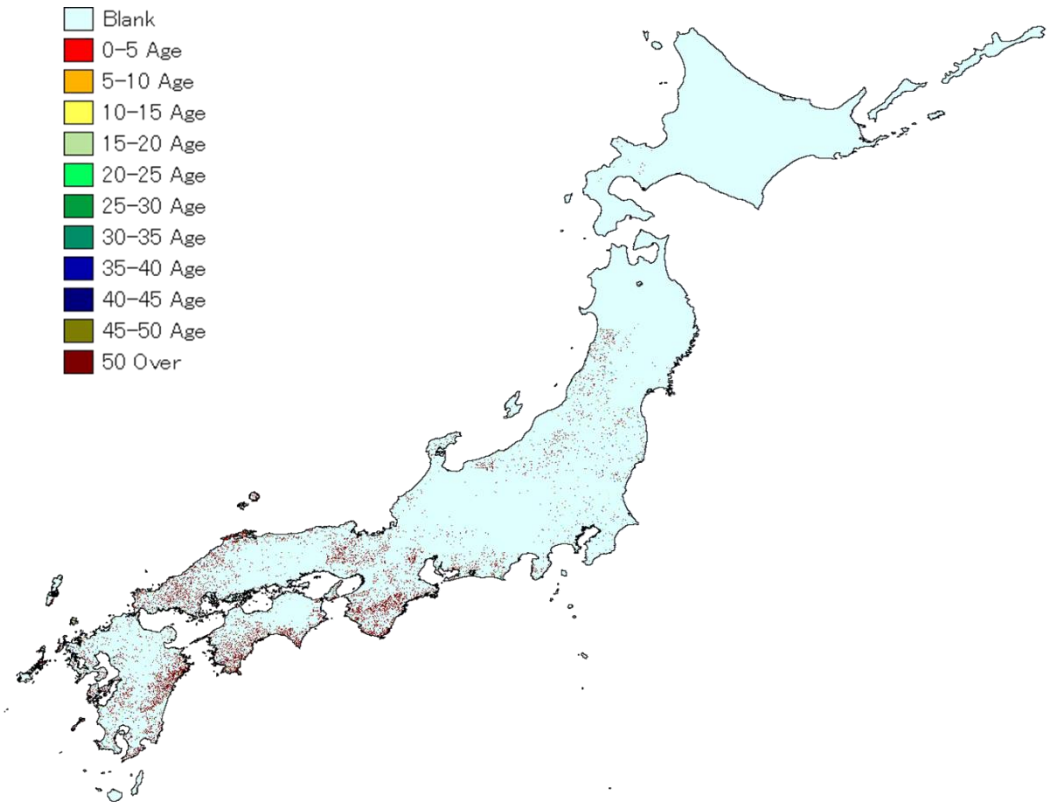

Figure 26. Tree age map transformed from the stem volume map for the **(a)** coniferous, **(b)** deciduous broadleaf and **(c)** evergreen broadleaf forests.

Distribution among the tree ages in a bar graph for the total area for each tree age range in Figure 27 shows better interpretation of the amount which the forests growing stages lies. For the coniferous, it can be seen widely distributed among the tree ages, the most in the 25-30 years range for site 1 (high growth rate regions) and 30-35 years range for site 2 (moderate growth rate regions) and 35-40 years range for site 3 (low growth rate regions). We can also confirm some size of areas over 75 years of age and it can be said that those areas are left naturally and it is kept growing without any management, while the areas with lower tree ages are places where plantations or forest management is at operation. However the accuracy of those needs to be validated in the future works. Compared to the coniferous, deciduous and evergreen broadleaf forests can be seen with the majority of tree ages over 50 years. Simply comparing this with the coniferous trees, there is completely less or mostly none areas that are working with plantations and it is just left naturally to grow resulting large size of areas being at a high aged classes.

(a)

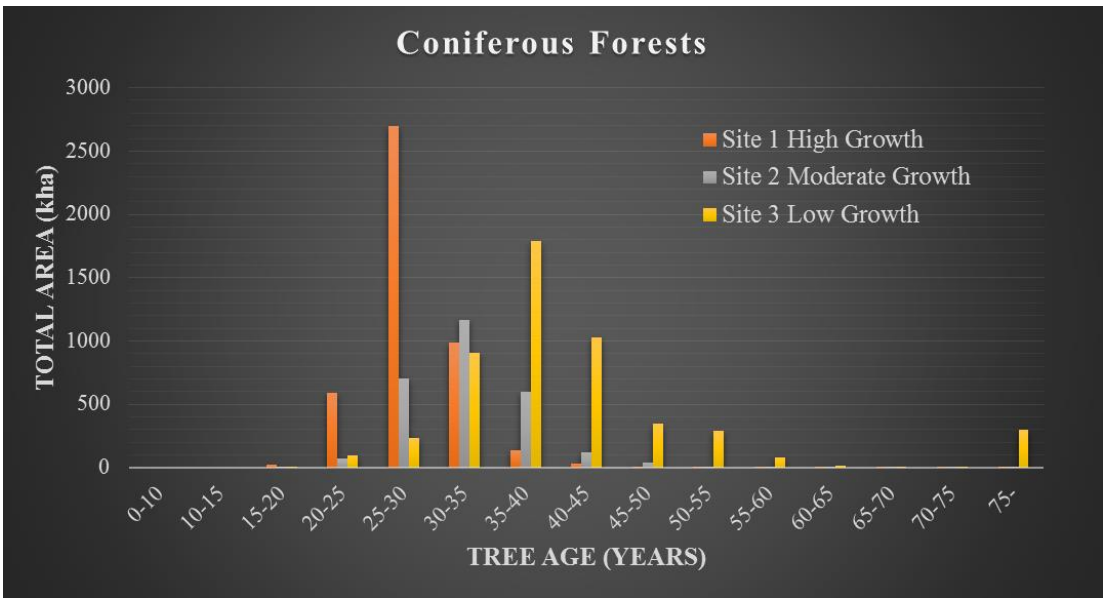

(b)

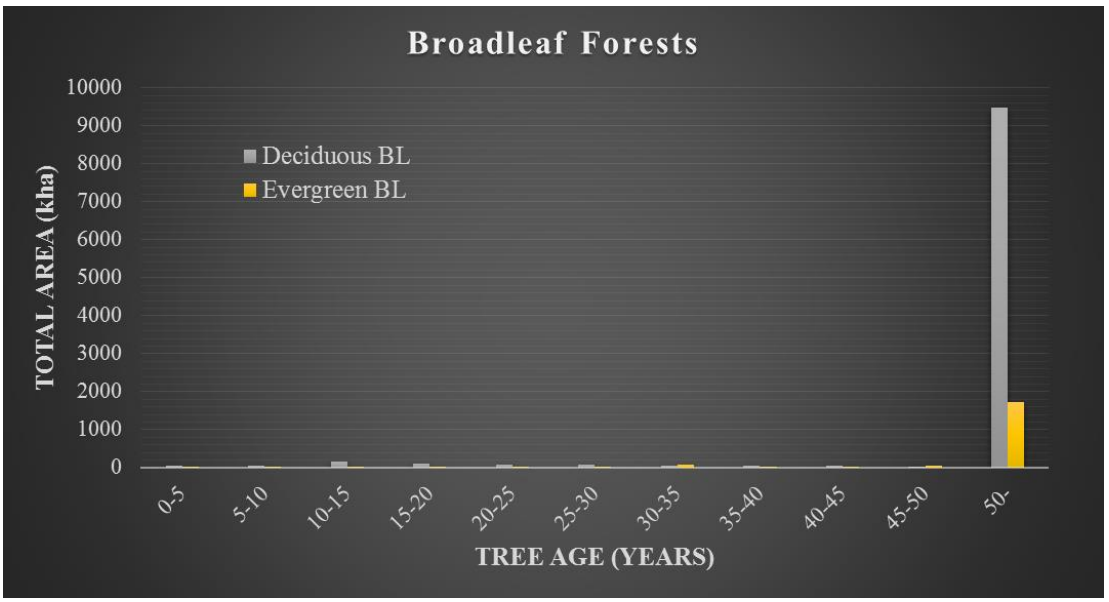

Figure 27. Statistical distribution of the forests area per tree ages for the **(a)** coniferous and **(b)** deciduous/evergreen broadleaf forests in Japan.

5.4.2. CO_2 Sequestration by Tree Ages

Table 6 to Table 8 shows the total CO_2 sequestration estimates for coniferous, deciduous broadleaf and evergreen broadleaf forests per age category respectively. The sequestration values were modified from the reference data published by the Tochigi Prefectural Government by taking an mean value of each tree types per tree age range for deciduous and evergreen

broadleaf forests, using the tree data information of sawtooth oak, Japanese beech, Japanese zelkova and hornbeam for deciduous broadleaf, while evergreen oak and chinquapin oak is used for the evergreen broadleaf forests. For the coniferous forests, an weighted mean value of the Sugi (cedar) and Hinoki (cypress) trees were taken as 7:3 because the distribution of those trees are around that ratio for whole Japan.

Table 6. CO_2 sequestration of coniferous forests per tree age using the PALSAR data and the stem volume method.

Forest Type	**Age (years)**	**tCO_2/ha/yr**			**Area (ha)**			**Total $MtCO_2$**		
		Site 1	Site 2	Site 3	Site 1	Site 2	Site 3	Site 1	Site 2	Site 3
Coniferous	0-5 5-10	3.38	2.56	1.70	0	0	0	0	0	0
	10-15	13.23	9.57	6.20	0	0	0	0	0	0
	15-20	16.11	11.45	6.76	22,826	6,575	7,332	0.37	0.08	0.05
	20-25	12.21	8.49	5.83	592,573	69,564	97,357	7.24	0.59	0.57
	25-30	10.05	7.83	5.34	2,700,597	705,043	230,650	27.15	5.52	1.23
	30-35	8.16	6.74	5.21	989,309	1,168,617	904,797	8.07	7.87	4.72
	35-40	6.42	5.87	4.89	137,687	600,268	1,791,110	0.88	3.52	8.76
	40-45	5.61	5.07	4.41	31,225	122,804	1,023,606	0.18	0.62	4.51
	45-50	5.41	4.63	3.78	7,835	38,352	349,890	0.04	0.18	1.32
	50-55	4.84	4.20	3.30	2,179	5,265	287,697	0.01	0.02	0.95
	55-60	4.08	3.61	2.91	684	7,685	78,352	0.00	0.03	0.23
	60-65	3.35	2.92	2.29	183	877.37	15,174	0.00	0.00	0.03
	65-70	2.47	1.78	1.40	1.57	1,986	9,501	0.00	0.00	0.01
	70-75	2.17	1.41	1.03	0.79	190.96	9,136	0.00	0.00	0.01
	75 over	1.18	0.42	0.42	30.57	1,098	296,715	0.00	0.00	0.13
Total					**4,485,131**	**2,728,325**	**5,101,317**	**43.95**	**18.44**	**22.52**
Overall					**12,,314,773**			**85.0**		

Table 7. CO_2 sequestration of deciduous broadleaf forests per tree age using the PALSAR data and the stem volume method.

Forest Type	Age (years)	$tCO_2/ha/yr$	Area (ha)	Total $MtCO_2$
Deciduous Broadleaf	0-5	2.91	38,756	0.11
	5-10	6.33	58,850	0.37
	10-15	6.50	151,418	0.98
	15-20	6.89	91,892	0.63
	20-25	5.96	90,147	0.54
	25-30	5.20	78,751	0.41
	30-35	5.09	62,852	0.32
	35-40	3.79	48,437	0.18
	40-45	3.52	57,704	0.20
	45-50	3.13	36,219	0.11
	50 over	1.87	9,475,569	17.74
Total			**10,190,332**	**21.61**

Table 8. CO_2 sequestration of evergreen broadleaf forests per tree age using the PALSAR data and the stem volume method.

Forest Type	Age (years)	$tCO_2/ha/yr$	Area (ha)	Total $MtCO_2$
Evergreen Broadleaf	0-5	2.46	35,540	0.09
	5-10	6.43	33,957	0.22
	10-15	6.57	15,752	0.10
	15-20	6.93	17,987	0.12
	20-25	6.27	20,771	0.13
	25-30	5.32	23,800	0.13
	30-35	5.38	68,927	0.37
	35-40	3.93	31,164	0.12
	40-45	3.74	36,252	0.14
	45-50	3.23	41,367	0.13
	50 over	1.87	1,716,706	3.21
Total			**2,042,228**	**4.76**

(a)

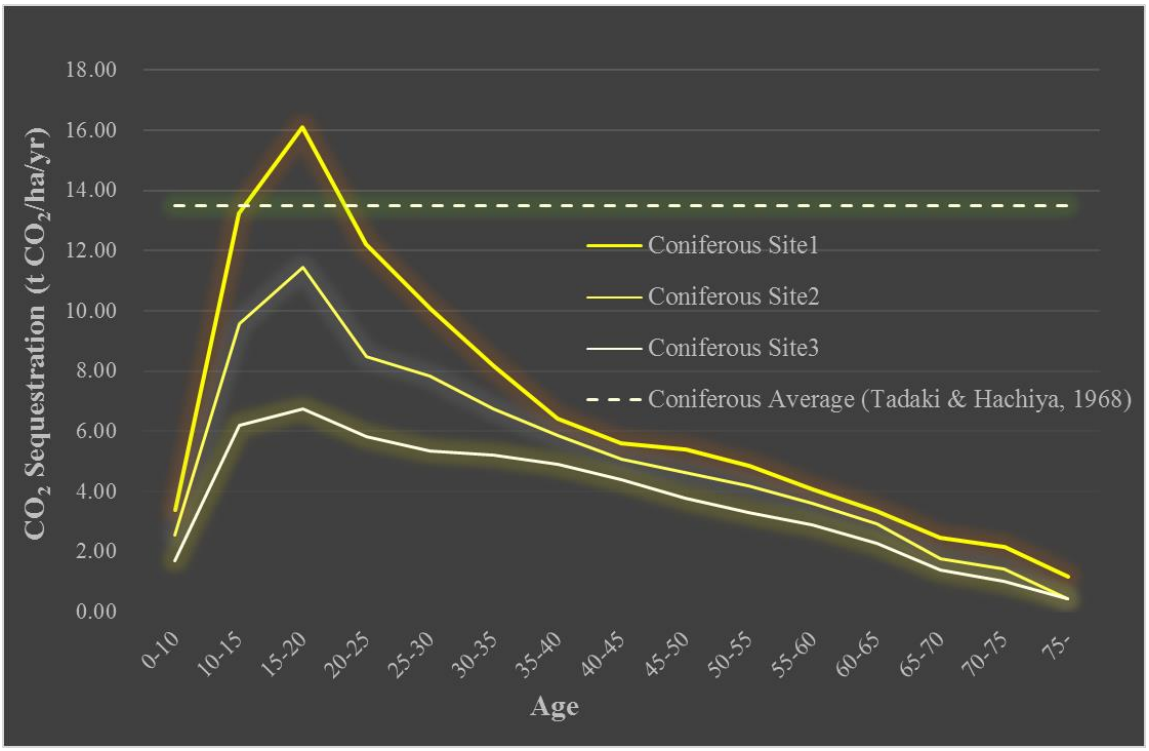

(b)

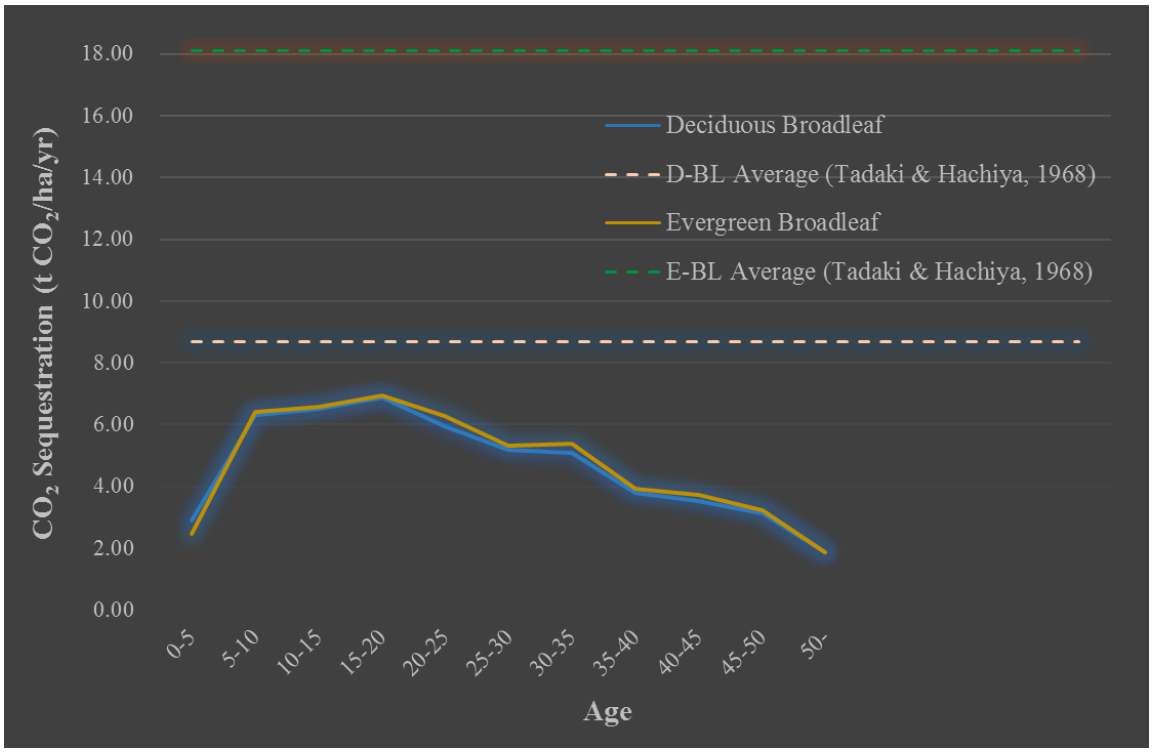

Figure 28. Trend of CO_2 values per tree age classes for **(a)** coniferous and **(b)** deciduous/evergreen broadleaf forests.

Figure 28 **(a)** and **(b)** shows a graph of the sequestration value among each tree ages for coniferous and broadleaf forests respectively. Together with the sequestration value calculated, a mean sequestration value of each forest types from the reference by Tadaki and Hachiya (1968) have been plotted. The coniferous forests shows an peak value at around 15-20 age and then gradually decrease to around the similar value from 0-10 years when it reaches 75 years. Each site dependency for the growth rate clearly shows the difference in the total sequestration amount, where it could be seen that comparing with the trees at low growth rate areas, the high growth rate area trees have approximately 10 tCO_2/ha/yr difference at the peak value. For the broadleaf forests, in this study, the results give not big difference between the evergreen and deciduous broadleaf forests. The peak value can be seen around 15-20 years age and gradually decrease, similar to the coniferous forests, however the total amount of sequestration value is much less than the coniferous. It is obvious that Japan has planned to operate an large plantation process using the Sugi or Hinoki trees because of the fast growing characteristics of those types which the values also confirms on this aspect. By using the detailed sequestration values per tree ages, sequestration overestimates that implicitly occur with the estimation method using averaged values (Tadaki and Hachiya, 1968) for coniferous trees of less than 10 years of age and for trees of more than 20 years of age, as well as the underestimation for the peak tree ages (15-20 years), can altogether be avoided. Similar can also be said for deciduous and evergreen broadleaf forests, compared to the averaged values for all ages their values per tree age show lower result.

Finally on Figure 29, shows the overall output of the final work which is the map developed first time so far, interpreting the CO_2 sequestration values from the forests in Japan.

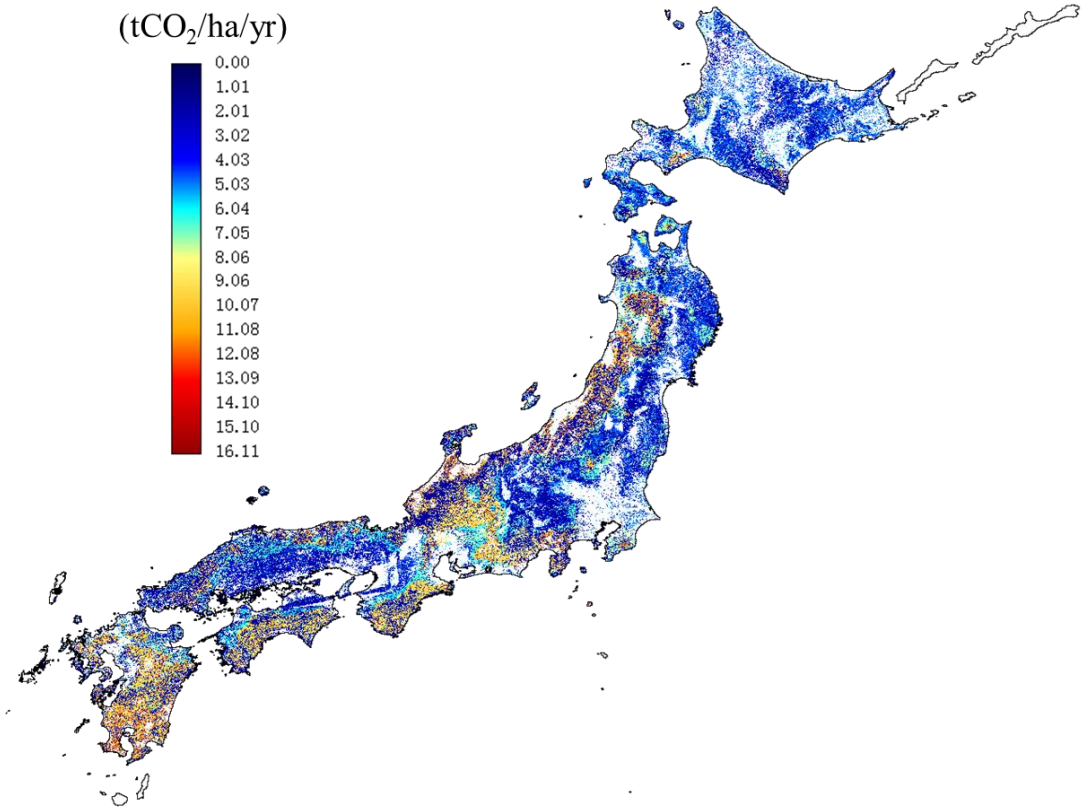

Figure 29. CO_2 sequestration map of Japan.

5.5. Discussion

5.5.1. CO_2 Sequestration Estimates, Errors and Limitations

The conventional method (Tadaki and Hachiya, 1968) used alone for the estimation of the CO_2 sequestration results in large errors of the total amount compared to when no special attention to the tree age is taken. The stem volume method for discriminating tree ages among each forest types clearly show the importance of those aspects to avoid such overestimations or underestimations depending on the growing stages of those forests. The use of PALSAR data made this discrimination possible, yielding sequestration rates per tree age, of up to trees of 75 years of age for the coniferous and 50 years of age for deciduous and evergreen broadleaf forests. It is thus clearly established that sequestration rates of 13.5 tCO2/ha/yr (Tadaki and Hachiya, 1968) is only valid for 10-15 year old coniferous forests on high growth rate regions, while the deciduous broadleaf forests reach just below the 8.7 tCO_2/ha/yr threshold only at 15-20 year old range. For the evergreen broadleaf forests, this is a big issue when applying with

the conventional method since it shows around 3 times more value than what is seen from the results in this study, meaning that there would be a large overestimation of the forests carbon sink capacity if such value is applied. High sequestration value from the evergreen broadleaf forests is difficult to confirm on the reasons. However, the amount of sequestration by the evergreen trees in Japan is acknowledged that it depends on the total solar radiation and also air temperature. Gross Primary Product (GPP) is resulted by the total radiation, and the Net Primary Product (NPP) is set from the amount of respiration subtracted from the GPP (Matsumoto, 2001). In this case higher air temperature leads to higher respiration and decreases the NPP, on the other hand, even if the total radiation is low, but if the air temperature is low also, respiration rate decreases and NPP becomes the same or even more compared from higher radiation periods (Perry et al., 2008). So depending on the season and location of the observation, the average value of the evergreen broadleaf forests should differ, and it might well be understood that the large value from Tadaki and hachiya (1968) is resulted from such perspective.

It is very important to note that, the averaged sequestration value for the coniferous forest type matches the sequestration value per tree ages obtained here for the 10-15 year old coniferous trees at Site 1. This is also the category of the second most fast-growing period for coniferous trees on that site location. The same is also true for the deciduous broadleaf forests for the 15–20 year old trees, just a little lower than the average value. This strongly implies that, if estimation is made based on the averaged values alone, it will round up the values for other trees in different growth stages, giving way to an overall overestimation of the carbon sink capacity, both for natural or planted forests. The results emphasize the fact that sequestration differs among tree ages: this has to be considered, otherwise erroneous values of forests' sequestration capacity will be obtained, and a number of negative consequences in the further use of these values can be foreseen.

Here it has been calculated and outputted the total estimation of the CO_2 from the forests of Japan, in consideration of both forest types and tree ages. As it is understood, discriminating the accuracy of this result is quite difficult, since there is no such "true value" of this information. However, it is necessary to note that there are always errors when coming with such estimation and it is itemized here what errors that could possibly come up which would concern on the results of the estimation. Four potential errors can be explained:

1. Accuracy of the land cover map (forest cover map)
2. Dependency on the backscattering model for stem volume estimation
3. Stem volume – age relationship curve
4. Sequestration value

For number 1, it is simply the errors from the misclassification of each forest types. As it is acknowledged in the work, total area size of the forest types is an important factor in the calculation of the total CO_2 sequestration since the sequestration value per unit area is multiplied by the total area of each forest types. Figure 30 shows the concept of the accuracy and errors of each forest types in reference from the error matrix (Table 5).

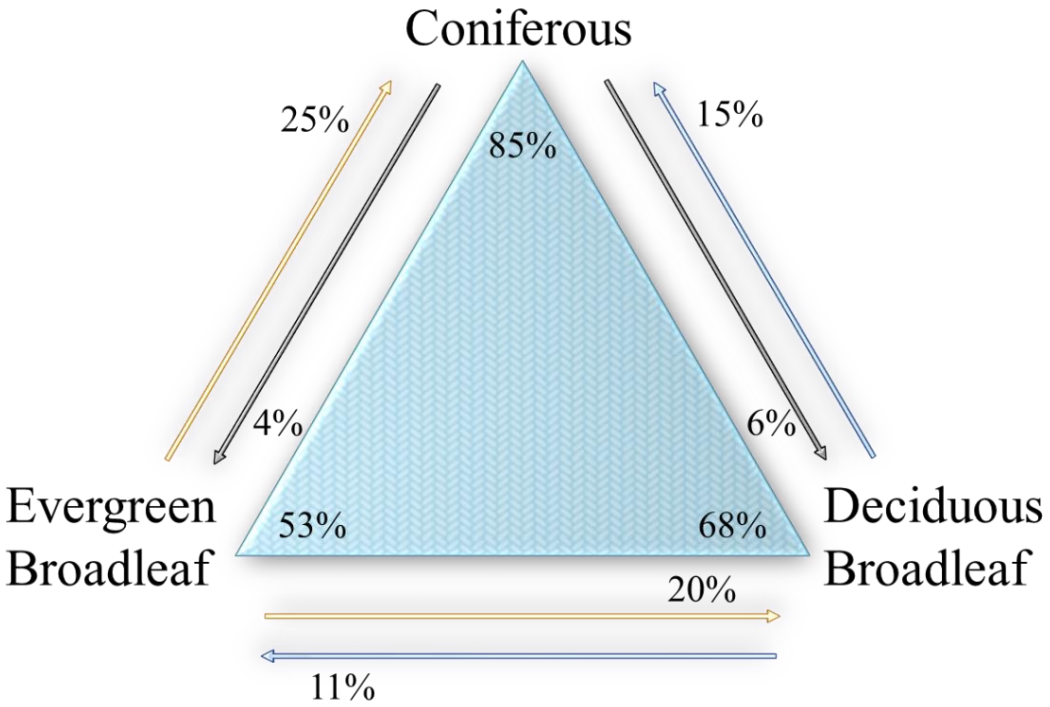

Figure 30. Triangular relationship of the forest classes and its accuracy and errors.

The figure shows the relationship between the classes which is outputted in the classification scheme. It indicates the producer's accuracy (percentage value inside the triangle) and the errors of omission (outside the triangle). The arrows indicate the misclassification of the classes that were supposed to be classified (beginning of the arrow) but was classified into a different class (end of the arrow). So, for example coniferous forests were 85 % accuracy in classification while 4 % was misclassified into evergreen broadleaf and 6 % were misclassified into deciduous broadleaf forests. Same can be explained for the other two classes. So here it can be said that 85 % for coniferous can be true, while there are 4 % and 6 % of chances making errors from evergreen and deciduous broadleaf forests respectively in the calculation of the total CO_2 amount. Same can be said for other classes, *mutatis mutandis*. Evergreen broadleaf shows 20 % and 25 % chances of error from deciduous broadleaf and coniferous forests respectively and deciduous broadleaf shows 11 % and 15 % chances of error from evergreen broadleaf and coniferous forests respectively.

For number 2, the errors in the backscattering model can be explained by the RMSE calculated from the estimated stem volume versus the ground truth volume information (Figure 16). As it has been explained in the earlier chapter, the RMSE of the backscattering model resulted 105.58 m^3/ha. This can lead to errors in where the stem volume was transformed into the tree age information, and thus become an error in the estimation of the CO_2. For example, in the coniferous trees at high growth rate areas, 100 m^3/ha difference can differ the tree age by ±6 years. Larger differences are seen at lower growth rate areas, for example at Site 3 (low growth rate region) 100 m^3/ha can differ the tree age by ±13 years by looking at the stem volume – age relationship data from the Oita Prefectural Government. 6 years difference can for sure change the estimation values in this case, for example the forested areas of coniferous at the peak ages can be possible to lie on the classes on earlier age or older age, and *vice versa*, the older age class could lie onto the peak tree age classes. So this is one of the potential that is described for the actual errors in the estimation.

For number 3, the tree age transformation was done by using the reference data provided by the Oita Prefectural Government and from Sasaki et al. (1989). According to this growth curve, the stem volume information was reclassified for the whole area of Japan. The issue here is that does this growth curve imply for other regions of Japan. This study used the reference information as a representative growth curve for each tree types, and using the precipitation data, it has been assumed that the other regions of Japan would lie similar to one of those growth curves. To make sure, additional references were collected to compare this curve information for other regions of Japan. Figure 31 shows the tree growth curve information from Kagoshima region and Aomori region to simply see the difference from the southern and northern regions environment affecting the tree growth.

(a)

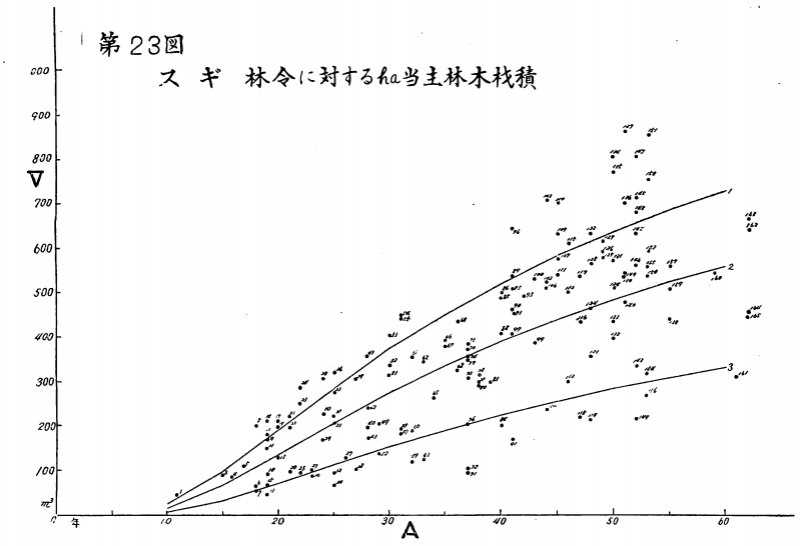

(b)

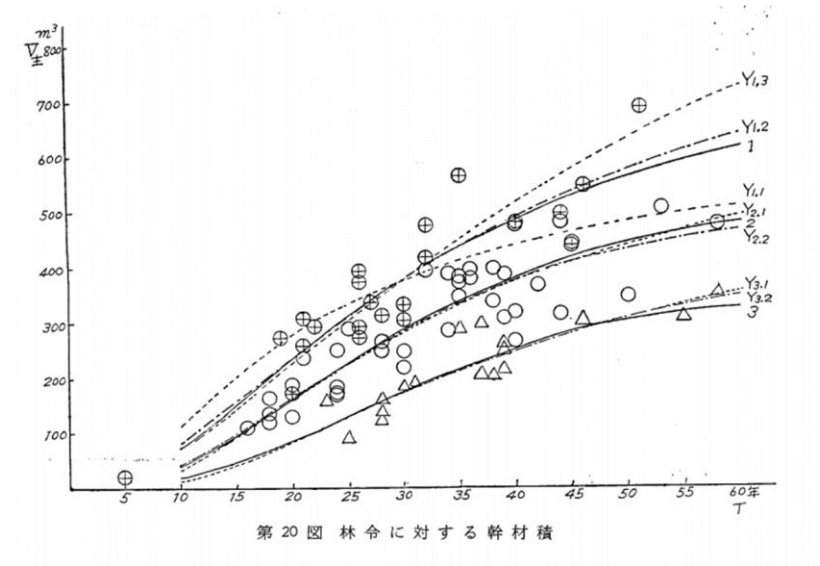

Figure 31. Stem volume – tree age curve for the sugi (coniferous) trees from **(a)** Aomori and **(b)** Kagoshima region (Forest Agency, 1962; 1965).

As far as the figure shows, there are differences in the growth curves depending on the different site productivity areas, however comparing the two figures it cannot confirm a big difference of the growing curves even at an opposite environmental regions (warmer Kagoshima region, and cooler Aomori region). It is known that there are a most suitable growth curves existing for each Prefectures of Japan, but on this case it has been considered for this fact and challenged to normalize the differences of the growth curve by using the precipitation data and setting the threshold. Thus it can be said that the growth curve differences among each regions are managed well to average out and reduced to the least in the

errors from this aspect. Still, this is one point that could be considered as one of potential errors in the estimation.

Finally, for number 4, the sequestration information was modified from the Tochigi Prefectural Government by taking the mean or weighted mean of each tree types and used the value as the representative of each forest types per tree age classes. The errors that can appear from this is the sequestration value used for the multiplication with the total area, which would be different if it actually broke down further in detail for each specific tree types. Because there are trees that capture more or less CO_2 compared to other tree types of the same forest types, but those values were averaged in the case of this study. Another is the minimum and the maximum sequestration value for each tree age classes, since it is difficult to discriminate each forest by one year age distribution, the tree ages were classified in a 5 year interval range. The mean value within that range is used and there are minimum and maximum values for those categories, and that can make errors in the estimation also. Table 9 shows the minimum and the maximum sequestration values for each forest types at each tree age class ranges. As it is seen, there are some classes that has high sequestration value in the peak age of the coniferous trees (10-15 years) at site 1 region, which is little higher even than the average value from the evergreen broadleaf forests of Tadaki and Hachiya (1968), and also similar for the deciduous broadleaf forests. Looking through all the ages, the biggest difference of maximum and minimum is seen at the peak aged forests classes. This point is one of the most possible errors that could generate other than from the land cover errors.

Table 9. CO_2 sequestration minimum and the maximum values for each forest types and tree age classes.

	Coniferous (tCO_2/ha/yr)							**Deciduous Broadleaf (tCO_2/ha/yr)**		**Evergreen Broadleaf (tCO_2/ha/yr)**	
	Site 1		Site 2		Site 3						
Age (years)	Min	Max	Min	Max	Min	Max	**Age (years)**	Min	Max	Min	Max
0-5	3.26	3.49	1.95	2.75	1.23	1.84	0-5	1.72	4.16	1.56	3.44
5-10							5-10	3.80	9.92	3.43	10.29
10-15	11.75	18.43	8.70	11.78	5.38	8.64	10-15	5.06	8.44	5.14	8.57
15-20	14.23	18.08	9.90	13.15	5.99	8.88	15-20	5.17	8.33	5.14	8.57
20-25	11.13	13.23	7.70	9.49	5.29	7.31	20-25	5.08	7.20	5.32	7.60
25-30	9.55	10.93	7.50	8.20	4.68	5.98	25-30	3.97	5.56	4.18	5.70
30-35	7.99	8.71	6.39	6.98	5.03	5.95	30-35	3.60	5.45	3.80	5.70
35-40	6.30	6.71	5.63	6.61	4.55	5.27	35-40	2.12	4.81	2.28	4.94
40-45	5.19	5.91	4.61	5.40	3.85	4.78	40-45	1.86	4.34	1.90	4.56
45-50	4.37	5.89	3.79	5.01	3.46	4.51	45-50	1.86	3.70	1.90	3.80
50-55	3.44	5.75	3.23	4.94	3.02	3.78	50 over	0.60	3.41	1.50	3.61
55-60	2.79	5.82	2.72	4.55	2.58	3.78					
60-65	2.08	5.28	2.01	3.65	1.71	2.93					
65-70	1.32	4.35	1.04	2.77	0.97	1.98					
70-75	1.32	3.89	0.97	2.39	0.97	1.22					
75 over	0.59	2.06	0.22	0.79	0.24	0.53					

5.5.2. Actual CO_2 Estimates Considering the Errors

The CO_2 sequestration amounts by the forest in Japan were calculated for when each error were taken in consideration as stated in section 5.5.1. Table 10 shows the summary of the final output of the total CO_2 when errors are considered.

Table 10. Summary of the total CO_2 sequestration estimated from when each of the error cases is considered.

Forest Types / Errors	**Coniferous**		**Deciduous Broadleaf**		**Evergreen Broadleaf**		**Total CO_2 Sequestration**	
	Unit: $MtCO_2$							
Land Cover Mapping	Min_{tot}: 50.94	Max_{tot}: 89.67	Min_{tot}: 20.29	Max_{tot}: 25.50	Min_{tot}: 4.57	Max_{tot}: 11.94	Min_{tot}: 75.80	Max_{tot}: 127.11
Backscattering Model	(Avg_{val}) Min_{tot}: 65.46	(Avg_{val}) Max_{tot}: 99.81	N/A (21.61)		N/A (4.76)		Min_{tot}: 91.83	Max_{tot}: 126.18
Tree Age Curve	N/A		N/A		N/A		N/A	
Sequestration Value	Min_{tot}: 78.80	Max_{tot}: 90.97	Min_{tot}: 7.38	Max_{tot}: 31.94	Min_{tot}: 6.55	Max_{tot}: 14.78	Min_{tot}: 92.73	Max_{tot}: 137.69
Backscattering Model + Sequestration Value	(Min_{val}) Min_{tot}: 64.65	(Min_{val}) Max_{tot}: 91.45	N/A (21.61)		N/A (4.76)		(Min_{val}) Min_{tot}: 91.02	(Min_{val}) Max_{tot}: 117.82
	(Max_{val}) Min_{tot}: 75.03	(Max_{val}) Max_{tot}: 110.64					(Max_{val}) Min_{tot}: 101.4	(Max_{val}) Max_{tot}: 137.01

In the table the summary of the total CO_2 calculated from this study is listed and when each of the error case is considered. Four different cases of the potential error were stated: land cover misclassification, reliability of backscattering model, dependency of tree age curve and the sequestration value. For tree age curve, it is putted as N/A because it is simply the errors caused by the growth trend of the trees, and giving an estimation such as using other Prefectural Governments tree age curve information will become similar to what is was showed here in the results using the Oita data. However for the errors from the land cover mapping

misclassification, backscattering model and the sequestration value, along with adding the backscattering model and sequestration value errors together, the estimation was made.

In the table, Avg_{val} Min_{val} and Max_{val} represent the average, minimum and maximum sequestration value used for the estimation respectively. Min_{tot} and Max_{tot} represent the minimum total and maximum total CO_2 sequestration by each category respectively. So in the case of backscattering model error case on coniferous category, total CO_2 amount is estimated using the average sequestration value which is the value listed on Table 6. Values in the brackets written after N/A is the total sequestration value outputted stated in the tables of deciduous and evergreen broadleaf forests (Table 7, Table 8).

Errors of misclassification were considered by the percentage of the total area of each distributed forest classes added or subtracted based on the actual misclassification percentage showed on Figure 30. For example, 4 % and 6 % of coniferous classes were misclassified to evergreen broadleaf and deciduous broadleaf forests respectively. So 4 % and 6 % of total area from those forest classes respectively were subtracted and added to the coniferous class (this status is determined as the maximum value). At this moment, the deciduous and evergreen broadleaf status is determined as the minimum value. On the other hand 25 % and 15 % were misclassified to coniferous class which was likely to be evergreen and deciduous broadleaf forests respectively. Those percentage of the total area from the coniferous forests were subtracted and added to each of those forest classes (this status is determined as the minimum value). Again, at this moment, the deciduous and evergreen broadleaf status is determined as the maximum value. The dependency of the classification results to the errors in estimates of sequestration were assumed in such method. As a result, minimum total of the sequestration was 75.80 $MtCO_2$, while the maximum was 127.11 $MtCO_2$. Here, the sequestration value per tree age class for each forest types doesn't change, and only the total area of the forests fluctuates. We can see how total size of the forested area is one of the important factors which contribute to the total sequestration.

Error of backscattering model was considered from the RMSE of the model developed which was resulted as 105.58 m^3/ha. According to the stem volume – tree age curve information, the difference of that stem volume results 6 year, 7 year and 10 year difference for the coniferous trees on site 1, site 2 and site 3 respectively. Using this fact, the estimation of the CO_2 of coniferous forests were re-assessed by shifting the age range by the above tree age year difference, and the minimum and maximum resulted 65.46 and 99.81 $MtCO_2$ respectively. The total CO_2 is then calculated using this value along with the total value of other forest types (deciduous broadleaf (DBL) and evergreen broadleaf (EBL)). Estimation was made only for the coniferous forests in this case because the actual error values of the model developed by Wijaya (2009) were not found.

For the sequestration value errors, as listed on Table 9. This minimum and maximum value was applied multiplying with the total forested area of each forest types. Overall total CO_2 resulted 92.73 and 137.69 $MtCO_2$ for minimum and maximum total respectively. This case would be easier to interpret compared to other errors since all forest classes can be estimated clearly.

Finally both the errors from the backscattering model and the sequestration value were added then re-assessed the estimation. Again for this, it was only done for the coniferous class which has resulted as 64.65 and 91.45 $MtCO_2$ for minimum and maximum amount when the minimum sequestration value (Table 9) was used respectively and 75.03 and 110.64 $MtCO_2$ for minimum and maximum amount when the maximum sequestration value (Table 9) was used respectively.

In overall, the estimated total CO_2 lies between from 75.80 to 137.69 $MtCO_2$, where the minimum amount comes from the land cover error and the maximum from the sequestration error. It can be assumed that these two parameters are the most important factors when sequestration amount is estimated. When the results of this study are looked where it was 111.27 $MtCO_2$, the fluctuation of the estimated amount is around 23 to 32 % difference. Of

course if the information of the errors for the DBL and EBL class for the backscattering model errors could be obtained, some change could be seen to the results, however it may determine that even so it will not make that huge difference from what it is resulting now. Thus this result strongly gives confidence to the practical usage of the methodology.

5.5.3. Comparison to other References

For further of knowledge, other estimation methods was investigated in comparison to the results of this study. Four main methods is examined and checked, one is from this study, second is from using the conventional method by Tadaki and Hachiya (1968), third is the work done by Sasaki and Kim (2009), and the last is from the National Institute for Environmental Studies (NIES) (2014) of the IPCC report for the forest carbon sink. The total CO_2 estimation is summarized in Table 11 for all the methods stated. For the conventional method, the value is used along with the total forest areas obtained from our work.

Table 11. Summary of the total CO_2 sequestration estimated by various methodology taken among different studies.

Methods	**Total CO_2 Sequestration**
Conventional (Tadaki and Hachiya, 1968)	308.51 $MtCO_2$
Sasaki and Kim (2009)	73.7 $MtCO_2$
NIES (2014)	77.67 $MtCO_2$
Stem Volume Method (our work)	111.27 $MtCO_2$

The stem volume method obtained in this study, shows a result of 111.27 $MtCO_2$ by considering the forests types together with the tree age information (coniferous: 85.0 $MtCO_2$; deciduous broadleaf: 21.61 $MtCO_2$; evergreen broadleaf: 4.76 $MtCO_2$). When taking a look at the conventional method using the averaged value compared to the results in this study, it can be seen that it shows a large overestimation of the sequestration because of the sequestration values that sums up all into one category omitting the information of tree ages ignoring the lower sequestration stages leading to high overestimation of the result. Sasaki and Kim (2009)

and NIES (2014) shows a similar estimation value, however for the former studies, the result is obtained by using the land use model and carbon stock growth model and estimates the sequestration value classifying the forests as planted and natural forests. Planted forests showed an estimation of 56.1 $MtCO_2$ and 17.6 $MtCO_2$ for the natural forests, summing up the total result as 73.7 $MtCO_2$. The most interesting result is by the NIES, which they made the approach by using the forest registration data from each prefectural government, and differentiating the forests by each tree types collecting annual growth information for each tree types, then perform estimation by multiplying the annual sequestration value with the total forested areas of each tree types. They have not only calculated for the aboveground but also for the litter and soil, however majority of the sequestration is resulted from the aboveground biomass (aboveground: 76.53 $MtCO_2$; litter: 0.41 $MtCO_2$; soil: 2.58 $MtCO_2$; dead tree: -1.85 $MtCO_2$). If the methods by the NIES are assumed to be the most exact likely estimation of the nature environment, the remote sensing method applied in the study shows only 43 % overestimation compared from their results. This difference can be explained from the errors in the former section, and if there is a method to improve those potential errors, our results may lie somewhat similar to the results by the NIES. However, even the NIES results give some questions to parts such as the uncertainty of the total forest area, which is important because as mentioned, total CO_2 is calculated by multiplying the sequestration value with the total forest area. The data from the prefectural government is sometimes unclear, especially in terms of the area of the forest covers, so maybe there is a possibility that NIES are underestimating the forests capacity. What is significant about our work compared to the NIES is that this method can be totally performed through various time seasons further in the future with more less time and lower labor costs with the use of remote sensing data. The work done by NIES is possible in countries where a large database of the forests information is compiled for the use in application, but in countries where this is not well achieved, it will become very difficult to implement such method. On the other hand, the method developed in this study can be applied

in any countries on the globe as long as there are the necessary data sets available. Moreover, the uncertainty of the forest area compared to NIES can be overcome using our methodology because we are looking at the correct amount and size and location of the forests. So in that sense, overall comment to this study can be explained that, the result showed much lower than the conventional method where it seems to result with high overestimation, and comparing with NIES results, estimation of this study does not show such underestimation and it's around between those two. It could be confirmed that the results achieved through the methodology in this study showed the improvement and the potential of obtaining better results than others through the remote sensing way. Just to note that the term of sequestration used in this study can be described as NPP, while the NIES result can be described as Net Ecosystem Production (NEP) since it also considers for the decomposers. In future, the improvements of the methodology would like to take this in consider and obtain NEP values of the forests so we can estimate precise value and the extent of the forest and so that understanding of the material cycle and fluxes of the nature environment could be explored in-depth.

This method can work as detecting or estimating more precise information of the forests resources which is more likely to provide the decision makers with a sound basis for more effective policies and actions aiming at the sustainable use and conservation of the environmental resource.

5.6. Summary

In this chapter the estimation of CO_2 sequestration from the forests of Japan were examined. The objective of the work were accomplished by transforming the stem volume information obtained from the PALSAR imagery into tree age information for each forest types (coniferous, deciduous broadleaf and evergreen broadleaf), then applying the sequestration value per forest types at each tree age classes multiplying it with the total forested areas. The result showed an impressive result comparing to the conventional method and the method by the NIES, since our

work has reduced the high overestimation of the sequestration result compared to the conventional method by taking attention to the specific tree type and age. Moreover, comparing with the time consuming and high labor cost method by the NIES, this studies result showed only 43 % higher estimation then by the NIES and even though comparing, we can assume that this study was successful in avoiding such underestimation which the NIES are possibly making. There are still some potential errors that could be discussed in the work, however if those errors can be overcome, more precise estimation would become possible. The remote sensing method for estimating CO_2 sequestration by the forests of Japan gave a successful result through the work.

6. Concluding Remarks

This research has employed LANDSAT OLI and ALOS PALSAR data from a series of dates and field data collected in Japan, to estimate the CO_2 sequestration potential of the forests in Japan. It is shown that sequestrations obtained by using averaged values for natural or planted forests without forest type and tree age discrimination can lead to large overestimations of the sink capacity of forests. It has been made clear here that, by combining the optical and SAR remote sensing data; it became possible to obtain more realistic CO_2 sequestration amounts by the forests, based on detailed discrimination of forest type and tree age. Moreover, the detailed information about the spatial location and the status of the forest resources is more likely to provide the decision makers with a sound basis for more effective policies and actions aiming at the sustainable use and conservation of the environmental resources.

In this study, the retrieval of tree ages using the stem volume information extracted from SAR data was implemented for coniferous, deciduous broadleaf and evergreen broadleaf forests taking Sugi (cedar), Kunugi (sawtooth oak) and Ubame oak trees as representatives of those forest types, respectively. With this method, more realistic sequestration amounts was obtained than compared with the other methods. This methodology can thus help to investigate more in-depth the CO_2 sequestration values for trees of different ages and types, especially for the coniferous and also for deciduous or evergreen broadleaf forests, which are found over Japan. It is foreseen that this would lead to even more realistic estimation of the CO_2 sequestration of the real environment.

Further extension of our knowledge is needed for the development of better correlation with the SAR information and the forests stand characteristics. Using only backscattering intensity as a relationship analysis is rather difficult to discriminate the true relationship between the biophysical parameters because of various scattering components that affect the radar scattering. It is known that ALOS-2 PALSAR-2 is in operation and coming up soon for the data to be distributed to the public. Through the use of this data, and additional field

observation, improved methods for detecting the correct stand characteristics using SAR information should become possible to carry out. In this study the stem volume information was analyzed, and not the aboveground biomass as how various studies implements. This is because biomass is an information of the accumulation of the forests which could be used as estimating the potential amount of fuel energy, however, it is difficult to understand the current status of the forests in terms of the growing stages (i.e. tree age) which would lead to results in the total CO_2 sequestration estimates. Moreover, by estimating stem volume it becomes possible to estimate the total biomass, however the other way round is difficult to obtain. So from such perspective, detecting the growing stages using stem volume information is important, and this needs to be taken care on the analysis also, since the two parameters (biomass, stem volume) can react differently in the radar scattering, and thus lead to different correlation model.

For the future works, it is important to recognize the actual growing rates of each region precisely for to not only obtain more realistic amount of the CO_2 estimation, but for further use of its information to effectively manage on new plans that would be more strategically and useful for decision makings in such field. In this study, the growing rates of the forests were considered by zoning the area using precipitation data as one of the limiting factors for the growth of the forests. If precise information of what factor affects the actual growth of the forests is considered and could be mapped, then zoning the areas into several potential growing rates areas, that would lead to more improvements to the final results and also it can be utilized as a scientific live information for the policy makers to deal with better plans and approaches for forest management to actually mange those resources sustainable.

At last the conclusion, findings, issues and future works are itemized:

1. Estimation of CO_2 sequestration was performed integrating optical and microwave remote sensing data
2. Optical data were used for land cover mapping, SAR was used for stem volume mapping

3. The originality of this work is that discrimination of tree age for each forest types using PALSAR L-band was achieved for more precise estimation
4. The result estimated 111.27 $MtCO_2$ giving only 43 % higher estimate compared from the NIES (2014)
5. There are issues that needs to overcome for better estimation as to be the future works: **(a)** improving land cover mapping **(b)** improving SAR - biophysical parameter modeling **(c)** discrimination of tree age for each region at different environments **(d)** observation of actual CO_2 sequestration for each tree types **(e)** further field work for the validation of the final outputs.
6. In the future works, it is considered to analyze the site productivity of the forests area and zone them to make more precise evaluation of the forests carbon extent and for the use as a data for the decision makers in their policy planning.

Acknowledgments

The author is very grateful to the members and the faculty of the Center for Environmental Remote Sensing (CEReS), Chiba University for the informative remarks and suggestions during the elaboration of this work. The author kindly appreciate the professors who have given us informative comments and advise to brush up the content of this work, especially a special appreciation to Professor Dr. Ryutaro Tateishi, for supervising throughout the whole work. Also to the thesis committee: Professor Dr. Akihiko Kondo, Professor Dr. Atsushi Higuchi and Professor Dr. Josaphat Tetuko Sri Sumantyo, a grateful appreciation for their encouragement, insightful comments and much more that made this piece of work to reach beyond the limits. The author would like to give a big appreciation to Professor Dr. Kazadi Sanga-Ngoie which has supervised the author in the early times for how to research and to be as a researcher, you have been a tremendous mentor for me and I truly thank the chance, opportunity and the experiences which made me to continue on this field. The author also thanks Oita Prefectural Government, Forest Management Division Department of Agriculture Affairs along with the Chiba Prefectural Government for providing the forest inventory data.

At last, the author gives his deep heartfelt appreciation to the parents. Words cannot express how grateful he is to his mother, Keiko Iizuka and father-in-law, Lennart Nils Ahl for raising me, supporting me, and for all the experiences you have brought to me. Thank you also to all my brothers and sisters for understanding and accepting me to be as a family. I kindly give my gratefulness to all the people who has related in my life, because I know that I have grown as what I am today thanks to all of you.

References and Notes

1. Abbott, K. N., Leblon, B., Staples, G. C., Maclean, D. A. and Alexander, M. E. (2007) Fire danger monitoring using RADARSAT-1 over northern boreal forests. *International Journal of Remote Sensing.* **28**, 1317-1338.
2. Armston, J., Carreiras, J., Lucas, R. and Shimada, M. (2010) ALOS PALSAR backscatter mosaics for Queensland, Australia. Proceedings of the 15th Australasian Remote Sensing & Photogrammetry Conference. September 2010, Australia.
3. Balzter, H., Baker, J., Hallikainen, M. T. and Tomppo, E. (2002) Retrieval of timber volume and snow water equivalent over a Finnish boreal forest from airborne polarimetric Synthetic Aperture Radar. *International Journal of Remote Sensing.* **23**, 3185–3208.
4. Bibilis, E. J., Brinker, R., Carino, H. F. and Mckee, C. W. (1993) Effect of stand age on flexural properties and grade compliance of lumber from loblolly pine plantation timber. *Forest Products Journal,* **43**, 23-28.
5. Bird, M. (2010) Monitoring the carbon cycle in Tropical forests. *Environmental Opinion Leaders for the Asia Pacific 2010 International Symposium Official Report*, Ritsumeikan Asia Pacific University, Japan, 39-54.
6. Brolly, M. and Woodhouse, L. H. A. (2012) "Matchstick Model" of microwave backscatter from a forest. *Ecological Modelling.* **237-238**, 74-87.
7. Brown de Colstoun Eric, C., Story Michael, H., Thompson, C., Commisso, K., Smith Timothy, G. and Irons James, R. (2003) National Park vegetation mapping using multitemporal Landsat 7 data and a decision tree classifier. *Remote Sensing of Environment,* **85**, 316-327.
8. Cartus, O., Santoro, M. and Kellndorfer, J. (2012) Mapping forest aboveground biomass in the Northeastern United States with ALOS PALSAR dual-polarization L-band. *Remote Sensing of Environment.* **124**, 466-478.
9. Castel, T., Beaudoin, A., Stach, N., Stussi, N., Le Toan, T. and Durand, P. (2001) Sensitivity of space-borne SAR data to forest parameters over sloping terrain. Theory and experiment. *International Journal of Remote Sensing.* **22**, 2351–2376.
10. Champion, I., Dubois-Fernandez, P., Guyon, D., Cottrel, M. (2008) Radar image texture as a function of forest stand age, *International Journal of Remote Sensing,* **29**, 1795-1800.
11. Chen, E., Li, Z., Ling, F., Lu, Y., He, Q. and Fan, F. (2009) Forest Volume Density Estimation Capability of ALOS PALSAR Data over Hilly Region. *Proceedings of 4th International Workshop on Science and Applications of SAR Polarimetry and Polarimetric Interferometry - PolInSAR 2009,* Frascati, Italy, 26–30 January 2009.
12. Chiras, D. D. (2006) Environmental Science Seventh Edition, Jones and Bartlett, United Kingdom, p.458.
13. Congalton, R. G. and Mead, R. A. (1983) A Quantitative Method to Test for Consistency and Correctness in Photointerpretation. *Photogrammetric Engineering and Remote Sensing.* **49**, 69-74.
14. Congalton, R. G. and Green, K. (2009) *Assessing the accuracy of remotely sensed data; principles and practices*, second edition; CRC/Taylor & Francis: New York.

15. DiMiceli, C. M., Carroll, M. L., Sohlberg, R. A., Huang, C., Hansen, M. C. and Townshend, J. R. G. (2011) Annual Global Automated MODIS Vegetation Continuous Fields (MOD44B) at 250 m Spatial Resolution for Data Years Beginning Day 65, 2000 - 2010, Collection 5 Percent Tree Cover. University of Maryland: College Park, MD, USA.
16. Dobson, M. C., Pierce, L., Sarabandi, K., Ulaby, F. T. and Sharik, T. (1992a) Preliminary analysis of ERS-1 SAR for forest ecosystem studies. *IEEE Transactions on Geoscience and Remote Sensing.* **30**, 203-210.
17. Dobson, M. C., Ulaby, F. T., Le Toan, T., Beaudoin, A., Kasischke, E. S. and Christensen, N. (1992b) Dependence of radar backscatter on coniferous forest biomass. *IEEE Transactions on Geoscience and Remote Sensing.* **30**, 412–415.
18. Dobson, M. C., Ulaby, F. T. and Pierce, L. E. (1995) Land-Cover Classification and Estimation of Terrain Attributes Using Synthetic Aperture Radar. *Remote Sensing of Environment.* **51**, 199-214.
19. Eastman, J. Ronald. (2006) *IDRISI Andes Guide to GIS and Image Processing*, Clark Labs, Clark University.
20. Fernandez-Ordonez, Y., Soria-Ruiz, J. and Leblon, B. (2008) Forest Inventory using Optical and Radar Remote Sensing, In: Gary Jedlovec, Ed., *Advances in Geoscience and Remote Sensing*, InTech, Rijeka, Croatia.
21. Forestry Agency (1962) Aomori Region Sugi tree Rinbun-Shukaku-Hyou (Japanese) http://www.ffpri.affrc.go.jp/labs/shukakushiken/02gyoken/02gyoken_28.pdf (accessed on 19 October 2014)
22. Forestry Agency (1965) Kagoshima Region Sugi tree Rinbun-Shukaku-Hyou (Japanese) http://www.ffpri.affrc.go.jp/labs/shukakushiken/02gyoken/02gyoken_33.pdf (accessed on 19 October 2014)
23. Fransson, J. E. S. and Israelsson, H. (1999) Estimation of stem volume in boreal forests using ERS-1 C- and JERS-1 L-band SAR data. *International Journal of Remote Sensing.* **20**, 123–137.
24. French, N. H. F., Kasischke, E. S., Bourgeau-Chavez, L. L. and Harrell, P. A. (1996) Sensitivity of ERS-1 SAR to variations in soil water in fire-disturbed boreal forest ecosystems. *International Journal of Remote Sensing.* **17**, 3037-3053.
25. Gopal, S. and C. Woodcock (1994) Theory and methods for accuracy assessment of thematic maps using fuzz sets. *Photogrammetric Engineering and Remote Sensing,* **60**, 181-188.
26. Hamdan, O., Aziz, H. K. and Rahman, K. A. (2011) Remotely Sensed L-band SAR Data for Tropical Forest Biomass Estimation. *Journal of Tropical Forest Science.* **23**, 318-327.
27. Harrell, P. A., Bourgeau-Chavez, L. L., Kasischke, E. S., French, N. H. F. and Christensen, N. L. (1995) Sensitivity of ERS-1 and JERS-1 radar data to biomass and stand structure in Alaskan boreal forest. *Remote Sensing of Environment.* **54**, 247-260.
28. Harrell, P., Kasischke, E. S., Bourgeau-Chavez, L. L., Haney, E. and Christensen, N. L. (1997) Evaluation of approaches to estimating aboveground biomass in Southern pine forests using SIR-C data. *Remote Sensing of Environment.* **59**, 223–233.
29. Hess, L. L., Melack, J. M. and Simonett, D. S. (1990) Radar detection of flooding beneath

the forest canopy: a review. *International Journal of Remote Sensing.* **11**, 1313-1325.
30. Hewitt C. N. and Jackson A. (2003) Handbook of Atmospheric Science: Principles and Applications; Blackwell, United Kingdom, pp. 368-370.
31. Hiroshima, T. and Nakajima, T. (2006) Estimation of sequestered carbon in article-3.4 private planted forests in the first commitment period in Japan. *Journal of forest research*, **11**, 427-437.
32. Hoekman, D. and Quinones, M. J. (2000) Land cover type and biomass classification using AirSAR data for evaluation of monitoring scenarios in the Colombian Amazon. *IEEE Transactions on Geoscience and Remote Sensing.* **38**, 685–696.
33. J. R. Holton (1992) An Introduction to Dynamic Meteorology Third Edition; Academic Press, California.
34. Hyyppä, J. M., Hyyppä, H. J., Inkinen, M. and Engdahl, M. E. (2000) Accuracy comparison of various remote sensing data sources in the retrieval of forest stand attributes. *Forest Ecology and Management.* **128**, 109–120.
35. Iizuka, K. and Tateishi, R. (2013) Analysis of Backscattering Characteristics of L-Band SAR over the Mountainous Region of Chiba Japan, using 50 m PALSAR Mosaic Product. *Proceedings of International Symposium on Remote Sensing*, Chiba, Japan, 15-17 May 2013.
36. Imhoff, M. L. (1995) Radar backscatter and biomass saturation: Ramifications for global biomass inventory. *IEEE Transactions on Geoscience and Remote Sensing.* **33**, 511– 518.
37. IPCC (1996) Revised 1996 IPCC Guidelines for National Greenhouse Gas Inventories. J.T. Houghton, L.G. Meira Filho, B. Lim, K. Treanton, I. Mamaty, Y. Bonduki, D.J. Griggs, and B.A. Callander (eds.). Intergovernmental Panel on Climate Change, Meteorological Office, Bracknell, United Kingdom.
38. Ishii, T. (2007) Estimation of forest leaf area index using remote sensing data and its applications to predicting forest carbon sequestration and water budget (Japanese), Ph.D. Thesis, Waseda University, Tokyo, Japan.
39. Janssens Ivan, A., Freibauer, A., Ciais, P., Smith, P., Nabuurs, G-J., Folberth, G., Schlamadinger, B., Hutjes Ronald, W. A., Ceulemans, R., Schulze, E-D., Valentini, R. and Dolman, A. J. (2003) Europe's Terrestrial Biosphere Absorbs 7 to 12% of European Anthropogenic CO_2 Emissions. *Science.* **300**, 1538-1542.
40. JAXA (2009). PALSAR Calibration Factor Updated. http://www.eorc.jaxa.jp/en/about/distribution/info/alos/20090109en_3.html (accessed on 2 October 2014).
41. Karjalainen, M., Pyysalo, U., Karila, K. and Hyyppa, J. (2008) Forest Biomass Estimation using ALOS PALSAR Images in Challenging Natural Forest Area in Finland. *Proc. of the ALOS PI 2008 Symposium*, November 2008, Greece.
42. Kasischke, E. S., Christensen, N. L. Jr. and Bourgeau-Chavez, L. L. (1995) Correlating radar backscatter with components of biomass in loblolly pine forests. *IEEE Transactions on Geoscience and Remote Sensing.* **33**, 643-659.

43. Kasischke, E. S. and Bourgeau-Chavez, L. (1997) Monitoring South Florida wetlands using ERS-1 SAR imagery. *Photogrammetric Engineering and Remote Sensing.* **63**, 281-291.
44. Kato, M. (2004) Forestry Remote Sensing - Basics to Application. Japan Forestry Investigation Committee, Toyko (in Japanese).
45. Kawazumi, K., Oda, K. and Tsutsumi, J. (1991) Heartwood Moisture Content of Sugi (*Cryptomeria japonica*) Cultivars Grown in a Given Stand. *Science Bulletin of the Faculty of Agriculture, Kyushu University.* **1-2**, 79-84.
46. Kellndorfer, J. M., Dobson, M. C., Vona, J. D. and Clutter, M. (2003) Toward precision forestry: Plot-level parameter retrieval for slash pine plantations with JPL AIRSAR. *IEEE Transactions on Geoscience and Remote Sensing.* **41**, 1571–1582.
47. Kobayashi S. and Sanga-Ngoie, K. (2008) The integrated radiometric correction of optical remote sensing imageries, *International Journal of Remote Sensing*, **29**, 5957-5985.
48. Kobayashi, S., Widyorini, R., Kawai, S., Omura, Y., Sanga-Ngoie, K. and Supriadi, B. (2012a) Backscattering characteristics of L-band polarimetric and optical satellite imagery over planted acacia forests in Sumatra, Indonesia. *Journal of Applied Remote Sensing.* **6**, 063519–063525.
49. Kobayashi, S., Omura, Y., Sanga-Ngoie, K., Widyorini, R., Kawai, S., Supriadi, B. and Yamaguchi, Y. (2012b) Characteristics of Decomposition Powers of L-band Multi-polarimetric SAR in Assessing Tree Growth of Industrial Plantation Forests in the Tropics. *Remote Sensing.* **4**, 3058-3077.
50. Kuplich, T. M., Salvatori, V., Curran, P. J. (2000) JERS-1/SAR backscatter and its relationship with biomass of regenerating forests, *International Journal of Remote Sensing*, **21**, 2513-2518.
51. Leblon, B., Kasischke, E. S., Alexander, M. E., Doyle, M. and Abbott, M. (2002) Fire Danger Monitoring Using ERS-1 SAR Images in the Case of Northern Boreal Forests. *Natural Hazards.* **27**, 231-255.
52. Leckie, D. G. (1990) Advanced in remote sensing technologies for forest surveys and management. *Canadian Journal of Forest Research.* **20**, 464-483.
53. Le Toan, T., Beaudoin, A. and Guyon, D. (1992) Relating forest biomass to SAR data. *IEEE Transactions on Geoscience and Remote Sensing.* **30**, 403–411.
54. Lo, C. P. and Choi, J. (2004) A hybrid approach to urban land use/cover mapping using Landsat 7 enhanced thematic mapper plus (ETM+) images. *International Journal of Remote Sensing*, **25**, 2687-2700.
55. Lucas, R. M., Armston, J., Fairfax, R., Fensham, R., Accad, A., Carreiras, J., Kelley, J., Bunting, P., Clewley, D., Bray, S., Metcalfe, D., Dwyer, J., Bowen, M., Eyre, T., Laidlaw, M. and Shimada, M. (2010) An evaluation of the ALOS PALSAR L-band backscatter—above ground biomass relationship Queensland, Australia: Impacts of surface moisture condition and vegetation structure. *IEEE Journal of Selected Topics in Applied Earth Observations and Remote Sensing.* **3**, 576–593.

56. Luckman, A., Baker, J., Honzak, M. and Lucas, R. (1998) Tropical forest biomass density estimation using JERS-1 SAR: Seasonal Variation, Confidence Limits, and Application to Image Mosaics. *Remote Sensing of Environment.* **63**, 126-139.
57. MAFF (2010a) Annual Report on Forest and Forestry in Japan (summary). http://www.rinya.maff.go.jp/j/kikaku/hakusyo/22hakusho/pdf/22_e.pdf (accessed on 2 October 2014).
58. MAFF (2010b) Function of the sequestration of forests/trees http://www.rinya.maff.go.jp/kinki/hyogo/mori-grow/mori-co2.html (accessed on 2 October 2014) (Japanese).
59. Matsumoto, M. (2001) Carbon Stock and Carbon Sequestration by the Forests of Japan, *Shinrin Kagaku*, **33** (Japanese).
60. METI (Ministry of Economy, Trade and Industry) (2005) Kyoto Protocol Target Achievement Plan. http://www.meti.go.jp/policy/energy_environment/global_warming/study_policy.html (accessed on 2 October 2014) (Japanese).
61. Minato, K., Ujiie, M. and Hishinuma, Y. (1989) Growth and Wood Quality of Sugi and Hinoki Trees in the Plantations of the Wakayama Experiment Forest. *Research Bulletins of the College Experiment Forests.* **46**, 223-247.
62. MOE (Ministry of Environment of Japan) (2013) National Survey on the Natural Environment. http://www.biodic.go.jp/english/J-IBIS.html (accessed on 2 October 2014).
63. Motohka, T., Shimada, M., ISoguchi, O., Ishihara, M. I. and Suzuki, S. N. (2011) Relationships Between PALSAR Backscattering Data and Forest Above Ground Biomass in Japan. *Proceedings of IEEE International Geoscience and Remote Sensing Symposium 2011*, Vancouver, Canada, 24-29 July, 2011.
64. National Institute for Environmental Studies (NIES), Japan, Center for Global Environmental Research (CGER) (2014) National Greenhouse gas Inventory Report of JAPAN http://www-gio.nies.go.jp/aboutghg/nir/2014/NIR-JPN-2014-v3.0.pdf (accessed on 18 October 2014)
65. Perry, D. A., Oren, R. and Hart, S. C. (2008) *Forest Ecosystems 2nd edition*: The Johns Hopkins University Press; Maryland, USA.
66. Pulliainen, J. Y., Mikkela, P. J., Hallikainen, M. T. and Ikonen, J. P. (1996) Seasonal dynamics of C-band backscatter with applications to biomass and soil moisture estimation. *IEEE Transactions on Geoscience and Remote Sensing.* **34**, 758-770.
67. Ranson, K. J. and Sun, G. (1994) Mapping biomass of a northern forest using multifrequency SAR data. *IEEE Transactions on Geoscience and Remote Sensing.* **32**, 388–396.
68. Ranson, K. J. and Sun, G. (2000) Effects of environmental conditions on boreal forest classification and biomass estimates with SAR. *IEEE Transactions on Geoscience and Remote Sensing.* **38**, 1242–1252.
69. Richards J. A. and Jia, X. (1999) *Remote Sensing Digital Image Analysis: An Introduction. Third, Revised and Enlarged Edition*; Springer; New York.
70. Richards, J. A. (2009) *Remote Sensing with Imaging Radar*. Springer; New York, USA.

71. Saatchi, S. S. and Moghaddam, M. (2000) Estimation of crown and stem water content and biomass of boreal forest using polarimetric SAR imagery. *IEEE Transactions on Geoscience and Remote Sensing.* **38**, 697–709.
72. Sandberg, G., Ulander, L. M. H., Fransson, J. E. S., Holmgren, J. and Le Toan, T. (2011) Land P-band backscatter intensity for biomass retrieval in hemiboreal forest. *Remote Sensing of Environment.* **115**, 2874–2886.
73. Sanga-Ngoie, K. (2003) Quantitative estimation of CO_2 sequestration by forest systems in Mie using GIS and Remote Sensing, *2003 Annual Conference for The Mie University GIS Society: GIS and Remote Sensing -Powerful tools for eco-climatic analysis*- **3**, 75-78.
74. Sanga-Ngoie, K. and Kobayashi, S. (2003) A perspective on the integration of the land-use/land-cover classification results using GIS and LANDSAT data. 2*003 Annual Conference for The Mie University GIS Society: GIS and Remote Sensing -Powerful tools for eco-climatic analysis*- **3**, 69-74 (Japanese).
75. Santoro, M., Fransson, J. E. S., Eriksson, L. E. B., Magnusson, M., Ulander, L. M. H. and Olsson, H. (2009) Signatures of ALOS PALSAR L-band backscatter in Swedish forest. *IEEE Transactions on Geoscience and Remote Sensing.* **47**, 4001–4019.
76. Santoro, M., Beer, C., Cartus, O., Schmullius, C., Shvidenko, A., McCallum, I., Wegmüller, U. and Wiesmann, A. (2011) Retrieval of growing stock volume in boreal forest using hyper-temporal series of Envisat ASAR ScanSAR backscatter measurements. *Remote Sensing of Environment.* **115**, 490-507.
77. Sasaki, H., Hayashi, H. and Ise, S. (1989) Considerations on the selective logging updating of evergreen broadleaf forests. *Tokushima Prefecture Forestry Research Center Report*. **27**, 22-29.
78. Sasaki, N. and Kim, S. (2009) Biomass carbon sinks in Japanese forests: 1966-2012. *Forestry*, **82**, 113-123.
79. Shi, J., Wang, J., Hsu, A. Y., O'Neill, P. E. and Engmann, T. (1997) Estimation of bare surface soil moisture and surface roughness parameter using L-Band SAR image data. *IEEE Transactions on Geoscience and Remote Sensing.* **35**, 1254-1265.
80. Shimada, M. (2010) Ortho-Rectification and Slope Correction of SAR Data Using DEM and Its Accuracy Evaluation. *IEEE Journal of Selected Topics in Applied Earth Observations and Remote Sensing*. **3**, 657-671.
81. Small, D. (2011) Flattening gamma: Radiometric terrain correction for SAR imagery. *IEEE Transactions on Geoscience and Remote Sensing.* **49**, 3081–3093.
82. Suzuki, R., Kim, Y. and Ishii, R. (2013) Sensitivity of the backscatter intensity of ALOS PASLAR to the above-ground biomass and other biophysical parameters of boreal forest in Alaska. *Polar Science.* **7**, 100-112.
83. Tadaki, Y. and Hachiya, K. (1968) Forest ecosystems and their productivity, *Ringyo Kagakugijutsu Shinkosho,* p. 64 (Japanese)
84. Tsushima, S., Fujioka, Y., Oda, K., Matsumura, J. and Shiraishi, S. (2006) Variations of Wood Properties in Forests of Seedlings and Cutting Cultivars of Hinoki (*Chamaecyparis obtusa*). *Mokuzai Gakkaishi.* **52**, 277-284.

85. Tucker, C. J. (1979) Red and photographic infrared linear combinations for monitoring vegetation. *Remote Sensing of Environment,* **8**, 127-150.
86. Turner, D. P., Guzy, M., Lefsky, M. A., Ritts, W. D., Tuyl, S. V. and Law, B. E. (2004) Monitoring Forest Carbon Sequestration with Remote Sensing and Carbon Cycle Modeling. *Environmental management,* **33**, 457-466.
87. Ulaby, F. T., Sarabandi, K., McDonald, K., Whitt, M. and Dobson, C. (1990) Michigan microwave canopy scattering model. *International Journal of Remote Sensing.* **11**, 1223-1253.
88. Ulander, L. M. H. (1996) Radiometric Slope Correction of Synthetic-Aperture Radar Images. *IEEE Transactions on Geoscience and Remote Sensing.* **34**, 1115-1122.
89. Umebayashi, T., Koga, S., Utsumi, Y., Inoue, S., Shiiba, Y., Nagasawa, H., Osaki, S., Kubota, K., Inoue, S., Matsumura, J. and Oda, K. (2011) Green moisture content and basic density of 95 woody species growing in Kyushu University Forests, Japan. *Bulletin of the Kyushu University Forest.* **92**, 33-44.
90. UNFCCC (1998) Kyoto Protocol to the United Nations Framework Convention on Climate Change. http://unfccc.int/resource/docs/convkp/kpeng.pdf (accessed on 2 October 2014).
91. USGS (United States Geological Survey), Earth Explorer: Satellite Images, Aerial Photographs and Maps. http://earthexplorer.usgs.gov/ (accessed on 18 October 2014)
92. Uyemura, T. (1960) Dielectrical Properties of Woods as the Indicator of the Moisture. *Bulletin of the Forestry and Forest Products Research Institute.* **119**, 95-172.
93. Watanabe, M., Shimada, M., Rosenqvist, A., Tadano, T., Matsuoka, M., Romshoo, S. A., Oha, K., Furuta, R., Nakamura, K. and Moriyama, T. (2006). Forest Structure Dependency of the Relation between L-Band σ^0 and Biophysical Parameters. *IEEE Transactions on Geoscience and Remote Sensing.* **44**, 3154-3165.
94. Wijaya, A. (2009) Evaluation of ALOS-PALSAR mosaic data for estimating stem volume and biomass: A case study from tropical rainforest of central Indonesia. *Jurnal Geografi.* **2**, 14-21.
95. Xiuwan, C. (2002) Using remote sensing and GIS to analyse land cover change and its impacts on regional sustainable development. *International Journal of Remote Sensing,* **23**, 107-124.

Integration of Optical and Microwave Remote Sensing Data for the Estimation of CO_2 Sequestration by the Forests in Japan

2015 年 3 月 2 日発行

著　者　　飯塚 浩太郎

発　行　　株式会社 サンヨー
〒101-0051 東京都千代田区神田神保町 1-30
TEL 03-3294-4950
FAX 03-3294-4962

Printed in Japan